

Department of Chemistry



*Probing Dynamic Disorder in Single-
Molecule Event Statistics*

*Thesis submitted in the partial fulfilment of
requirements for the degree of*

Doctor of Philosophy

By Divya Singh

Registration No.: 20153406

Date: 17.12.2020

Dedicated to my family...

Certificate

This is to certify that the submitted thesis constitutes the research work performed by Divya Singh during her doctoral tenure (August 2015 to December 2020). Any section of this work had has not been submitted anywhere else as a thesis/dissertation. Motivations and backgrounds associated with the already existing literature had have been properly cited wherever necessary. To best of my knowledge, the presented thesis is not plagiarised.

Ph.D. Supervisor: Dr. Srabanti Chaudhury



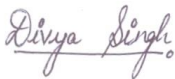
Place: IISER Pune

Date: 17.12.2020

Declaration

I Divya Singh hereby declare that the presented work in the thesis is non-plagiarised research carried out under the supervision of Dr. Srabanti Chaudhury, in the Department of Chemistry, IISER Pune India. The theoretical methods, data, figures and analyses are works not submitted anywhere else as a thesis/dissertation. I have performed these works exclusively during my Ph.D. tenure (August 2015 to December 2020). Due credits and citations have been given in different sections of the thesis for referring to the existing literature. To best of my knowledge, there is no conflict of interest.

Name of Ph.D. Student: Divya Singh



Place: IISER Pune

Date: 17.12.2020

Acknowledgments

A journey is a reward in itself. Sparking sand, the water content in a seashell, the whispering wind, lake whirlpools, they all comprise magnificent stories of time journeys in themselves. Like those, life is a journey of moments covering several aspects of learning, living, gathering specific expertise and excelling with the earned experiences.

With the submission of this thesis, I would like to express my sincere gratitude towards people who have been my comrades, companions, colleagues, acquaintances and well-wishers throughout this journey. Firstly, I wholeheartedly thank my Ph.D. supervisor Dr. Srabanti Chaudhury, for her continuous support and encouragements throughout the tenure. As my mentor, she was there for the formal/informal discussions and providing suggestions for resolving research issues. She always emphasized on consistency, opting for the methodology wisely and working hard for addressing problems in time.

I would like to thank my RAC (Research Advisory Committee) members, Dr. Anirban Hazra (IISER Pune) and Dr. Sarika M. Bhattacharyya (CSIR-NCL Pune) for their critical comments, continuous evaluation and feedback. I would also like to thank my collaborator Prof. Anatoly B. Kolomeisky (Rice University, U.S.A.) for a wonderful collaboration and providing an opportunity for enhancing my conceptual understanding of biophysical problems.

Sincerely I would like to thank my personal, time-independent support system: my beloved family. Without their unconditional affection, care and belief, this day would not have come. I am quite fortunate to have parents who happened to be my teachers and friends as well. I am thankful to my wonderful siblings Shweta and Avanish for being there with me in my thick and thins, addressing my occasional tantrums and trying their best to complement me while cheering me up. I am indebted to Anant and Pragya for being my friends cum family. I especially want to acknowledge Dr. Deenanath Chaubey and Dr. R. B. Singh for their valuable guidance and inspiration. I thank the soul supreme for everything.

Friends are the family we choose. I thank God for blessing me with such warm, cute and chaotic creatures. I thank my complementary lab mate and friend Bappa for being there (literally!) for all the meetings, seminars, snacks and discussing dynamic ‘trajectories’. I want to thank Mahesh, Meghna and Avdhoot for the scientific/non-scientific discussions in our

shared lab space. I will always cherish the moments spend together, be it the weekend dinners, magic tricks, dumb charades and dedicated poor joke sessions.

I would also like to acknowledge the ‘new arrivals of C-202’ Mrityunjay, Kinjal, Bhawakshi, Akash and Rugved who are ever ready with their puns, situational comedy and some cute little things. I especially want to thank Kinjal for teaming up for a project and making work fun. I would also like to thank Prabhat, Ardhara, Rakesh, Praveen, Debashish, Kanika, Subrahmanyam and all other computational group members of IISER Pune who provided a friendly neighborhood. I want to express my gratitude to my batch mates Jyoti, Manu and Satish for their friendly gestures and companionship. I would especially like to thank Yashwant for the enzymology discussions and being a friend indeed. This list would be incomplete if I do not mention my perennial friends Swati, Arpana, Rashmi and Vartika for all the conversations we had in these years, which cemented our relationship. I would like to acknowledge Swasti for the laughter we have shared. I want to thank Juhi for really being there at the time of need. I wish my friends good health and luck in all their carrier endeavors.

I would like to thank IISER Pune and CSIR for my fellowship. I thank present and former Directors of IISER Pune for providing excellent research facilities and infrastructure. I am obliged to Dr. Alope Das for facilitating a great working experience during my teaching assistantships and the trust he showed in us.

I express my gratitude towards all the members of different departments like the IT, Accounts and Academic office at IISER Pune. I genuinely thank Tushar Sir, Mayuresh Sir, Sayalee Ma’am, Neeta Ma’am, Shailesh Sir and Sachin Sir for their availability and efficiency, which ensures smooth functioning of IISER Pune. I would like to acknowledge DST-SERB for sanctioning the international travel grant. I thank Infosys foundation and Department of Chemistry for covering the accommodation charges associated with the travel.

At last but not the least, I would like to remember all my teachers from the school and professors who taught me in the Banaras Hindu University for introducing me to the world of knowledge.

Thesis Outlook

The molecular aspect of a reaction governs the applied methodology and the corresponding properties of a reaction under investigation. Unlike ensemble measurement techniques, single-molecule (SM) studies provide platforms for analysing individual molecular activities and accessing several dynamics aspects like as the lifetime of intermediates, the temporal fluctuations in the reaction rates, the rate-determining step, predicting reaction mechanisms, the correlation between events, the probability distribution function (PDF) associated with a stochastic process and related statistical measurements. For analytically analysing these stochastic networks, one requires appropriate theoretical frameworks for constructing the PDF of interest.

The thesis titled ‘Probing Dynamic Disorder in Single-Molecule Event Statistics’ emphasises on some applications of the theoretical formalisms (the first-passage time distribution formalism and the waiting-time distribution formalism) for mathematically modelling SM reaction networks associated with an enzyme and a nanoparticle (NP). We have implemented discrete state models on enzymatic systems undergoing reversible interconversions between different conformational states and calculated the noise. We have also applied these frameworks on NP catalysed reactions for exploring the underlying dynamics of chemical reactions and quantifying the temporal activity fluctuations.

Stochastic processes can also be modelled using continuous modelling methods. We have developed a theoretical method to derive the PDF of time taken by a molecule in crossing a barrier (the transit time distribution) using a generalized Langevin Equation (GLE) comprising different force components.

All these theoretical investigations and numerical analyses provide platforms for a better understanding of biochemical/biophysical processes.

List of Contents

1. Introduction	(11)
1.1 SM measurements and their relevance	(12-13)
1.2 Experimental techniques and applied methodology	(13-15)
1.3 Conventional enzyme catalysis	(15-16)
1.4 Analyses at the SM level and fluctuation measurements	(16-21)
1.5 Theoretical formalisms to construct the PDF	(21)
1.5.1 The first-passage time distribution formalism	(21-23)
1.5.2 The waiting-time distribution formalism	(23-27)
1.6 Thesis chapters in brief	(27-33)
1.7 References	(33-36)
2. Statistical properties of fluctuating enzymes with dynamic cooperativity using a first passage time distribution formalism	(37)
2.1 Introduction	(38-39)
2.2 Reaction Models and Analyses	(39-46)
2.3 Conclusions	(46-47)
2.4 References	(47)
3. Theoretical study of the conditional non-monotonic off rate dependence of catalytic reaction rates in single enzymes in the presence of conformational fluctuations	(48)
3.1 Introduction	(49-50)
3.2 Reaction Models and Analyses	(51-63)
3.3 Conclusions	(63-64)
3.4 References	(64)

4. Single molecule kinetics of an enzyme in the presence of multiple substrates	(65)
4.1 Introduction	(66-67)
4.2 Reaction Models and Analyses	(67-79)
4.3 Conclusions	(79-80)
4.4 References	(80)
5. Effect of substrate number fluctuations in stochastic enzyme kinetics	(81)
5.1 Introduction	(82-83)
5.2 Reaction Models and Analyses	(83-98)
5.3 Conclusions	(98-99)
5.4 References	(99)
6. Single-molecule kinetics of an enzyme in the phosphorylation-dephosphorylation cycle	(100)
6.1 Introduction	(101-103)
6.2 Reaction Models and Analyses	(103-117)
6.3 Conclusions	(117-118)
6.4 References	(118)
7. A stochastic theoretical approach to study the size-dependent catalytic activity of metal nanoparticle at the single molecule level	(119)
7.1 Introduction	(120-122)
7.2 Reaction Model and Analyses	(122-129)
7.3 Conclusions	(129-130)
7.4 References	(130)
8. Theoretical investigations of the dynamics of chemical reactions on nanocatalysts with multiple active sites	(131)
8.1 Introduction	(132-133)
8.2 Reaction Models and Analyses	(133-142)

8.3 Conclusions	(142)
8.4 References	(142)
9. Effect of memory and inertial contribution on transition time distributions: theory and simulations	(143)
9.1 Introduction	(144-146)
9.2 Model and Analyses	(146-155)
9.3 Conclusions	(155-156)
9.4 References	(156-157)
10. Conclusions and Future Directions	(158)
10.1 An Overall Outlook	(159-161)
10.2 References	(161)
List of Publications	(162)
Rights and Permissions	(163-166)

1. Introduction

1.1 SM measurements and their relevance:

Scientific experimentation, methodology and associated analyses provide signatures of the system constituents and its environment. Obtained inferences enhance the existing fundamentals and provide new platforms for future developments. Along with the details describing a system under investigation like as the starting material, reactant, catalyst, prerequisite experimental conditions for the reaction initiation and so on, the molecular aspect of a measurement also regulates the consequent characterization and observation. For example, the bulk measurement techniques give ensemble-average reaction properties of a set of molecules subjected to similar physio-co-chemical constraints and variables. These averages do not reflect the individual contribution from each molecule.¹⁻⁵ Discrete molecular activity in the course of a reaction remains hidden due to the cumulative nature of the outcome. For instance, a fraction of molecule behaving differently from the rest of the bulk can either facilitate or hamper the kinetics and dynamics of an ongoing process. The heterogeneity of reaction environment can play crucial roles in determining properties dependent on the local surrounding of molecules.⁶⁻⁸ Therefore, for exploring the individual molecular properties and addressing dynamical aspects, single-molecule (SM) measurement techniques are required.

Beginning from the initial historical developments to the current advancements in the field of single molecule detection (SMD) and single molecule spectroscopy (SMS), a lot changed in regards to the instrumentation, designing and characterization.⁹⁻¹⁶ In the year 2014, the Nobel Prize in Chemistry went to the three pioneer scientists namely, William E Moerner, Eric Betzig and Stefan W Hell for their remarkable contribution in the field of single molecule detection (SMD) and high-resolution microscopic techniques.¹⁷⁻²⁰ Single molecule spectroscopy (SMS) can unravel several dynamical aspects like as conformational fluctuations of a protein in a heterogeneous environment, detecting short-lived intermediates, suggesting suitable mechanisms as per the experimental evidence obtained by examining literally ‘one

molecule' at a time.²¹⁻²⁴ SM measurements are free from the ensemble and time averages and additionally provide tools for the quantification of the static and dynamic changes. When compared to the bulk measures, SM data shows enhanced activity with better spatial and temporal resolutions of the spectral fingerprints of a sample.²⁵ SM experiments are the platforms for clarifying the effects of interactions between the molecular species, dynamics of conformational transitions and many more photo-physical and photochemical aspects, which were once inaccessible using the ensemble measurement techniques.^{26,27}

1.2 Experimental techniques and applied methodology:

SM can be analysed either by observing the fluorescence phenomenon or by applying force microscopic measurements. To refer a few, scanning probe microscopic techniques like the atomic force microscopy (AFM), scanning electron microscopy (SEM), tunnelling electron microscopy (TEM) and many more provide measures for the characterization of sample surfaces using an efficient probe.^{26,28-33} Another, category of structural characterization incorporates the use of optical and magnetic tweezers for trapping the biomolecules of interest and determining changes in the physical and chemical properties as a response to an applied external force. Usually, proteins have stable thermodynamic structures but many proteins exist in their near-native/partially unfolded structures and undergo rapid conformational transitions.^{34,35} The applied force on protein introduces conformational modifications. Using optical trapping techniques, one can study the formation of RNA from a DNA template catalysed by the RNA polymerase and other force pulling experiments.^{36,37} These structural changes facilitate an ongoing biochemical process by ensuring easier accessibility of ligand to the active site of a protein.

SMD techniques based on the fluorescence spectroscopy like fluorescence resonance energy transfer (FRET) employs determination of the structural³⁸ and

thermodynamic properties of different protein conformers.^{26,39,40} This energy transfer depends on the distance between the donor and acceptor moieties present in a bio-molecule. The conformational change from a folded to an unfolded state modifies the intra and inter-molecular distance and hence affects the fluorescence intensity. The confocal fluorescence microscopy enables the SMD of molecules in the solution phase at room temperature. In this microscopy, molecular diffusion in and out of the focal volume leads to fluctuations in the fluorescence intensity. The timescales of conformational interconversions between different protein subpopulations (states) shorter than the residence time inside the confocal volume are tweakable using the viscogenic solvents under controlled experimental measures.^{41,42} It enables the measurement of translational diffusion by combining it with the fluorescence correlation spectroscopy (FCS). The dependence of functional properties of a protein on its state (native, denatured, globular), can be examined using FCS.⁴³⁻⁴⁵ It has several other applications like determining the size and growth of nanoparticles. Therefore, SM measurements and associated analyses are quite advantageous when subjected to chemical, biophysical and biochemical systems. The change in the protein conformation modifies the binding affinity, path selectivity, mechanistic pathways and intermediates. Ensemble averaged solution-phase measurements cannot capture the protein fluctuation dynamics, the coexistence of the structure dependent sub-populations and associated inhomogeneous aspects contributed by the reaction environment in complex multi-step reactions.⁴⁶⁻⁴⁹ There are theoretical studies based on the stochastic description of different states of protein for explaining the long-time tails in experimental observations. These mechanisms either supported discrete transitions between multiple intermediate states to reach the folded conformer or simple two state stochastic model descriptions characterized by the high activation energy barriers.⁵⁰⁻⁵³ Many experiments and theoretical frameworks have shown the existence of correlated events at the SM level.⁵⁴⁻⁵⁶

Analysing a single molecule under specific physiological conditions, one can characterize the spatial and temporal fluctuations in the reaction rates. These data give relevant information related to the mechanism like as the rate-determining step, number of intermediates and the conformational transitions between them, the complete distribution of the experimentally measured reaction times and the correlation between events.⁵⁷⁻⁶⁰ The stochastic fluctuations in biochemical processes reflect kinetic details of the underlying reaction pathways. For example, two biochemical processes may report the same average rates but have different variances (fluctuations about the mean value) that depend on the number, lifetime of intermediates and conformational interconversions between them.

1.3 Conventional enzyme catalysis:

Catalysis received a lot of scientific attention and investigation for centuries. Enzymes are the biocatalysts performing processes at the intra and intercellular level necessary for the sustenance of life like as nerve impulse transmission, transportation of chemical substances, oxidation of biomolecules and many more.⁶¹ For instance, the well-known Michaelis-Menten (MM) mechanism $E + S \rightleftharpoons ES \rightarrow E + P$, describes enzyme kinetics by considering reversible substrate-binding event leading to an enzyme-substrate complex formation.⁶² This complex can either irreversibly dissociate to give the product with the regeneration of free-enzyme or can simply revert to the free enzymatic state without undergoing turnover. The substrate binding, reversion and product formation events are respectively, denoted by the rate constants k_1, k_{-1} and k_2 . Applying the quasi-steady-state approximation (QSSA), the reaction rate shows a hyperbolic substrate dependence indicated by an initial linear rise followed by the saturation at higher substrate concentrations. The Michaelis-Menten constant and maximum rate of reaction can be determined from the curve.

$$v = \frac{k_2[E_0][S]}{[S] + K_M} \quad (1.1)$$

where $[E_0] = [E] + [ES]$ represents the total enzyme concentration, $[S]$ is the substrate concentration and $K_M = \frac{k_{-1}+k_2}{k_1}$, is the Michaelis-Menten constant. Another more efficient way of representing the reaction time for enzymatic reactions is the Line-Weaver-Burke (LWB) plot where one can determine the variation in reaction time against the reciprocal of substrate concentration, which follows a straight-line curve.

$$\frac{1}{v} = \frac{1}{k_2[E_0]} + \frac{K_M}{k_2[E_0][S]} \quad (1.2)$$

In this double reciprocal plot, slope and intercept of the curve directly give the kinetics parameters unlike the velocity versus $[S]$ plot. All these conventional methods employed for studying kinetics at the classical ensemble level, are for a particular enzymatic concentration (number per unit volume). This is why the properties obtained represent an average effect of a certain number of molecules subjected to the same physical-chemical conditions. Consequently, masking individual contributions.

1.4 Analyses at the SM level and fluctuation measurements:

Enzymes are dynamic entities. Owing to the small dynamic range of data obtained from the classical measurements, asynchronous enzyme activities remain hidden. The observation of individual enzyme molecules enables one to capture dynamical aspects inaccessible from the ensemble studies. The probability distribution function (PDF) of the stochastic waiting times, obtained from the long SM trajectories on enzyme β -galactosidase, shows significant deviation from the expected exponential behaviour at higher substrate concentrations.^{63,64} Additionally, the catalytic rate constant attains a distribution rather than a specific value. Single molecule fluorescence resonance energy transfer (FRET) measurements revealed protein conformational changes on a broad range of time scales.⁶⁵ Fluorescence intensity profiles exhibit multiexponentiality because the equilibrium distance between the

donor-acceptor pair fluctuates with the fluorescence lifetime measurements. If these conformational fluctuations are slower or comparable to the timescale of the product formation event, then it will lead to a distribution of the catalytic rate constants. The phenomenon describing these temporal activity fluctuations is termed as dynamic disorder.⁶⁶ As pointed by several studies, fluctuations can be static as well as dynamic in nature depending upon the heterogeneity type.^{58,67-69}

Dynamic disorder varies from the static heterogeneity, usually observed between different molecules exhibiting different molecular activities due to the change in the activation energy barriers and the reaction rate constants. SM studies have shown the memory effects, unusual statistical data attributed to rare events and different reaction timescales confirmed from the autocorrelation functions.^{43,55,70} The inhomogeneity observed in the reaction rates of an individual molecule signifies dynamic disorder. One can employ the rate formalisms and classical Newtonian treatments to probe dynamic disorder characterized by a discrete and continuous random variables, respectively.⁶⁶ For modelling the kinetics of SM reactions, discrete stochastic approaches were formulated which comprised distinct intermediates. A biomolecule traverses the entire continuum of internal states (conformers) before accomplishing the target state (turnover event in case of enzymes), which leads to a distribution of the reaction rates. Studies related to dynamic disorder involved protein structural dynamics explained through the fluctuating bottleneck model.^{71,72} Dynamics of a physical process, involving crossing of a cellular membrane by a biomolecule like RNA, DNA or polypeptide, starting from a specific entry point to reach a defined target are prone to the stochastic fluctuations of the reaction coordinate. These fluctuations regulate the reaction properties like as the residence time, translocation probability and event correlations.^{73,74}

The physics and chemical principles associated with an experimental observation revolve around the fundamental concepts of diffusion of molecular species during the course

of reaction, surface absorption/adsorption of the reactant (promotor/inhibitor/catalyst) and its chemical property, reaction kinetics and catalysis. Catalysts can be homogenous as well as heterogeneous. Unlike enzymes, reactions catalysed by nanoparticles are associated with intrinsic heterogeneity due to the structural dispersions, non-uniform distribution of surface sites and dynamic surface restructuring.⁷⁵ Experiments have shown preference of a particular pathway depending upon the physical conditions, variations in the binding affinities for different NPs and change in the adsorption equilibrium dynamics, which are prone to the spontaneous or catalysis induced surface restructuring.⁷⁶⁻⁷⁸ Thus there is heterogeneity associated with NP catalysed reactions. The autocorrelation functions of the stochastic waiting times indicate the presence of activity fluctuations. The timescales of these fluctuations are different for different NPs. Thus, catalysis associated with stochastic SM systems are susceptible to fluctuations and using statistical treatments one can characterize them.^{79,80}

These fluctuations observed in single molecule measurements can provide insights into the underlying kinetics and hidden intermediates. Such inferences are unobtainable from the average rate measurements. In SM confocal microscopy measurements, a single immobilized enzyme catalyses the conversion of a non-fluorescent reactant to a fluorescent product.^{21,64} The fluorescence burst from product marks the turnover event with the regeneration of the free enzyme. In this way, recording multiple realizations in a definite time window gives a set of data. Actually, experiments yield the waiting times between two consecutive events. From the histogram of occurrences divided into a certain number of time bins, one can obtain the corresponding waiting time distribution. SM data analyses have shown that PDFs of the stochastic waiting times exhibit non-Poissonian behaviour at higher substrate concentrations. Slower conformational fluctuations between different protein states lead to deviation from the mono-exponential behaviour. To address the phenomenon describing the distribution of catalytic rates, scientists extended the simple MM reaction model to a discrete state stochastic

model comprising N number of free and bound enzymatic states where each bound conformer can potentially lead to a turnover.⁶³⁻⁶⁵ Different free and bound enzymatic states are mutually interconverting in a reversible manner. The first moment of PDF gives the mean reaction time for a single product formation. The LWB plot analysis shows linearity even in the presence of temporal fluctuations. Thus, the rate measurements cannot capture the fluctuation characteristics. How to quantify these fluctuations?

The PDF ($f(t)$) contains signatures of the stochastic system. Noise present can be quantified using higher moments of the PDF like as variance, skewness, kurtosis and many other measures of the central tendency.

$$\langle t^n \rangle = \int_0^\infty t^n f(t) dt \quad (1.3)$$

For stochastic model systems, statistical quantities like the Fano factor, Poisson indicator, Mandel's parameter, randomness parameter were calculated which emphasized on exploring the mechanistic details, determination of the statistical nature of data and quantification of the temporal fluctuations.⁸¹⁻⁸³ For example, a widely used measure for characterizing these fluctuations in enzymatic behaviour is the randomness parameter, R, represented as a dimensionless ratio of the variance of PDF to the mean square. It qualitatively predicts the shape of the catalytic time distribution and indicates multiple competing reaction timescales.

$$R = \frac{\langle t^2 \rangle - \langle t \rangle^2}{\langle t \rangle^2} \quad (1.4)$$

Here t is the time between two consecutive turnover events.

If a distribution shows a mono-exponential behavior then a single rate-determining step dominates the reaction. The numerical value of R will be unity in this case. If a kinetic process has multiple rate-determining steps (dynamic disorder) then the distribution profile becomes non-exponential and R deviates from unity. In the context of single enzyme reactions, at low

and high substrate concentrations, the substrate binding and product formation event become the rate-determining step, respectively. Thus in these scenarios, the value of R saturates to unity. At intermediate substrate concentrations, multiple transitions from the bound enzymatic states lead to significant deviation in the value of R from unity.⁶³⁻⁶⁵ If the PDF has a peak followed by a decay, then the randomness parameter will be less than one. On the other hand, if the distribution has long multi-exponential tails, the randomness parameter's magnitude would exceed from unity due to higher dispersions. For simple exponentially distributed functions, the randomness parameter equates to one. Thus, this parameter allows one to predict the shape of the catalytic time distribution. Earlier studies have confirmed that the numerical value of R also provides information about the number of steps (intermediates) present in a stochastic system.⁸⁴⁻⁸⁶ Any deviation in the value of R from unity is a manifestation of dynamic disorder. Another common statistical parameter, widely used to quantify fluctuations associated with the flux production from the stochastic networks is the Fano factor.⁸⁷ Its functional form is

$$F = \frac{\langle n^2 \rangle - \langle n \rangle^2}{\langle n \rangle}. \quad (1.5)$$

Here ' n ' represents the number of molecules produced (flux) during a definite course of reaction. For example, in the context of molecular motors, one can measure the physical distance moved by the motor to obtain the number of products in a given time window. On the similar grounds, computing a parameter called as the Poisson indicator can mark the statistical behavior of data as Poissonian or non-Poissonian. Its mathematical representation is as follows

$$P = \frac{\langle t^2 \rangle - 2 \langle t \rangle^2}{\langle t \rangle^2}. \quad (1.6)$$

If the numerical value of P is zero, then the expectation value of the distribution will be equal to the variance.⁸² Any other value corresponds to multiple competing reaction timescales.

Thus, fluctuation analysis is a valuable tool for the characterization of SM kinetics. The implementation of a statistical approach adopted for obtaining the distribution of the reaction completion times for a complex scheme incorporating different reactions pathways, can be challenging. Using appropriate analytical methods one can determine the dependence of the statistical quantities on input kinetic parameters. For example, analytical solutions can be especially good for the examination of limiting cases where a single event governs the reaction.

To date, many analytical approaches have had been developed to find the distribution of reaction times. In this thesis, we describe theoretical frameworks employed to obtain PDFs of the stochastic model systems related to enzyme and NP catalyses at the SM level.^{63,79} As discussed in the former paragraphs, we focus on obtaining the analytical expression of the PDF. The mean reaction time, randomness parameter or any other statistical quantities of interest are derivable from the moments of PDF. We have used two approaches to model the reaction kinetics at the SM level, namely, the first passage-time distribution formalism and the waiting-time distribution formalism.

1.5 Theoretical formalisms for constructing the PDF:

1.5.1 The first-passage time distribution formalism:

A catalyst accelerates the rate of a reaction by providing an alternative path for its completion with a lower activation energy requirement. It does not alter the position of equilibrium. After one turnover, the enzymatic concentration (or number) remains the same and this will lead to the commencement of the next cycle. The probability distribution function is a fundamental quantity to measure in any renewal process.

To understand how to formulate the first-passage time distribution function, let us consider a discrete state stochastic model comprising an arbitrary finite number of internal states, n .



Figure 1: Schematic representing a discrete state stochastic model.

One state can reversibly interconvert to its adjacent state. An irreversible step characterizes reaching the final state from the last but one state.⁸² This step in modelling is equivalent to fluorescence product formation. The first passage time distribution function represents PDF for reaching the n^{th} state at time t for the first time, provided the process began from the zeroth state. It is possible for the process to start and reach the target state successfully in one ultimate go without any reversions. However, reversions are probable to happen from any of the existing intermediates. In these scenarios, the process will begin again to accomplish the monitored event i.e. reaching the target state. In this manner, the process continues reaching the n^{th} state at once or by reverting-back to the starting state for once, twice, thrice and so on. The distribution of these stochastic times gives the first passage time distribution.

$$\begin{aligned} \hat{f}(s) = & \hat{Q}_{1 \rightarrow n}(s) + \hat{Q}_{1 \rightarrow 1}(s)\hat{Q}_{1 \rightarrow n}(s) + \left(\hat{Q}_{1 \rightarrow 1}(s)\right)^2 \hat{Q}_{1 \rightarrow n}(s) + \left(\hat{Q}_{1 \rightarrow 1}(s)\right)^3 \hat{Q}_{1 \rightarrow n}(s) \\ & + \dots \left(\hat{Q}_{1 \rightarrow 1}(s)\right)^n \hat{Q}_{1 \rightarrow n}(s) \end{aligned} \quad (1.7)$$

Performing some mathematical modifications leads to

$$\begin{aligned} \hat{f}(s) = & \hat{Q}_{1 \rightarrow n}(s) \left(1 + (-1) \frac{\left(-\hat{Q}_{1 \rightarrow 1}(s)\right)}{1!} + (-1)(-1-1) \frac{\left(-\hat{Q}_{1 \rightarrow 1}(s)\right)^2}{2!} \right. \\ & \left. + (-1)(-1-1)(-1-2) \frac{\left(-\hat{Q}_{1 \rightarrow 1}(s)\right)^3}{3!} + \dots n! \frac{\left(-\hat{Q}_{1 \rightarrow 1}(s)\right)^n}{n!} \right). \end{aligned} \quad (1.8)$$

Further, rearranging in the form of a binomial series we get

$$\hat{f}(s) = \frac{\hat{Q}_{1 \rightarrow n}(s)}{1 - \hat{Q}_{1 \rightarrow 1}(s)}. \quad (1.9)$$

Here $\hat{f}(s)$ is the Laplace transform of $f(t)$; $\hat{f}(s) = \int_0^\infty e^{-s t} f(t) dt$.

$\hat{Q}_{1 \rightarrow n}(s)$ represents the convoluted waiting probabilities for the monitored event and $\hat{Q}_{1 \rightarrow 1}(s)$ corresponds to the probability per unit for the unmonitored transitions. For the simple MM reaction, where the free enzyme state E forms the product P via the enzyme-substrate complex ES , it is probable that ES complex reverts to E without leading to an enzymatic turnover event. The first passage time distribution will have the following functional form

$$\hat{f}(s) = \frac{\hat{Q}_{E \rightarrow ES}(s) \hat{Q}_{ES \rightarrow P}(s)}{1 - \hat{Q}_{E \rightarrow ES}(s) \hat{Q}_{ES \rightarrow E}(s)}. \quad (1.10)$$

Here the substrate-binding event is the only transition dependent on $[S]$, represented as an exponentially distributed function, $Q_{E \rightarrow ES}(t) = k_1 [S] e^{-k_1 [S] t}$. The catalytic step and reversions are independent of $[S]$ and their explicit forms are not important. From the moment generation formula, we can find out the mean reaction time and higher moments of the first passage time distribution to quantify the temporal fluctuations.

$$\langle t^n \rangle = (-1)^n \left(\frac{\partial^n \hat{f}(s)}{\partial s^n} \right)_{s=0} \quad (1.11)$$

As discussed earlier, similar systems can show the same substrate dependence in the mean reaction time.^{81,82} Variance calculation can give information about the internal kinetic states and temporal fluctuations in different systems. This was our first approach of deriving PDF of the stochastic processes. Next, we describe another framework to formulate the distributions.

1.5.2 The waiting-time distribution formalism:

SM fluorescence microscopy measurements record the waiting time between two consecutive turnover events. To understand and apply the waiting formalism theoretically, we need to

construct the chemical master equation (CME) which represents the time evolution of the joint probability distribution. This distribution incorporates the change in the number of all species present in a reaction system.

Consider a simple reversible reaction, where X transforms to Y ; $X \rightleftharpoons Y$. Rate constants k_f and k_b , respectively characterize the forward and backward transitions. The forward step will lead to decrement in the number of X units by unity ($x \rightarrow x - 1$) and the backward transition corresponds to one unit increment ($x \rightarrow x + 1$). For simplicity and understanding purposes, consider changes in X only. For determining the probability of finding a certain number of X (x) at some higher time ($t + dt$), provided there were already some numbers of X (x') at a prior time (t'), one needs to consider probabilities of all possible stochastic transitions.⁸⁸

$$\begin{aligned}
 P[x, t + dt | x', t'] &= t^-(x + 1) dt P[x + 1, t | x', t'] + t^+(x - 1) dt P[x - 1, t | x', t'] \\
 &+ \{1 - (t^+(x) + t^-(x)) dt\} P[x, t | x', t']
 \end{aligned}
 \tag{1.12}$$

In the above equation, the first term represents the probability of decrement in x by one unit, associated with decomposition transition probability per unit time ($t^-(x + 1)$). The second term corresponds to increment in x by unity, involving the formation transition probability ($t^+(x - 1)$) and the third term describes the probability of not undergoing any such transition. Further, simplification using the First Principle gives

$$\begin{aligned}
 \frac{dP[x, t | x', t']}{dt} &= t^-(x + 1) P[x + 1, t | x', t'] + t^+(x - 1) P[x - 1, t | x', t'] \\
 &- (t^+(x) + t^-(x)) P[x, t | x', t'].
 \end{aligned}
 \tag{1.13}$$

The rate of change in the probability density represents its evolution in the forward time. Thus, the name forward chemical master equation. Following the similar rational, one can also construct the equivalent backward CME.

The CME for the MM model, $E + S \rightleftharpoons ES \rightarrow E^{(0)} + P$; $E^{(0)} \rightarrow E$ can be written as

$$\begin{aligned}
& \frac{\partial P[n_E, n_{ES}, n_{E^{(0)}}, n_P; t]}{\partial t} \\
&= \left[k_1[S](n_E + 1)Y_{n_E}Y_{n_{ES}}^- + k_{-1}(n_{ES} + 1)Y_{n_E}^-Y_{n_{ES}} \right. \\
&+ k_2(n_{ES} + 1)Y_{n_{ES}}Y_{n_{E^{(0)}}}^- Y_{n_P}^- \\
&\left. - \{k_1[S]n_E + (k_{-1} + k_2)n_{ES}\} \right] P[n_E, n_{ES}, n_{E^{(0)}}, n_P; t]
\end{aligned} \tag{1.14}$$

Rate constants k_1 , k_{-1} and k_2 characterize the substrate binding, reversion and product formation events, respectively. Kinetic rate constant δ_0 represents the instantaneous step leading to regeneration of the free enzyme ($E^{(0)} \rightarrow E$). The step operator Y relates the change in the number of species involved in a particular step.⁸⁹ For example, $Y_{n_E}Y_{n_{ES}}^-P[n_E, n_{ES}, n_{E^{(0)}}, n_P; t]$ gives $P[n_E + 1, n_{ES} - 1, n_{E^{(0)}}, n_P; t]$.

The above equation holds only under the substrate abundance assumption. Thus, the joint probability distribution does not reflect any change in the substrate number. Owing to the mutual exclusivity of different enzymatic states i.e. at a particular instant of time, the enzyme would exist in a particular conformer. CME reduces to a set of ordinary differential equations.

$$\frac{\partial P_E(t)}{\partial t} = -k_1[S]P_E(t) + k_{-1}P_{ES}(t) + \delta_0P_{E^{(0)}}(t) \tag{1.15.a}$$

$$\frac{\partial P_{ES}(t)}{\partial t} = k_1[S]P_E(t) - (k_{-1} + k_2)P_{ES}(t) \tag{1.15.b}$$

$$\frac{\partial P_{E^{(0)}}(t)}{\partial t} = k_2 P_{ES}(t) - \delta_0 P_{E^{(0)}}(t) \quad (1.15.c)$$

The instantaneous step associated with the free enzyme regeneration is very fast ($\delta_0 \rightarrow \infty$).

Thus, $\frac{\partial P_{E^{(0)}}(t)}{\partial t} \approx 0$. The corresponding waiting time distribution function, $f(t)$ represents the rate of change in the probability density of the product state.⁹⁰

$$f(t) = \frac{\partial P_P(t)}{\partial t} = k_2 P_{ES}(t) \quad (1.16)$$

To obtain the required PDF, one needs to solve these differential equations by taking their Laplace transforms ($\hat{f}(s) = \int_0^\infty e^{-s t} f(t) dt$).

$$(s + k_1[S])\hat{P}_E(s) - k_{-1}\hat{P}_{ES}(s) - \delta_0\hat{P}_{E^{(0)}}(s) = 1 \quad (1.17.a)$$

$$-k_1[S]\hat{P}_E(s) - (s + k_{-1} + k_2)\hat{P}_{ES}(s) = 0 \quad (1.17.b)$$

$$s\hat{P}_{E^{(0)}}(s) = 1 \quad (1.17.c)$$

Further, the application of appropriate initial conditions and normalization constraints would yield the probability density of each state. At the beginning of the reaction, the enzyme would be exclusively present as E because neither the product nor bound-enzymatic state would exist. At any time, the sum of these probability densities should always be unity.

$$P_E(0) = 1, P_{ES}(0) = 0, P_{E^{(0)}}(0) = 0, P_P(0) = 0 \quad (1.18)$$

$$P_E(t) + P_{ES}(t) + P_{E^{(0)}}(t) = 1 \quad (1.19)$$

Arranging in the form of a matrix we get

$$\begin{bmatrix} s + k_1[S] & -k_{-1} & -\delta_0 \\ -k_1[S] & (s + k_{-1} + k_2) & 0 \\ 0 & 0 & s \end{bmatrix} \begin{bmatrix} \hat{P}_E(s) \\ \hat{P}_{ES}(s) \\ \hat{P}_{E^{(0)}}(s) \end{bmatrix} = \begin{bmatrix} 1 \\ 0 \\ 0 \end{bmatrix} \quad (1.20)$$

Further, taking the inverse and performing the matrix multiplication one can obtain

$$\begin{bmatrix} \hat{P}_E(s) \\ \hat{P}_{ES}(s) \\ \hat{P}_{E^{(0)}}(s) \end{bmatrix} = \begin{bmatrix} \frac{k_{-1}+k_2+s}{k_{-1}s+(k_2+s)(s+k_1[S])} \\ \frac{k_1[S]}{k_{-1}s+(k_2+s)(s+k_1[S])} \\ 0 \end{bmatrix}. \quad (1.21)$$

Using the probability density of the bound enzymatic state, we obtain PDF for the turnover event.

$$\hat{f}(s) = k_2 * \hat{P}_{ES}(s) = \frac{k_1 k_2 [S]}{k_{-1}s+(k_2+s)(s+k_1[S])} \quad (1.22)$$

In this way, one can derive the waiting time distribution for a catalytic system by constructing the CME, fragmenting it to obtain the rate of change in density of respective states and solving the coupled differential equations using the initial and normalization conditions.

16.1 Thesis chapters in brief:

This thesis covers some applications of the first-passage time distribution formalism and the waiting-time distribution formalism on enzyme and NP catalytic systems with varying number of internal states (discrete) and interconversions at the SM level. Stochastic processes can also be modelled using continuous modelling methods. We have developed a theoretical method to derive the PDF of time taken by a molecule in crossing a barrier (the transit time distribution) using a generalized Langevin Equation (GLE) comprising different force components. The obtainable PDFs provide us a measure of significant statistical quantities for characterizing the systems, providing molecular mechanistic details and capturing stochastic behaviour inaccessible from ensemble rate measurements. The succeeding sections comprise respective thesis chapters, briefed below.

Chapter 2:

Experiments have already shown that the temporal effects like as the distribution of catalytic rates, molecular memory and correlation between the stochastic events attributed to the

conformational fluctuations in SM reaction systems.^{23,36,63,65,68,69} To understand such fluctuations from a theoretical point of view, several discrete state models consisting of many free and bound enzymatic conformers were constructed. We wanted to build up some minimal models, which are capable of capturing these experimental observations. Using the first-passage time distribution formalism, we examined the effect of different types of enzymatic interconversions between the free and bound states. We have studied the statistical properties of a fluctuating enzyme existing in multiple conformers, exhibiting dynamic cooperativity and dynamic disorder due to many competing reaction timescales.

Chapter 3:

The reaction rate studies usually involve the change in the rate of product formation with respect to the binding rate or in terms of the catalytic rate constant. If one examines the classical turnover expression obtained under the QSSA, it is quite evident that with an increase in the magnitude of unbinding rate, the velocity decreases. Study based on mathematical arguments and analytical reasoning, confirms that the turnover rate can show an occasional rise with the unbinding rate, which was restricted to some prerequisite conditions.⁹¹ Further modifications in the mechanistic models, involved incorporation of the bound-enzyme conformational dynamics. It also led to the reaction-rate acceleration effect pertaining to certain limits.⁹²

In the previous model, owing to the conformational equilibrium between the free-enzymatic states, there is a single free state. It had has been reported that free-enzyme fluctuations lead to the dynamic cooperative effect. We modified the existing mechanisms by incorporating the free-enzyme interconversions along with the substrate-bound fluctuations and formulated the CME for different reaction models. In general, the reaction rate decreases monotonically with the unbinding rate. The conditional non-monotonicity is obtainable under

special limits corresponding to a particular parameter space, which shows an initial rate enhancement followed by a maximum value and ultimately, a gradual fall.

Chapter 4:

Previous chapters dealt with the SM enzyme kinetics in the presence of a single type of substrate. There are several reactions in the organic Chemistry involving binding with multiple substrates. For these mechanisms, along with the binding site, the sequence of binding also governs the reaction kinetics. Based on the binding sequence, they have been classified into two categories, namely, the sequential and non-sequential binding mechanisms.⁹³ The deterministic treatments cannot differentiate between these mechanisms as the functional form of the velocity shows similar substrate dependence. Using a stochastic approach for determining the mean reaction time and other statistical quantities to characterize multiple-substrate binding models, one can mark the clear distinction. We apply the waiting-time distribution formalism to obtain the PDF for the turnover event and quantify the fluctuations present in the multi-substrate binding reactions occurring at the SM level.

Chapter 5:

In the classical chemical kinetics, the substrate concentration is significantly greater than that of the enzyme catalysing the reaction. Even in the SM enzyme catalysed reactions, the substrate concentration is quasi-statically fixed. This is equivalent to experiments where one monitors the turnover event during the initial transient phase of the reaction. However, for intracellular compartment reactions, the substrate abundance assumption breaks down due to the comparable concentrations of the substrate and enzyme involved.^{94,95} To model the kinetics of intracellular reactions constituting irreversible or bidirectional substrate flow, we incorporated the substrate number fluctuations in the CME. For different systems comprising a varying number of intermediates, we deduced the velocity under the SSA, which shows a non-MM

behaviour and calculated the coefficient of variation (CV) representing fluctuations in the substrate numbers. The noise present in such systems depend on its internal states and the associated steady substrate flow.

Chapter 6:

Enzymes perform several vital functions necessary for the sustenance of life. ERK II is a mitogen-activated protein kinase enzyme involved in the extracellular cell signalling pathways and phosphorylation of the targeted substrate molecules.⁹⁶ Many experimental and theoretical studies have shed light on its mechanism.⁹⁷ Recent experimental data have shown an enhanced enzymatic activity due to some mutations in the docking sites.⁹⁸ For theoretically modelling this effect, a network comprising three coupled MM pathways was analysed where the mean time followed the MM law.⁹⁹

We wanted to investigate the temporal fluctuations present in such phosphorylation and de-phosphorylation networks by incorporating more internal states and associated transitions in the mechanism. Using the waiting-time distribution formalism, one can also examine the effect of activity or inactivity of an intermediate. The rate-determining step changes under different physical scenarios depending on the concentration of species involved. We have studied randomness present in different networks as a function of the substrate concentration for different values of the activator and deactivator concentrations.

Chapter 7:

All of the above thesis chapters based on SM enzyme catalysis with one/multiple substrate types, with/without the substrate number fluctuations, deal with homogenous catalysis. On the contrary, nanoparticles (NPs) are intrinsically heterogeneous and show the temporal fluctuations in the rates.^{75,77,100} As observed from the single molecule experiments, a catalytic cycle constitutes an off and an on event, respectively representing the fluorescent product

formation and dissociation processes. Based on these experimental observations, the proposed mechanism (modified MM) consisted of two product dissociation pathways. Theoretical studies have quantified the temporal fluctuations in the activity of NPs.^{79,80}

Experiments have also shown the size-dependent metal NP catalysis.⁷⁶ An increase in NP's dimension enhanced the reaction rates for the fluorescent product formation and dissociation events. The effect of size on several physical properties like as the binding affinity, adsorption equilibrium constants, fractional-coverage of the active sites, spontaneous and induced surface restructuring, was illustrated. We wanted to examine the size-dependent catalysis theoretically by including the effects from all sites. Using a stochastic approach based on the superposition of renewal processes, we could obtain the first-passage time distribution for the off and on events with a certain number of sites. The size of a NP is directly proportional to the number of active sites. This was the rationale behind the applied concept. From the moments of the PDF, we obtained the exact analytical expression for the mean time and randomness parameter.

Chapter 8:

NPs have a multitude of surface sites on which chemical reactions occur simultaneously. In the previous theoretical model, the PDF for a system with a given number of catalytic sites depends on the distribution of one site, corresponding to the respective off and on events. The methodology applied involves recording the statistical output from a pool of events. Considering the realistic picture of heterogeneous catalysis with an aim of capturing stochasticity, one needs to establish a connection between the experimentally measured time between the two consecutive product formation events and the corresponding distribution of time obtained from the analytical methods.^{75,77}

To model such heterogeneous systems with multitude of active sites, one must focus on the mechanistic details of the chemical reaction. We construct a model comprising N number of

independent identical catalytic sites. These reactions can have an arbitrary number of intermediates and for the product formation to happen from multiple sites, the system will be in a particular bound state. Here we apply the first-passage time distribution formalism to determine the PDF for an event to happen from any possible site. The statistical measurements successfully captured the stochastic effects, which depend on the mechanism.

Chapter 9:

In our previous thesis chapters, we have implemented different discrete state stochastic approaches for determining the statistical quantities related to the catalytic reaction networks at the SM level. The PDF constructed for various model systems emphasized on the occurrence of a particular event (reaching a definite state for the first time; marking the monitored transition). This gives the first-passage distribution. We have also employed the waiting-time distribution formalism to determine the catalytic turnover time distribution by taking into consideration the change in the number of different species participating in a reaction.

Apart from these approaches, one can also implement the continuous modelling methods to obtain the PDF. The methodology involves the use of a generalized Langevin equation (GLE), which comprises different forces subjected on a particle crossing a barrier.^{101,102} By examining the change in the position of the reaction co-ordinate of the system, one can model its dynamics. From this GLE, we can obtain the corresponding Fokker Planck equation (FPE), whose solution gives the required PDF (the first-passage time distribution). With advancements in the SM techniques, one can explicitly measure the time taken by a molecule in crossing a biological pore. This only takes into account the successful trajectories and gives the corresponding transit time distribution (TTD).^{103,104} Previous theoretical studies covered Markovian systems with/without the inertial effect.^{105,106} However, studies related to protein folding-unfolding dynamics and conformational rearrangements have shown anomalous diffusion.^{41,107} There are studies describing the dynamics of non-Markovian

systems in the overdamped limit.^{108,109} It is important to include the inertial contribution along with the memory effect. In this chapter, we describe a theoretical method for deriving the TTD for a particle crossing an inverted parabolic potential, subjected to a frictional force associated with a power-law memory kernel, and a correlated random force (coloured noise).

All these theoretical investigations and numerical analyses provide platforms for a better understanding of biochemical/biophysical processes.

1.6 References:

- (1) Moerner, W. E. *J. Phys. Chem. B* **2002**, *106*, 910.
- (2) Nath, A.; Koo, P. K.; Rhoades, E.; Atkins, W. M. *J. Am. Chem. Soc.* **2008**, *130*, 15746.
- (3) Bagh, S.; Paige, M. F. *J. Phys. Chem. A* **2006**, *110*, 7057.
- (4) Terentyeva, T. G.; Hofkens, J.; Komatsuzaki, T.; Blank, K.; Li, C.-B. *J. Phys. Chem. B* **2013**, *117*, 1252.
- (5) Tamarat, P.; Maali, A.; Lounis, B.; Orrit, M. *J. Phys. Chem. A* **2000**, *104*, 1.
- (6) de Vries, H.; Wiersma, D. A. *J. Chem. Phys.* **1980**, *72*, 1851.
- (7) Orłowski, T. E.; Zewail, A. H. *J. Chem. Phys.* **1979**, *70*, 1390.
- (8) Kondo, T.; Chen, W. J.; Schlau-Cohen, G. S. *Chem. Rev.* **2017**, *117*, 860.
- (9) Ambrose, W. P.; Basché, T.; Moerner, W. E. *J. Chem. Phys.* **1991**, *95*, 7150.
- (10) Bjorklund, G. C.; Levenson, M. D.; Lenth, W.; Ortiz, C. *Appl. Phys. B* **1983**, *32*, 145.
- (11) Güttler, F.; Irgartinger, T.; Plakhotnik, T.; Renn, A.; Wild, U. P. *Chem. Phys. Lett.* **1994**, *217*, 393.
- (12) Kummer, S.; Basché, T.; Bräuchle, C. *Chem. Phys. Lett.* **1995**, *232*, 414.
- (13) Kummer, S.; Kulzer, F.; Kettner, R.; Basché, T.; Tietz, C.; Glowatz, C.; Kryschi, C. *J. Chem. Phys.* **1997**, *107*, 7673.
- (14) Moerner, W. E.; Kador, L. *Phys. Rev. Lett.* **1989**, *62*, 2535.
- (15) Moerner, W. E.; Lenth, W.; Bjorklund, G. C. In *Persistent Spectral Hole-Burning: Science and Applications*; Moerner, W. E., Ed.; Springer Berlin Heidelberg: Berlin, Heidelberg, 1988, p 251.
- (16) Orrit, M.; Bernard, J. *Phys. Rev. Lett.* **1990**, *65*, 2716.
- (17) Betzig, E.; Chichester, R. J. *Science* **1993**, *262*, 1422.
- (18) Betzig, E.; Lewis, A.; Harootunian, A.; Isaacson, M.; Kratschmer, E. *Biophys J* **1986**, *49*, 269.
- (19) Betzig, E.; Trautman, J. K.; Harris, T. D.; Weiner, J. S.; Kostelak, R. L. *Science* **1991**, *251*, 1468.
- (20) Hell, S. W.; Wichmann, J. *Opt. Lett.* **1994**, *19*, 780.
- (21) Michalet, X.; Weiss, S.; Jäger, M. *Chem. Rev.* **2006**, *106*, 1785.
- (22) Nie, S.; Zare, R. N. *Annu. Rev. Biophys. Biomol. Struct.* **1997**, *26*, 567.
- (23) Tinnefeld, P.; Sauer, M. *Angew. Chem., Int. Ed.* **2005**, *44*, 2642.
- (24) Xie, X. S.; Trautman, J. K. *Annu. Rev. Phys. Chem.* **1998**, *49*, 441.
- (25) Martyn, T. A.; Moore, J. L.; Halterman, R. L.; Yip, W. T. *J. Am. Chem. Soc.* **2007**, *129*, 10338.
- (26) He, Y.; Lu, M.; Cao, J.; Lu, H. P. *ACS Nano* **2012**, *6*, 1221.
- (27) Zhang, J.; Campbell, R. E.; Ting, A. Y.; Tsien, R. Y. *Nat. Rev. Mol. Cell Biol.* **2002**, *3*, 906.
- (28) Cyr, D. M.; Venkataraman, B.; Flynn, G. W. *Chem. Mater.* **1996**, *8*, 1600.

- (29) Han, B.; Nia, H. T.; Wang, C.; Chandrasekaran, P.; Li, Q.; Chery, D. R.; Li, H.; Grodzinsky, A. J.; Han, L. *ACS Biomater. Sci Eng.* **2017**, *3*, 2033.
- (30) Liljeroth, P.; Swart, I.; Paavilainen, S.; Repp, J.; Meyer, G. *Nano Lett.* **2010**, *10*, 2475.
- (31) Shapir, E.; Sagiv, L.; Borovok, N.; Molotski, T.; Kotlyar, A. B.; Porath, D. *J. Phys. Chem. B* **2008**, *112*, 9267.
- (32) Velegol, S. B.; Pardi, S.; Li, X.; Velegol, D.; Logan, B. E. *Langmuir* **2003**, *19*, 851.
- (33) Lee, G.; Abdi, K.; Jiang, Y.; Michaely, P.; Bennett, V.; Marszalek, P. E. *Nature* **2006**, *440*, 246.
- (34) Nettels, D.; Müller-Späth, S.; Küster, F.; Hofmann, H.; Haenni, D.; Rügger, S.; Reymond, L.; Hoffmann, A.; Kubelka, J.; Heinz, B.; Gast, K.; Best, R. B.; Schuler, B. *Proc. Natl. Acad. Sci. U.S.A.* **2009**, *106*, 20740.
- (35) Solanki, A.; Neupane, K.; Woodside, M. T. *Phys. Rev. Lett.* **2014**, *112*, 158103.
- (36) Abbondanzieri, E. A.; Greenleaf, W. J.; Shaevitz, J. W.; Landick, R.; Block, S. M. *Nature* **2005**, *438*, 460.
- (37) Cecconi, C.; Shank, E. A.; Bustamante, C.; Marqusee, S. *Science* **2005**, *309*, 2057.
- (38) Groll, J.; Amirgoulova, E. V.; Ameringer, T.; Heyes, C. D.; Röcker, C.; Nienhaus, G. U.; Möller, M. J. *Am. Chem. Soc.* **2004**, *126*, 4234.
- (39) Cornish, P. V.; Ha, T. *ACS Chem. Biol.* **2007**, *2*, 53.
- (40) Seelig, J.; Leslie, K.; Renn, A.; Kühn, S.; Jacobsen, V.; van de Corput, M.; Wyman, C.; Sandoghdar, V. *Nano Lett.* **2007**, *7*, 685.
- (41) Ladurner, A. G.; Fersht, A. R. *Nat. Struct. Biol.* **1999**, *6*, 28.
- (42) Jacob, M.; Schindler, T.; Balbach, J.; Schmid, F. X. *Proc. Natl. Acad. Sci. U.S.A.* **1997**, *94*, 5622.
- (43) Ambrose, W. P.; Goodwin, P. M.; Jett, J. H.; Van Orden, A.; Werner, J. H.; Keller, R. A. *Chem. Rev.* **1999**, *99*, 2929.
- (44) Mohraz, A.; Solomon, M. J. *Langmuir* **2005**, *21*, 5298.
- (45) Wilkerson, C. W.; Goodwin, P. M.; Ambrose, W. P.; Martin, J. C.; Keller, R. A. *Appl. Phys. Lett.* **1993**, *62*, 2030.
- (46) Schuler, B.; Lipman, E. A.; Eaton, W. A. *Nature* **2002**, *419*, 743.
- (47) Gopich, I. V.; Szabo, A. J. *Chem. Phys.* **2006**, *124*, 154712.
- (48) Chirico, G.; Cannone, F.; Beretta, S.; Diaspro, A.; Campanini, B.; Bettati, S.; Ruotolo, R.; Mozzarelli, A. *Protein Sci* **2002**, *11*, 1152.
- (49) Dickson, R. M.; Norris, D. J.; Tzeng, Y.-L.; Moerner, W. E. *Science* **1996**, *274*, 966.
- (50) Garcia-Mira, M. M.; Sadqi, M.; Fischer, N.; Sanchez-Ruiz, J. M.; Muñoz, V. *Science* **2002**, *298*, 2191.
- (51) Yang, H.; Luo, G.; Karnchanaphanurach, P.; Louie, T.-M.; Rech, I.; Cova, S.; Xun, L.; Xie, X. S. *Science* **2003**, *302*, 262.
- (52) Jackson, S. E. *Fold. Des.* **1998**, *3*, R81.
- (53) Alexander, P.; Fahnestock, S.; Lee, T.; Orban, J.; Bryan, P. *Biochemistry* **1992**, *31*, 3597.
- (54) Craig, D. B.; Arriaga, E. A.; Wong, J. C. Y.; Lu, H.; Dovichi, N. J. *J. Am. Chem. Soc.* **1996**, *118*, 5245.
- (55) Edman, L.; Rigler, R. *Proc. Natl. Acad. Sci. U.S.A.* **2000**, *97*, 8266.
- (56) Xue, Q.; Yeung, E. S. *Nature* **1995**, *373*, 681.
- (57) Svoboda, K.; Mitra, P. P.; Block, S. M. *Proc. Natl. Acad. Sci. U.S.A.* **1994**, *91*, 11782.
- (58) van Oijen, A. M.; Blainey, P. C.; Crampton, D. J.; Richardson, C. C.; Ellenberger, T.; Xie, X. S. *Science* **2003**, *301*, 1235.
- (59) Eizenberg, N.; Klafter, J. *J. Chem. Phys.* **1996**, *104*, 6796.
- (60) Sebastian, K. L. *J. Chem. Phys.* **2019**, *151*, 025101.
- (61) Segel, I. H. *Enzyme kinetics: behavior and analysis of rapid equilibrium and steady state enzyme systems*; Wiley New York, 1975; Vol. 115.
- (62) Johnson, K. A.; Goody, R. S. *Biochemistry* **2011**, *50*, 8264.

- (63) Min, W.; English, B. P.; Luo, G.; Cherayil, B. J.; Kou, S. C.; Xie, X. S. *Acc. Chem. Res.* **2005**, *38*, 923.
- (64) English, B. P.; Min, W.; van Oijen, A. M.; Lee, K. T.; Luo, G.; Sun, H.; Cherayil, B. J.; Kou, S. C.; Xie, X. S. *Nat. Chem. Biol.* **2006**, *2*, 87.
- (65) Min, W.; Luo, G.; Cherayil, B. J.; Kou, S. C.; Xie, X. S. *Phys. Rev. Lett.* **2005**, *94*, 198302.
- (66) Zwanzig, R. *Acc. Chem. Res.* **1990**, *23*, 148.
- (67) Zhuang, X.; Kim, H.; Pereira, M. J. B.; Babcock, H. P.; Walter, N. G.; Chu, S. *Science* **2002**, *296*, 1473.
- (68) Velonia, K.; Flomenbom, O.; Loos, D.; Masuo, S.; Cotlet, M.; Engelborghs, Y.; Hofkens, J.; Rowan, A. E.; Klafter, J.; Nolte, R. J. M.; de Schryver, F. C. *Angew. Chem. Int. Ed.* **2005**, *44*, 560.
- (69) Flomenbom, O.; Velonia, K.; Loos, D.; Masuo, S.; Cotlet, M.; Engelborghs, Y.; Hofkens, J.; Rowan, A. E.; Nolte, R. J. M.; Van der Auweraer, M.; de Schryver, F. C.; Klafter, J. *Proc. Natl. Acad. Sci. U.S.A.* **2005**, *102*, 2368.
- (70) Lu, H. P.; Xun, L.; Xie, X. S. *Science* **1998**, *282*, 1877.
- (71) Zwanzig, R. *J. Chem. Phys.* **1992**, *97*, 3587.
- (72) Robertson, J. W. F.; Kasianowicz, J. J.; Reiner, J. E. *J. Phys.: Condens. Matter* **2010**, *22*, 454108.
- (73) Bian, Y.; Wang, Z.; Chen, A.; Zhao, N. *J. Chem. Phys.* **2015**, *143*, 184908.
- (74) Chatterjee, D.; Cherayil, B. J. *J. Chem. Phys.* **2010**, *132*, 025103.
- (75) Xu, W.; Kong, J. S.; Yeh, Y.-T. E.; Chen, P. *Nat. Mater.* **2008**, *7*, 992.
- (76) Zhou, X.; Xu, W.; Liu, G.; Panda, D.; Chen, P. *J. Am. Chem. Soc.* **2010**, *132*, 138.
- (77) Xu, W.; Shen, H.; Liu, G.; Chen, P. *Nano Research* **2009**, *2*, 911.
- (78) Chen, T.; Zhang, Y.; Xu, W. *J. Am. Chem. Soc.* **2016**, *138*, 12414.
- (79) Xu, W.; Kong, J. S.; Chen, P. *J. Phys. Chem. C* **2009**, *113*, 2393.
- (80) Das, A.; Chaudhury, S. *Chem. Phys. Lett.* **2015**, *641*, 193.
- (81) Chaudhury, S.; Cao, J.; Sinitsyn, N. A. *J. Phys. Chem. B* **2013**, *117*, 503.
- (82) Chaudhury, S. *J. Phys. Chem. B* **2014**, *118*, 10405.
- (83) Li, X.; Kolomeisky, A. B. *J. Chem. Phys.* **2013**, *139*, 144106.
- (84) Kou, S. C.; Cherayil, B. J.; Min, W.; English, B. P.; Xie, X. S. *J. Phys. Chem. B* **2005**, *109*, 19068.
- (85) Moffitt, J. R.; Bustamante, C. *FEBS J.* **2014**, *281*, 498.
- (86) Floyd, D. L.; Harrison, S. C.; van Oijen, A. M. *Biophys J* **2010**, *99*, 360.
- (87) Barato, A. C.; Seifert, U. *J. Phys. Chem. B* **2015**, *119*, 6555.
- (88) Gardiner, C. W. *Handbook of stochastic methods : for the natural and social sciences*; Springer: Berlin; London, 2009.
- (89) Kampen, N. G. v. *Stochastic processes in physics and chemistry*; North - Holland: Amsterdam, 1981.
- (90) Kumar, A.; Maity, H.; Dua, A. *J. Phys. Chem. B* **2015**, *119*, 8490.
- (91) Reuveni, S.; Urbakh, M.; Klafter, J. *Proc. Natl. Acad. Sci. U.S.A.* **2014**, *111*, 4391.
- (92) Berezhkovskii, A. M.; Szabo, A.; Rotbart, T.; Urbakh, M.; Kolomeisky, A. B. *J. Phys. Chem. B* **2017**, *121*, 3437.
- (93) Wallace Cleland, W. *Biochim. Biophys. Acta.* **1989**, *1000*, 209.
- (94) Holwerda, E. K.; Lynd, L. R. *Biotechnol. Bioeng.* **2013**, *110*, 2389.
- (95) Grima, R.; Leier, A. *J. Phys. Chem. B* **2017**, *121*, 13.
- (96) Anderson, N. G.; Maller, J. L.; Tonks, N. K.; Sturgill, T. W. *Nature* **1990**, *343*, 651.
- (97) Misiura, M. M.; Kolomeisky, A. B. *J. Phys. Chem. B* **2016**, *120*, 10508.
- (98) Tanoue, T.; Adachi, M.; Moriguchi, T.; Nishida, E. *Nat. Cell Biol.* **2000**, *2*, 110.
- (99) Misiura, M.; Kolomeisky, A. B. *J. Chem. Phys.* **2019**, *150*, 155101.
- (100) Han, K. S.; Liu, G.; Zhou, X.; Medina, R. E.; Chen, P. *Nano Lett.* **2012**, *12*, 1253.
- (101) Chaudhury, S.; Cherayil, B. J. *J. Chem. Phys.* **2006**, *125*, 024904.
- (102) Chaudhury, S.; Chatterjee, D.; Cherayil, B. J. *J. Chem. Phys.* **2008**, *129*, 075104.

- (103) Neupane, K.; Ritchie, D. B.; Yu, H.; Foster, D. A. N.; Wang, F.; Woodside, M. T. *Phys. Rev. Lett.* **2012**, *109*, 068102.
- (104) Neupane, K.; Foster, D. A. N.; Dee, D. R.; Yu, H.; Wang, F.; Woodside, M. T. *Science* **2016**, *352*, 239.
- (105) Laleman, M.; Carlon, E.; Orland, H. *J. Chem. Phys.* **2017**, *147*, 214103.
- (106) Chaudhury, S.; Makarov, D. E. *J. Chem. Phys.* **2010**, *133*, 034118.
- (107) Kim, P. S.; Baldwin, R. L. *Annu. Rev. Biochem.* **1990**, *59*, 631.
- (108) Satija, R.; Makarov, D. E. *J. Phys. Chem. B* **2019**, *123*, 802.
- (109) Carlon, E.; Orland, H.; Sakaue, T.; Vanderzande, C. *J. Phys. Chem. B* **2018**, *122*, 11186.

2. Statistical properties of fluctuating enzymes with dynamic cooperativity using a first passage time distribution formalism

**Reprinted from “Singh, D.; Chaudhury, S., J. Chem. Phys. 2017, 146, 145103-145107.”
with the permission of AIP Publishing.**

2.1 Introduction:

According to the classical Michaelis-Menten (MM) reaction, the mean turnover time depends linearly on the inverse of the substrate concentration.¹ However, enzymatic reactions can be much more complex.²⁻⁴ Recent advances in single molecule spectroscopy allow us to study the dynamic behaviour of individual enzyme molecules in real-time.^{5,6} Single-molecule fluorescence studies on the enzyme beta-galactosidase⁷ show that the turnover time distributions follow a multi-exponential decay at high substrate concentrations. This experimental observation was explained theoretically with a discrete two-state model where the enzyme can exist in multiple conformations and switch reversibly between them.⁸ Such conformational fluctuations lead to dynamic disorder.^{9,10} In general, for this two-state model with slow enzymatic conformational fluctuations, the mean turnover time, does not follow the classical MM equation.⁴ Such a deviation in the MM behaviour can lead to dynamic cooperativity in a single enzyme. Cooperativity is the effect of multiple binding sites for a single enzyme. But under certain limiting conditions, for example in the quasi-static limit, when fluctuations between the free enzyme conformers are absent and only slow fluctuations between the enzyme-substrate conformers exist, the rate equation reduces to the ensemble MM equation.^{8,11} In complex enzymatic reactions with interconversion between several enzymatic states, the hyperbolic form of the MM relation is valid provided the detailed balance condition holds good.¹² Hence the measurement of the mean turnover time may not be sufficient to provide dynamic insights.

As described in the chapter I of the thesis, we calculate the randomness parameter to quantify the noise present in the catalytic systems, expressed in terms of the moments of the catalytic time distribution.¹¹⁻¹⁴ The randomness and its inverse provides qualitative information about the nature of the probability distribution.¹⁵ The measurement of R , gives the mechanistic insights.¹⁶ For a single substrate enzymatic reaction with multiple conformations, randomness parameter has been studied theoretically by Kou *et al.*⁸ Assuming that the inter-conversion between the free enzymes is absent and the inter-conversion among the two enzyme-substrate conformers is slow compared to the product formation rates (quasi-steady state approximation gives $R = 1$ at low $[S]$, but its value deviates from unity at intermediate to high substrate concentration. Many theoretical studies employed the chemical master equation (CME) approach to obtain the steady-state probabilities for different enzymatic states.

Kumar *et al.* have used the same approach for single enzyme reactions where product formation can occur through either parallel or off-pathway mechanisms.¹⁷ This study confirmed that free enzyme conformational fluctuations do not contribute to dynamic disorder.

In this chapter, we consider an alternative theoretical model based on the first-passage time distribution formalism to obtain the reaction time and the randomness parameter for a catalytic reaction with multiple inter-convertible states. This method has been used earlier to obtain the first passage time distribution for a simple MM reaction.¹⁸ Within this theoretical framework, one can obtain the closed-form analytical expressions for the statistical measures in the context of ion channel statistics and even for single nanoparticle catalysis.^{16,18} All the reaction motifs studied earlier using the first passage formalism correspond to a renewal process¹⁹ with a single substrate binding site. A fundamental measurable quantity in any renewal process is the first passage time distribution function between successive catalytic turnover events, which are referred to as monitored transitions.^{20,21} These events can be detected in single molecule fluorescence experiments owing to the fluorescent nature of the product.⁷ Earlier studies based on the first passage approach, covered renewal processes²² with only one active site.^{16,18} In this chapter, we consider complex kinetic schemes with multiple inter-convertible states by applying this formalism.

In section 2.2, we describe our different enzymatic reaction models with multiple interconvertible states and explain respective observations. We first consider two simple models of single enzymatic reaction with two active sites wherein fluctuations exist only between the free enzyme conformers. Both these reaction mechanisms can serve as minimal models to understand the effect of dynamic cooperativity. Next we consider a minimal model for the off-pathway mechanism that has been discussed earlier by Kumar *et al.*¹⁷, where conformational fluctuations are present only between the enzyme-substrate conformers. This model could rationalize the experimental findings, on single turnover statistics.

2.2 Reaction Models and Analyses

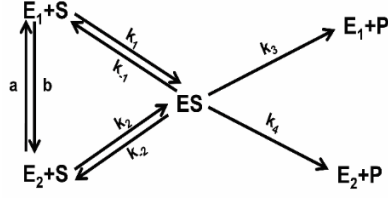


Figure 2.1: Reaction model for single enzyme catalysis with two interconvertible free conformers E_1 and E_2 .

We consider a very simple enzymatic reaction scheme as described in Figure 2.1. The enzyme can exist as two inter-convertible conformers E_1 and E_2 . Both these conformers can bind reversibly to the substrate S to form the ES complex, which can dissociate via two pathways forming the product P and E_1 and E_2 are regenerated. The first passage time distribution $\hat{\phi}(s)$ for this reaction scheme is an algebraic sum of four distributions given as

$$\hat{\phi}(s) = P_1 \hat{\phi}_{E_1 \rightarrow ES}(s) + P_2 \hat{\phi}_{E_2 \rightarrow ES}(s) + \hat{Q}_{ES \rightarrow E_1}(s) + \hat{Q}_{ES \rightarrow E_2}(s). \quad (2.1)$$

Here the first two terms correspond to the probability of forming ES starting E_1 and E_2 respectively and P_1 and P_2 are the corresponding weights such that $P_1 + P_2 = 1$. However, the expressions for these weights can be determined from normalized stationary fluxes.^{23,24} For Figure 2.1, P_1 and P_2 are constants and are independent of the substrate concentration. $\hat{\phi}_{E_1 \rightarrow ES}(s)$ has a contribution from two reaction pathways (a) $E_1 \rightarrow ES$ and (b) $E_1 \rightleftharpoons E_2 \rightarrow ES$. Similarly, $\hat{\phi}_{E_2 \rightarrow ES}(s)$ will also have two contributions (a) $E_2 \rightarrow ES$ and (b) $E_2 \rightleftharpoons E_1 \rightarrow ES$.

$$\hat{\phi}_{E_1 \rightarrow ES}(s) = \frac{\hat{Q}_{E_1 \rightarrow ES}(s) + \hat{Q}_{E_1 \rightarrow E_2}(s) \hat{Q}_{E_2 \rightarrow ES}(s)}{1 - \hat{Q}_{E_1 \rightarrow E_2}(s) \hat{Q}_{E_2 \rightarrow E_1}(s)} \quad (2.2)$$

$$\hat{\phi}_{E_2 \rightarrow ES}(s) = \frac{\hat{Q}_{E_2 \rightarrow ES}(s) + \hat{Q}_{E_2 \rightarrow E_1}(s) \hat{Q}_{E_1 \rightarrow ES}(s)}{1 - \hat{Q}_{E_1 \rightarrow E_2}(s) \hat{Q}_{E_2 \rightarrow E_1}(s)} \quad (2.3)$$

$\hat{Q}_{ES \rightarrow E_1}(s)$ and $\hat{Q}_{ES \rightarrow E_2}(s)$ in Eq. 1 are the probabilities of regenerating E_1 and E_2 , respectively starting from ES . The equation set below shows the explicit form of the waiting time probabilities for each transition.

$$\hat{Q}_{E_1 \rightarrow ES}(s) = \frac{k_1[S]}{s + k_1[S] + b} \quad (2.4a)$$

$$\hat{Q}_{E_2 \rightarrow ES}(s) = \frac{k_2[S]}{s+k_2[S]+a} \quad (2.4b)$$

$$\hat{Q}_{E_1 \rightarrow E_2}(s) = \frac{b}{s+b+k_1[S]} \quad (2.4c)$$

$$\hat{Q}_{E_2 \rightarrow E_1}(s) = \frac{a}{s+a+k_2[S]} \quad (2.4d)$$

$$\hat{Q}_{ES \rightarrow E_1}(s) = \frac{k_{-1}+k_3}{s+k_{-1}+k_{-2}+k_3+k_4} \quad (2.4e)$$

$$\hat{Q}_{ES \rightarrow E_2}(s) = \frac{k_{-2}+k_4}{s+k_{-1}+k_{-2}+k_3+k_4} \quad (2.4f)$$

Using the moment generation formula, we derive the average reaction time from Eq. 1.

$$\langle t \rangle = \frac{F[S]^2+H[S]+B}{E[S]^2+D[S]}. \quad (2.5)$$

Here $F = \frac{k_1 k_2}{k_{-1}+k_{-2}+k_3+k_4}$, $H = \frac{(ak_1+bk_2)}{k_{-1}+k_{-2}+k_3+k_4} + (k_1 P_2 + k_2 P_1)$, $B = a + b$, $E = k_1 k_2$ and $D = ak_1 +$

bk_2 . According to Eq. 5, the reaction rate does not follow the classical MM relation. Analysing the rate

of reaction in the quasi-static limit ($a \rightarrow 0$ and $b \rightarrow 0$), Eq. 5 reduces to the simple MM kind of

equation, $\langle t \rangle = A + \frac{I}{[S]}$. Here $A = \frac{1}{k_{-1}+k_{-2}+k_3+k_4}$, $I = \frac{k_1 P_2 + k_2 P_1}{E}$. Figure 2a shows the dependence of the

reaction rate as a function of the substrate concentration, $[S]$. When the binding of the substrate to one

enzyme conformer influences the substrate binding to another conformer ($k_1 > k_2$), there are

deviations from the MM equation. This indicates the emergence of dynamic cooperativity. In the

absence of conformation fluctuations ($a = b = 0$), the MM equation recovers. For the given set of

parameter values chosen in Figure 2a, in the presence of conformational fluctuations between E_1 and

E_2 , there is a steeper increase in the reaction rate with increasing $[S]$ than obtained in classical MM

kinetics indicating the presence of positive cooperativity.

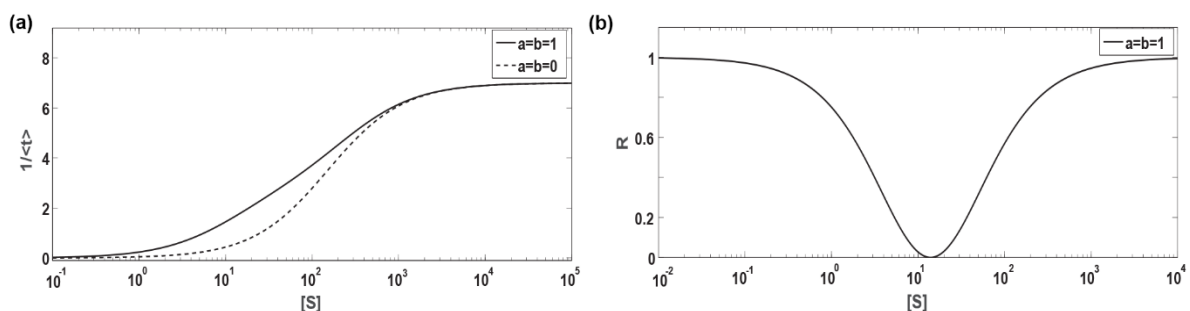


Figure 2.2: (a) Single molecule rate plot for the scheme shown in Figure 1, as a function of substrate concentration $[S]$ in non-dimensional units showing deviation from the MM equation and positive cooperativity at $a = b = 1$, (solid line). The MM relation recovers in the absence of enzyme conformational fluctuations $a = b = 0$ (dashed line). Common parameter values are $k_1 = k_{-1} = k_{-2} = 0.5, k_2 = 0.01, k_3 = 5, k_4 = 1, P_1 = 0.8, P_2 = 0.2$. (b) Randomness parameter R as a function of $[S]$ for the same model with $k_1 = k_{-1} = k_2 = k_{-2} = 0.5, a = b = 1, k_3 = 5, k_4 = 1, P_1 = 0.8, P_2 = 0.2$.

Figure 2.2b shows the randomness parameter as a function of the substrate concentration, $[S]$. In the presence of slow fluctuations between E_1 and E_2 conformers, the randomness parameter is equal to unity at low substrate concentration. At intermediate $[S]$, R deviates from unity due to the presence of multiple timescales of binding and dissociation events. Finally, at infinite substrate concentrations, R reduces to unity. Thus, the slow enzymatic conformational fluctuations do not affect the product formation step.

Unlike Figure 2.1, Figure 2.3 has two enzyme-substrate complexes, E_1S and E_2S .

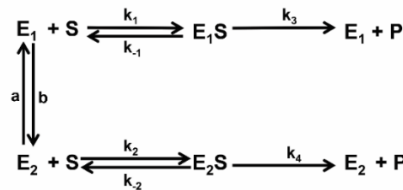


Figure 2.3: Reaction scheme for single enzyme catalysis with two interconvertible free conformers E_1 and E_2 . Both of them can bind with S to form different enzyme-substrate complexes.

Eq. 6 represents the first passage time distribution for the model presented in Figure 2.3.

$$\hat{\phi}(s) = \hat{\phi}_{E_1S}(s) + \hat{\phi}_{E_2S}(s) + P_5 \hat{Q}_{E_1S \rightarrow E_1}(s) + P_6 \hat{Q}_{E_2S \rightarrow E_2}(s) \quad (2.6)$$

$\hat{\phi}_{E_1S}(s)$ and $\hat{\phi}_{E_2S}(s)$ are the probability distributions for forming E_1S and E_2S from either E_1 and E_2 respectively. $\hat{\phi}_{E_1S}(s)$ has two contributions starting from E_1 and E_2 , respectively given as (a) $E_1 \rightarrow E_1S$ and (b) $E_2 \rightleftharpoons E_1 \rightarrow E_1S$ with corresponding weights P_1 and P_2 . Similarly, $\hat{\phi}_{E_2S}(s)$ will include two routes for the formation of E_2S via (a) $E_2 \rightarrow E_2S$ and (b) $E_1 \rightleftharpoons E_2 \rightarrow E_2S$ from E_1 and E_2 respectively with corresponding weights P_3 and P_4 .

$$\hat{\phi}_{E_1S}(s) = P_1 \frac{\hat{Q}_{E_1 \rightarrow E_1S}(s)}{1 - \hat{Q}_{E_1 \rightarrow E_2}(s) \hat{Q}_{E_2 \rightarrow E_1}(s)} + P_2 \frac{\hat{Q}_{E_2 \rightarrow E_1}(s) \hat{Q}_{E_1 \rightarrow E_1S}(s)}{1 - \hat{Q}_{E_1 \rightarrow E_2}(s) \hat{Q}_{E_2 \rightarrow E_1}(s)} \quad (2.7)$$

$$\hat{\phi}_{E_2S}(s) = P_3 \frac{\hat{Q}_{E_2 \rightarrow E_2S}(s)}{1 - \hat{Q}_{E_1 \rightarrow E_2}(s)\hat{Q}_{E_2 \rightarrow E_1}(s)} + P_4 \frac{\hat{Q}_{E_1 \rightarrow E_2}(s)\hat{Q}_{E_2 \rightarrow E_2S}(s)}{1 - \hat{Q}_{E_1 \rightarrow E_2}(s)\hat{Q}_{E_2 \rightarrow E_1}(s)} \quad (2.8)$$

The free enzymes regenerates from E_1S and E_2S conformers with probabilities $\hat{Q}_{E_1S \rightarrow E_1}(s)$ and $\hat{Q}_{E_2S \rightarrow E_2}(s)$. P_5 and P_6 are the corresponding weight factors. The set of equations listed below shows the functional form of the probability per unit time for each event.

$$\hat{Q}_{E_1 \rightarrow E_1S}(s) = \frac{k_1[S]}{s + k_1[S] + b} \quad (2.9a)$$

$$\hat{Q}_{E_2 \rightarrow E_2S}(s) = \frac{k_2[S]}{s + k_2[S] + a} \quad (2.9b)$$

$$\hat{Q}_{E_1 \rightarrow E_2}(s) = \frac{b}{s + k_1[S] + b} \quad (2.9c)$$

$$\hat{Q}_{E_2 \rightarrow E_1}(s) = \frac{a}{s + k_2[S] + a} \quad (2.9d)$$

$$\hat{Q}_{E_1S \rightarrow E_1}(s) = \frac{k_{-1} + k_3}{s + k_{-1} + k_3} \quad (2.9e)$$

$$\hat{Q}_{E_2S \rightarrow E_2}(s) = \frac{k_{-2} + k_4}{s + k_{-2} + k_4} \quad (2.9f)$$

Using Eq. 6, the first moment of $\hat{\phi}(s)$ gives the mean reaction time.

$$\langle t \rangle = \frac{U[S]^3 + X[S]^2 + Y[S] + Z}{E_0[S]^3 + F_0[S]^2 + D_0[S]} \quad (2.10)$$

$$\text{Here } U = k_1^2 k_2^2 [(k_{-1} + k_3)P_6 + (k_{-2} + k_4)P_5],$$

$$X = k_1 k_2 (k_{-1} + k_3)(k_{-2} + k_4)(k_1 P_3 + k_2 P_1) + 2k_1 k_2 (ak_1 + bk_2)[(k_{-1} + k_3)P_6 + (k_{-2} + k_4)P_5],$$

$$Y = (ak_1(ak_1 + 2bk_2) + b^2 k_2^2)[(k_{-1} + k_3)P_6 + (k_{-2} + k_4)P_5] + ((k_{-1} + k_3)(k_{-2} + k_4))[2k_1 k_2 (aP_1 + bP_3) + (k_1 + k_2)(ak_1 P_2 + bk_2 P_4)],$$

$$Z = ((k_{-1} + k_3)(k_{-2} + k_4))[a^2 k_1 + ab(k_1 + k_2)].$$

This expression does not follow the MM relation. If the conformational transitions between E_1 and E_2 are absent (i.e. $a = b = 0$) the mean reaction time reduces to a MM like equation,

$\langle t \rangle = J_0 + \frac{I_0}{[S]}$, where $J_0 = \frac{P_5}{k_{-1}+k_3} + \frac{P_6}{k_{-2}+k_4}$ and $I_0 = \frac{k_1 P_3 + k_2 P_1}{k_1 k_2}$. Figure 2.4a shows the reaction velocity as a function of $[S]$ where a less steep increase in the reaction velocity is observed in the presence of free enzyme fluctuations than allowed by a MM scheme. With the given set of parameters, slow enzyme conformational fluctuations lead to positive cooperativity.

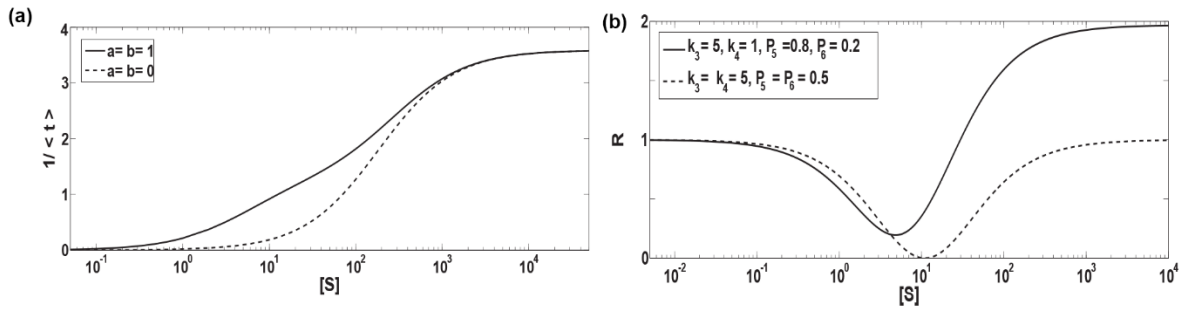


Figure 2.4: (a) Single molecule rate plot for the model presented in Figure 2.3 as a function of substrate concentration $[S]$ in non-dimensional units showing deviation from the MM equation and positive cooperativity at $a = b = 1$ (solid line). The MM relation recovers in the absence of enzyme conformational fluctuations, $a = b = 0$ (dashed line). (b) Randomness parameter R as a function of $[S]$, $k_3 = k_4 = 5, P_5 = P_6 = 0.5$ (dashed line), $k_3 = 0.5, k_4 = 0.1, P_5 = 0.8, P_6 = 0.2$ (solid line). Common parameters are $k_1 = k_{-1} = k_2 = k_{-2} = 0.5, P_1 = P_2 = P_3 = P_4 = 0.5, a = b = 0.1$.

Figure 2.4b shows the effect of enzyme conformational fluctuations on R for the schematic shown in Figure 2.3. At high substrate concentrations, when $k_3 = k_4$, R is equal to unity (dashed line in Figure 2.4b). If conformational fluctuations are present between the enzyme-substrate complexes at timescales comparable to catalytic step, the relative rates of product formation are different ($P_5 \neq P_6, k_3 \neq k_4$) and dynamic disorder arises at high substrate concentration (solid line). From both these schemes (Figure 2.1 and 2.3) discussed, we can conclude that slow fluctuations only between free enzyme conformers (E_1 and E_2) do not lead to dynamic disorder.¹⁷

Kumar *et al.* showed analytically that R is greater than unity at high substrate concentration when the catalytic rate constants are not equal ($k_3 \neq k_4$) or even when product formation occurs from only one enzyme-substrate conformer ($k_4 = 0$).¹⁷ This result indicates that we can consider a simpler mechanism where the free enzyme exists in only one active state ($k_2 = k_{-2} = 0$) and slow

conformational fluctuations are present between E_1S and E_2S , with only a single product formation pathway from E_1S ($k_4 = 0$). Figure 2.5a represents the reaction pathway, commonly known as the off-pathway mechanism.

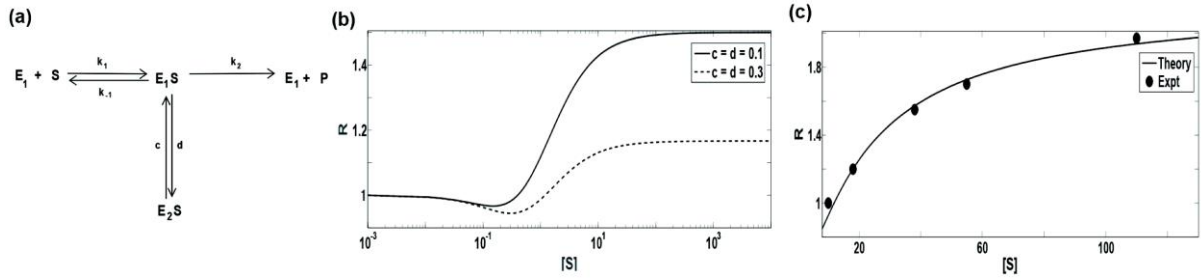


Figure 2.5: (a) Reaction model for single enzyme catalysis with interconversion between enzyme substrate conformers and only one product formation pathway. (b) Randomness parameter R as a function of $[S]$ in non-dimensional units with $c = d = 0.1$ (solid line) and $c = d = 0.3$ (dashed line). Common parameters are $k_1 = k_{-1} = 0.5, k_2 = 0.1$. (c) Comparison of randomness parameter with experimental data in Reference 7. Black circles represent experimental data points. The substrate concentration, $[S]$ on the x -axis is in micro-molar concentration. The solid line is the theoretical fit of Eq. 15 with parameter values with parameters $k_1 = 3.89 * 10^3 s^{-1}, k_{-1} = 5 * 10^3 s^{-1}, k_2 = 5 * 10^4 s^{-1}, c = 2 * 10^4 s^{-1}, d = 2.2 * 10^4 s^{-1}$.

The first-passage time distribution for this reaction mechanism is

$$\widehat{\varrho}(s) = \frac{\widehat{Q}_{E_1 \rightarrow E_1 S}(s) \widehat{Q}_{E_1 S \rightarrow P}(s)}{1 - \widehat{Q}_{E_1 \rightarrow E_1 S}(s) \widehat{Q}_{E_1 S \rightarrow E_1}(s) - \widehat{Q}_{E_1 S \rightarrow E_2 S}(s) \widehat{Q}_{E_2 S \rightarrow E_1 S}(s)} \quad (2.12)$$

The waiting time distributions for each step are as follows:

$$\widehat{Q}_{E_1 \rightarrow E_1 S}(s) = \frac{k_1 [S] p}{s + k_1 [S]} \quad (2.13a)$$

$$\widehat{Q}_{E_1 S \rightarrow E_1}(s) = \frac{k_{-1}}{s + d + k_{-1} + k_2} \quad (2.13b)$$

$$\widehat{Q}_{E_1 S \rightarrow P}(s) = \frac{k_2}{s + d + k_{-1} + k_2} \quad (2.13c)$$

$$\widehat{Q}_{E_1 S \rightarrow E_2 S}(s) = \frac{d}{s + d + k_{-1} + k_2} \quad (2.13d)$$

$$\widehat{Q}_{E_2 S \rightarrow E_1 S}(s) = \frac{c}{s + c} \quad (2.13e)$$

Using Eq. 2.12, we can obtain the mean reaction time.

$$\langle t \rangle = \frac{A + B[S]}{C[S]} \quad (14)$$

Here, $A = c(k_{-1} + k_2)$, $B = (c + d)k_1$ and $C = k_1k_2c$. Eq. 2.14 obeys the MM type of relation.

The randomness parameter for the off-pathway mechanism has the following form.

$$R = \left[1 + \frac{[S][G[S]-I]}{[m+[S]]^2} \right] \quad (2.15)$$

Here, $j = \frac{2k_2d}{(c+d)^2}$, $l = \frac{2k_2c}{(c+d)k_1}$ and $m = \frac{c(k_1+k_2)}{k_1(c+d)}$. Figure 2.5b shows the dependence of the randomness parameter on $[S]$. Due to the competition between timescales of enzyme-substrate conformational fluctuations and the product formation step, dynamic disorder is present at intermediate to high substrate concentrations. A small increase in the timescale of the enzyme-substrate conformational fluctuations can suppress the magnitude of temporal fluctuations and can reduce the value of R at high substrate concentrations (dashed line). At $[S] \rightarrow 0$, the rate determining step corresponds to the binding of the substrate only to E_1 and $R = 1$. In Figure 2.5c we compare the randomness parameter obtained from Eq. 2.15 with the experimental data on beta-galactosidase.⁷ By considering the case that the conformational fluctuations of the enzyme-substrate are slower than the catalytic step, and choosing suitable parameter values, we obtain an excellent agreement with the experimental data.

2.3 Conclusions:

In this chapter, we use the first-passage time distribution formalism to model the kinetics of a single enzyme that fluctuating between multiple conformations. We obtain exact expressions for the mean reaction time and the randomness parameter. In different schemes described above, conformational fluctuations of the free enzyme lead to dynamic cooperativity. In the absence of enzymatic conformational fluctuations, the MM relation holds. Thus, dynamic cooperativity in single enzyme arises due to the slow enzymatic (free enzyme) conformational fluctuations. The variation of the randomness parameter with $[S]$ provides information about the role of dynamic disorder in different reaction models with conformational fluctuations. In this chapter, for both the models based on free enzyme fluctuations, the randomness parameter is equal to unity at low and high $[S]$. On the contrary, the off-pathway mechanism obeys the MM kinetics and the randomness parameter is greater than unity at high substrate concentrations. A small increase in the timescale of the enzyme-substrate conformational fluctuations can suppress the magnitude of temporal fluctuations at high substrate

concentrations. All these studies indicate that randomness parameter at high substrate concentrations is determined only by the slow fluctuations of the enzyme–substrate conformers.

2.4 References:

- (1) Michaelis, L.; Menten., M. L.; *Biochem. Z.* 1913, 333 *Biochem. Z.* **1913**, 49, 333.
- (2) Segel, I. H. *Enzyme Kinetics: Behaviour and Analysis of Rapid Equilibrium and Steady State Enzymes Systems*; Wiley: New York, 1993.
- (3) Kolomeisky, A. B. *J. Chem. Phys.* **2011**, 134, 155101.
- (4) Qian, H. *Biophys. J.* **2008**, 95, 10.
- (5) Lu, H. P.; Xun, L.; Xie, X. S. *Science* **1998**, 282, 1877.
- (6) van Oijen, A. M.; Blainey, P. C.; Crampton, D. J.; Richardson, C. C.; Ellenberger, T.; Xie, X. S. *Science* **2003**, 301, 1235.
- (7) English, B. P.; Min, W.; van Oijen, A. M.; Lee, K. T.; Luo, G.; Sun, H.; Cherayil, B. J.; Kou, S. C.; Xie, X. S. *Nat. Chem. Biol.* **2006**, 2, 87.
- (8) Kou, S. C.; Cherayil, B. J.; Min, W.; English, B. P.; Xie, X. S. *J. Phys. Chem. B* **2005**, 109, 19068.
- (9) Zwanzig, R. *Acc. Chem. Res.* **1990**, 23, 148.
- (10) Zwanzig, R. *J. Chem. Phys.* **1992**, 97, 3587.
- (11) Min, W.; English, B. P.; Luo, G.; Cherayil, B. J.; Kou, S. C.; Xie, X. S. *Acc. Chem. Res.* **2005**, 38, 923.
- (12) Yang, Y.; Cao, J.; Silbey, R. J.; Sung, J. *Biophys. J.* **2011**, 101, 519.
- (13) Saha, S.; Sinha, S.; Dua, A. *J. Chem. Phys.* **2012**, 137, 045102.
- (14) Jung, W.; Yang, S.; Sung, J. *J. Phys. Chem. B* **2010**, 114, 9840.
- (15) Moffitt, J. R.; Bustamante, C. *FEBS J.* **2013**, 281, 498.
- (16) Chaudhury, S. *J. Phys. Chem. B* **2014**, 118, 10405.
- (17) Kumar, A.; Maity, H.; Dua, A. *J. Phys. Chem. B* **2015**, 119, 8490.
- (18) Chaudhury, S.; Cao, J.; Sinitsyn, N. A. *J. Phys. Chem. B* **2013**, 117, 503.
- (19) Cox, D. R. *Renewal Theory*; Methuen & Co. Ltd.: London, 1962.
- (20) Gopich, I. V.; Szabo, A. *J. Chem. Phys.* **2006**, 124, 154712.
- (21) Gopich, I. V.; Szabo, A. *J. Chem. Phys.* **2003**, 118, 454.
- (22) Cao, J.; Silbey, R. J. *J. Phys. Chem. B* **2008**, 112, 12867.
- (23) Cao, J. *J. Phys. Chem. B* **2006**, 110, 19040.
- (24) Cao, J. *Chem. Phys. Lett.* **200**, 327, 38.

3. Theoretical study of the conditional non-monotonic off rate dependence of catalytic reaction rates in single enzymes in the presence of conformational fluctuations

Reprinted from “Singh, D.; Chaudhury, S., Chem. Phys. 2019, 523, 150-159” with the permission from the Elsevier publishing.

© 2019 Published by Elsevier B.V.

3.1 Introduction

With the advancements in single molecule fluorescence measurements, one can explore the behaviour of individual molecules in time.^{1,2} The role of enzymatic conformational fluctuations affecting the dynamic properties of a reaction has also been studied theoretically.³⁻⁵ In the second chapter of the thesis, we have already discussed the effect of enzymatic interconversions for different reaction models. Systems with slow free enzyme conformational fluctuations show deviation from the classical MM behaviour and this effect vanishes in the quasi-static limit. Thus, the turnover rate showed the substrate hyperbolic dependence only under certain assumptions. In this chapter, we discuss the role of substrate unbinding using theoretical tools. According to the well-known Michaelis–Menten equation, an increase in the rate of substrate unbinding will decrease the rate of enzymatic turnover. However, Klafter and co-workers⁶ have analytically studied the role of substrate unbinding and demonstrated that reaction velocity can be accelerated by increasing the off dissociation rate under certain conditions. For understanding the unbinding-catalytic turnover relationship, they transformed the catalytic time distribution in terms of the unbinding rate ($\hat{f}_{cat}(k_{off}) = \int_0^\infty f_{cat}(t) e^{-k_{off} t} dt$) and classified the parameter space into monotonic/non-monotonic regimes. The rationale and physical arguments related to this study motivates experimental studies using single molecule techniques to achieve the unexpected rate enhancement effect by controlled variation of the unbinding rates. However, their analytical model did not cover the dynamical fluctuations between the enzyme-substrate complexes, which are evident in previous experimental and theoretical studies.

Recently, Kolomeisky and co-workers have employed a theoretical^{7,8} method that gives more physical understanding related to such observations. For examining the non-monotonic dependence of the velocity on the off dissociation rate, they have applied a theoretical formalism to a discrete two-state model where the enzyme-substrate complex

conformers can mutually interconvert. This mechanism serves as a minimal model to capture the effects of conformational fluctuation dynamics for the MM reaction at the SM level.^{5,9,10} If one of the substrate bound state is unproductive, then increasing the off dissociation rates gives the enzyme another chance to form the productive enzyme-substrate complex. In this study,⁷ reaction velocities for different schemes have been calculated assuming that the free enzyme conformers are in the state of conformational equilibrium.

However, it is probable that the free enzymes conformers are slowly interconverting among themselves. There are reported studies clarifying the effect of the free enzyme conformational fluctuations leading to dynamic cooperativity.^{10,11} Since, the mean time measurements do not capture the fluctuation characteristics present in the SM reaction networks, one requires to calculate the randomness parameter to quantify the temporal fluctuations.^{5,10,12,13}

In this chapter, we study the dependence of the enzymatic rate on the substrate unbinding rate for different reaction mechanisms comprising free and bound enzyme conformational fluctuations as shown in Figure 3.1(a) and 3.1(b). We consider a two-state discrete model that includes the conformational interconversions between the free enzyme (E_1 and E_2) and enzyme-substrate conformers (E_1S and E_2S) and assume that E_2S is an unproductive state and product formation can only take place from E_1S . The reaction schemes taken under consideration correspond to renewal kinetics with a single productive state. For a given scheme, we construct the chemical master equation (CME)¹⁴ and derive an exact analytical expression for the turnover velocity. We use these analytical results to mark a certain region of parameter space where it is probable to show a non-monotonic velocity dependence on the off dissociation rate. We also determine the randomness parameter and examine its dependence on the off rate at high substrate concentration.

3.2 Reaction Models and Analyses

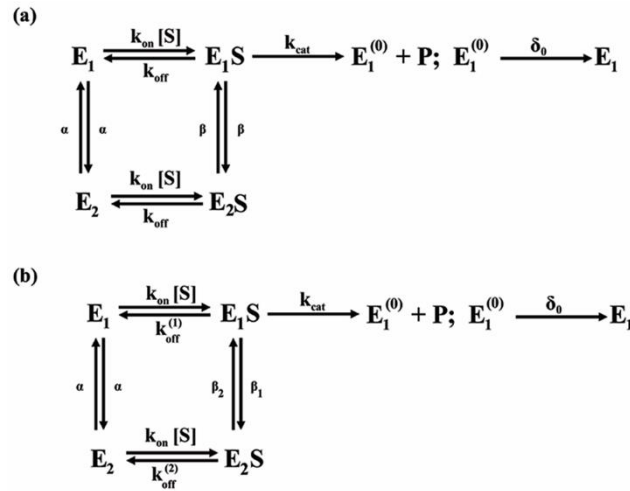


Figure 3.1: Schematic representation of the reaction schemes constituting discrete free and bound-enzyme conformers when (a) $k_{off}^{(1)} = k_{off}^{(2)} = k_{off}$ and (b) $k_{off}^{(1)} \neq k_{off}^{(2)}$.

In Figure 3.1(a), the two enzyme conformers E_1 and E_2 can bind to the substrate to form the complexes E_1S and E_2S , respectively or can interconvert among themselves. The rate constants characterizing these two processes are k_{on} , and α , respectively. The second state E_2S is unproductive and can only dissociate to the free enzyme with the rate constant k_{off} or can be converted to E_1S with a rate constant β . The E_1S state can decay to the free enzyme E_1 via the dissociation or the catalytic pathway or can be converted to E_2S with rate constants k_{off} , k_{cat} , and β , respectively. Initially, we assume the off dissociation rate is same for both the enzyme–substrate states. In order to consider the effect of conformational fluctuation of the enzyme–substrate complexes, one has to assume that the timescale characterizing these interconversions is longer than or comparable to the catalytic timescales. The chemical master equation (CME)^{9,10,15} for a Michaelis-Menten reaction includes the effect of stochasticity with discrete integer jump in the number of enzymes (n_{E_1}, n_{E_2}) and enzyme-substrate complexes (n_{E_1S}, n_{E_2S}), regenerated enzymes ($n_{E_1^{(0)}}$) and products (n_P). Grima and Leier have used the chemical master equation to calculate the mean time to produce one product molecule and also the average reaction rate at long times.¹⁶ In this chapter, we assume that the substrate is always present in

abundance. As pointed out in many works,^{17 18} this substrate abundance assumption holds good when the product formation rate is measured for a short period of time.

According to the chemical master equation formalism,¹⁹ if $n_{E_1}, n_{E_1S}, n_{E_2}, n_{E_2S}, n_{E_1^{(0)}}, n_P$ are discrete random variables that can take finite number of positive integral values, at any time t , the time evolution of the joint probability $P [n_{E_1}, n_{E_1S}, n_{E_2}, n_{E_2S}, n_{E_1^{(0)}}, n_P; t]$ for Figure 3.1(a) is given

$$\begin{aligned}
& \partial_t P [n_{E_1}, n_{E_1S}, n_{E_2}, n_{E_2S}, n_{E_1^{(0)}}, n_P; t] \\
&= \left(k_{on}[S](n_{E_1} + 1)(Y_{E_1} Y_{E_1S}^{-1}) + \alpha(n_{E_1} + 1)(Y_{E_1} Y_{E_2}^{-1}) \right. \\
&+ k_{off}(n_{E_1S} + 1)(Y_{E_1}^{-1} Y_{E_1S}) + \beta(n_{E_1S} + 1)(Y_{E_1S} Y_{E_2S}^{-1}) \\
&+ k_{cat}(n_{E_1S} + 1)(Y_{E_1S} Y_{E_1^{(0)}}^{-1} Y_P^{-1}) + k_{on}[S](n_{E_2} + 1)(Y_{E_2} Y_{E_2S}^{-1}) \\
&+ \alpha(n_{E_2} + 1)(Y_{E_1}^{-1} Y_{E_2}) + k_{off}(n_{E_2S} + 1)(Y_{E_2}^{-1} Y_{E_2S}) \\
&+ \beta(n_{E_2S} + 1)(Y_{E_1S}^{-1} Y_{E_2S}) \\
&- \left[(k_{on}[S] + \alpha)n_{E_1} + (\beta + k_{off} + k_{cat})n_{E_1S} + (k_{on}[S] + \alpha)n_{E_2} \right. \\
&\left. + (k_{off} + \beta)n_{E_2S} \right] P [n_{E_1}, n_{E_1S}, n_{E_2}, n_{E_2S}, n_{E_1^{(0)}}, n_P; t]
\end{aligned} \tag{3.1}$$

Due to the mutually exclusivity of different states, the CME reduces to a set of coupled differential equations listed below.

$$\frac{\partial P_{E_1}(t)}{\partial t} = -(k_{on}[S] + \alpha)P_{E_1}(t) + k_{off}P_{E_1S}(t) + \alpha P_{E_2}(t) + \delta_0 P_{E_1^{(0)}}(t) \tag{3.2.a}$$

$$\frac{\partial P_{E_1S}(t)}{\partial t} = k_{on}[S]P_{E_1}(t) - (\beta + k_{off} + k_{cat})P_{E_1S}(t) + \beta P_{E_2S}(t) \tag{3.2.b}$$

$$\frac{\partial P_{E_2}(t)}{\partial t} = \alpha P_{E_1}(t) - (k_{on}[S] + \alpha)P_{E_2}(t) + k_{off}P_{E_2S}(t) \tag{3.2.c}$$

$$\frac{\partial P_{E_2S}(t)}{\partial t} = \beta P_{E_1S}(t) + k_{on}[S]P_{E_2}(t) - (\beta + k_{off})P_{E_2S}(t) \quad (3.2.d)$$

$$\frac{\partial P_{E_1^{(0)}}(t)}{\partial t} = k_{cat}P_{E_1S}(t) - \delta_0 P_{E_1^{(0)}}(t) \quad (3.2.e)$$

At the beginning of the reaction, the enzyme exists in the free-state conformer E_1 . Also, at any instant of time the condition $P_{E_1}(t) + P_{E_1S}(t) + P_{E_2}(t) + P_{E_2S}(t) = 1$ should always be satisfied. We can solve these coupled differential equations following the methodology described in chapter I of the thesis.

$$(s + k_{on}[S] + \alpha)\hat{P}_{E_1}(s) - k_{off}\hat{P}_{E_1S}(s) - \alpha\hat{P}_{E_2}(s) - \delta_0\hat{P}_{E_1^{(0)}}(s) = 1 \quad (3.3.a)$$

$$-k_{on}[S]\hat{P}_{E_1}(s) + (s + \beta + k_{off} + k_{cat})\hat{P}_{E_1S}(s) - \beta\hat{P}_{E_2S}(s) = 0 \quad (3.3.b)$$

$$-\alpha\hat{P}_{E_1}(s) + (s + k_{on}[S] + \alpha)\hat{P}_{E_2}(s) - k_{off}\hat{P}_{E_2S}(s) = 0 \quad (3.3.c)$$

$$-\beta\hat{P}_{E_1S}(s) - k_{on}[S]\hat{P}_{E_2}(s) + (s + \beta + k_{off})\hat{P}_{E_2S}(s) = 0 \quad (3.3.d)$$

$$s\hat{P}_{E_1^{(0)}}(s) = 0 \quad (3.3.e)$$

Arranging them in the form of a matrix, we get Eq. 4.

$$\begin{bmatrix} s + k_{on}[S] + \alpha & -k_{off} & -\alpha & 0 & -\delta_0 \\ -k_{on}[S] & s + \beta + k_{off} + k_{cat} & 0 & -\beta & 0 \\ -\alpha & 0 & s + k_{on}[S] + \alpha & -k_{off} & 0 \\ 0 & -\beta & -k_{on}[S] & s + \beta + k_{off} & 0 \\ 0 & 0 & 0 & 0 & s \end{bmatrix} \begin{bmatrix} \hat{P}_{E_1}(s) \\ \hat{P}_{E_1S}(s) \\ \hat{P}_{E_2}(s) \\ \hat{P}_{E_2S}(s) \\ \hat{P}_{E_1^{(0)}}(s) \end{bmatrix} =$$

$$\begin{bmatrix} 1 \\ 0 \\ 0 \\ 0 \\ 0 \end{bmatrix} \quad (3.4)$$

Further rearrangement and taking an inverse gives Eq. 3.5.

$$\begin{bmatrix} \hat{P}_{E_1}(s) \\ \hat{P}_{E_1S}(s) \\ \hat{P}_{E_2}(s) \\ \hat{P}_{E_2S}(s) \\ \hat{P}_{E_1^{(0)}}(s) \end{bmatrix} = \begin{bmatrix} \frac{s^3 + \mu_1 s^2 + \mu_3 s + \mu_4}{s^4 + \mu_5 s^3 + \mu_6 s^2 + \mu_7 s + \mu_9} \\ \frac{k_{on}[S]s^2 + \mu_{10}s + \mu_8}{s^4 + \mu_5 s^3 + \mu_6 s^2 + \mu_7 s + \mu_9} \\ \frac{\alpha s^2 + \mu_2 s + \sigma_1}{s^4 + \mu_5 s^3 + \mu_6 s^2 + \mu_7 s + \mu_9} \\ \frac{\sigma_2 s + \sigma_3}{s^4 + \mu_5 s^3 + \mu_6 s^2 + \mu_7 s + \mu_9} \\ 0 \end{bmatrix}. \quad (3.5)$$

where $\mu_1 = k_{on}[S] + \alpha + 2\beta + 2k_{off} + k_{cat}$, $\mu_2 = \alpha(2\beta + 2k_{off} + k_{cat})$,

$$\mu_3 = \alpha\beta k_{cat} + k_{off}(\mu_2 - \alpha k_{off} + k_{on}[S]) + k_{on}[S](2\beta + k_{cat}) + \mu_2,$$

$$\mu_4 = \beta k_{on}[S]k_{cat} + \sigma_1, \mu_5 = \mu_1 + k_{on}[S] + \alpha,$$

$$\mu_6 = \beta k_{cat} + k_{off}(2\beta + k_{off} + k_{cat}) + k_{on}[S](\mu_1 + 2\beta + \alpha + k_{cat}) + 2\mu_2,$$

$$\mu_7 = 2\mu_4 + k_{on}[S]k_{cat}(k_{off} + k_{on}[S]) + 2\sigma_3,$$

$$\mu_8 = \beta k_{on}[S](k_{on}[S] + 2\alpha) + \alpha k_{on}[S]k_{off}, \mu_9 = k_{cat}\mu_8,$$

$$\mu_{10} = k_{on}[S](k_{on}[S] + k_{off}) + \sigma_2,$$

$$\sigma_1 = k_{off}(\mu_2 - \alpha k_{off} + \beta k_{on}[S]) + \alpha\beta k_{cat}, \sigma_2 = k_{on}[S](\alpha + \beta) \text{ and}$$

$$\sigma_3 = k_{on}[S](\mu_2 - \alpha k_{off} + \beta k_{on}[S]).$$

Eq. 7 represents the turnover time distribution for the scheme shown in Figure 3.1(a).

$$\hat{f}(s) = k_{cat}\hat{P}_{E_1S}(s) = \frac{k_{cat}(k_{on}[S]s^2 + \mu_{10}s + \mu_8)}{s^4 + \mu_5 s^3 + \mu_6 s^2 + \mu_7 s + \mu_9} \quad (3.6)$$

The first moment of Eq.6 gives the mean waiting time and its reciprocal gives the rate.

$$v_1 = \frac{k_{on}[S]k_{cat}(\alpha(2\beta + k_{off}) + \beta k_{on}[S])}{2\alpha(k_{off}(k_{cat} + k_{off}) + \beta(k_{cat} + 2k_{off})) + k_{on}[S](\alpha(4\beta + k_{cat} + 2k_{off}) + \beta(k_{cat} + 2k_{off})) + 2\beta k_{on}^2[S]^2} \quad (3.7)$$

Eq. 3.7 does not follow the Michaelis–Menten relation in the presence of enzymatic conformational fluctuations.¹⁰ If the free enzyme conformers interconvert quickly ($\alpha \rightarrow \infty$), then Eq. 3.7 reduces to

$$v_1(\alpha \rightarrow \infty) = \frac{k_{on}[S]k_{cat}(2\beta+k_{off})}{2(k_{off}(k_{cat}+k_{off})+\beta(k_{cat}+2k_{off}))+k_{on}[S](4\beta+k_{cat}+2k_{off})}$$

This expression resembles the form of the enzymatic velocity for the three state model discussed in Ref. 7. The limit $\alpha = 0$ yields the Michaelis–Menten-like equation.

$$v_1(\alpha \rightarrow 0) = \frac{k_{on}[S]k_{cat}(k_{on})}{(k_{cat}+2k_{off})+2k_{on}[S]}$$

Eq. 3.8 shows the normalized reaction velocity for the scheme shown in Figure 3.1 (a).

$$v_{ratio} = \frac{(\alpha(2\beta+k_{off})+\beta k_{on}[S])(2\alpha\beta k_{cat}+\alpha k_{on}[S](4\beta+k_{cat})+\beta k_{on}[S](k_{cat}+2k_{on}[S]))}{\beta(2\alpha+k_{on}[S])(2\alpha(k_{off}(k_{cat}+k_{off})+\beta(k_{cat}+2k_{off}))+\alpha k_{on}[S](4\beta+k_{cat}+2k_{off}))+\beta k_{on}[S](k_{cat}+2(k_{off}+k_{on}[S])))} \quad (3.8)$$

In Figure 3.1(b), the state E_2S is unproductive and can only dissociate to the free enzyme with $k_{off}^{(2)}$. It can also undergo a conformational transition to the state E_1S which is characterized by the rate constant β_2 . The E_1S state can decay to the free enzyme E_1 via the dissociation or catalytic pathway or can be converted to E_2S with rate constants $k_{off}^{(1)}$, k_{cat} and β_1 , respectively.

In this model we assume the off dissociation rate constants are different for both the enzyme–substrate states. The variables constituting the probability distributions are $n_{E_1}, n_{E_1S}, n_{E_2}, n_{E_2S}, n_{E_1^{(0)}}, n_P$ representing the number of enzyme molecules present in the state $E_1, E_2, E_1S, E_2S, E_1^{(0)}$, respectively and n_P is the number of product molecules formed at a time t . Eq. 3.9 represents the CME for Figure 3.1(b).

$$\begin{aligned}
& \partial_t P \left[n_{E_1}, n_{E_1S}, n_{E_2}, n_{E_2S}, n_{E_1^{(0)}}, n_P; t \right] \\
&= \left(k_{on}[S](n_{E_1} + 1)(Y_{E_1} Y_{E_1S}^{-1}) + \alpha(n_{E_1} + 1)(Y_{E_1} Y_{E_2}^{-1}) \right. \\
&+ k_{off}^{(1)}(n_{E_1S} + 1)(Y_{E_1}^{-1} Y_{E_1S}) + \beta_1(n_{E_1S} + 1)(Y_{E_1S} Y_{E_2S}^{-1}) \\
&+ k_{cat}(n_{E_1S} + 1)(Y_{E_1S} Y_{E_1^{(0)}}^{-1} Y_P^{-1}) + k_{on}[S](n_{E_2} + 1)(Y_{E_2} Y_{E_2S}^{-1}) \\
&+ \alpha(n_{E_2} + 1)(Y_{E_1}^{-1} Y_{E_2}) + k_{off}^{(2)}(n_{E_2S} + 1)(Y_{E_2}^{-1} Y_{E_2S}) \\
&+ \beta_2(n_{E_2S} + 1)(Y_{E_1S}^{-1} Y_{E_2S}) \\
&- \left[(k_{on}[S] + \alpha)n_{E_1} + (\beta_1 + k_{off}^{(1)} + k_{cat})n_{E_1S} + (k_{on}[S] + \alpha)n_{E_2} \right. \\
&\left. + (k_{off}^{(2)} + \beta_2)n_{E_2S} \right] P \left[n_{E_1}, n_{E_1S}, n_{E_2}, n_{E_2S}, n_{E_1^{(0)}}, n_P; t \right].
\end{aligned} \tag{3.9}$$

Since for a single enzyme the different enzymatic states are mutually exclusive, the CME reduces to these coupled differential equations

$$\frac{\partial P_{E_1}(t)}{\partial t} = -(k_{on}[S] + \alpha)P_{E_1}(t) + k_{off}^{(1)}P_{E_1S}(t) + \alpha P_{E_2}(t) + \delta_0 P_{E_1^{(0)}}(t) \tag{3.10a}$$

$$\frac{\partial P_{E_1S}(t)}{\partial t} = k_{on}[S]P_{E_1}(t) - (\beta_1 + k_{off}^{(1)} + k_{cat})P_{E_1S}(t) + \beta_2 P_{E_2S}(t) \tag{3.10b}$$

$$\frac{\partial P_{E_2}(t)}{\partial t} = \alpha P_{E_1}(t) - (k_{on}[S] + \alpha)P_{E_2}(t) + k_{off}^{(2)} P_{E_2S}(t) \tag{3.10c}$$

$$\frac{\partial P_{E_2S}(t)}{\partial t} = \beta_1 P_{E_1S}(t) + k_{on}[S]P_{E_2}(t) - (\beta_2 + k_{off}^{(2)})P_{E_2S}(t) \tag{3.10d}$$

$$\frac{\partial P_{E_1^{(0)}}(t)}{\partial t} = k_{cat}P_{E_1S}(t) - \delta_0 P_{E_1^{(0)}}(t) \tag{3.10e}$$

Let $k_{on}[S] + \alpha = \mu$, $\beta_1 + k_{off}^{(1)} + k_{cat} = \xi$ and $\beta_2 + k_{off}^{(2)} = \varepsilon$.

Following the same steps and methodology adopted for Figure 3.1(a), we get Eq. 3.11.

$$\begin{bmatrix} \hat{P}_{E_1}(s) \\ \hat{P}_{E_1S}(s) \\ \hat{P}_{E_2}(s) \\ \hat{P}_{E_2S}(s) \\ \hat{P}_{E_1^{(0)}}(s) \end{bmatrix} = \begin{bmatrix} \frac{s^3 + \xi_1 s^2 + \xi_2 s + \xi_3}{s^4 + \xi_4 s^3 + \xi_5 s^2 + \xi_6 s + \xi_7} \\ \frac{k_{on}[S]s^2 + \xi_8 s + \xi_9}{s^4 + \xi_4 s^3 + \xi_5 s^2 + \xi_6 s + \xi_7} \\ \frac{\alpha s^2 + \xi_{10} s + \varepsilon_1}{s^4 + \xi_4 s^3 + \xi_5 s^2 + \xi_6 s + \xi_7} \\ \frac{\varepsilon_2 s + \varepsilon_3}{s^4 + \xi_4 s^3 + \xi_5 s^2 + \xi_6 s + \xi_7} \\ 0 \end{bmatrix} \quad (3.11)$$

Eq. 12 shows the turnover time distribution for the scheme represented in Figure 3.1 (b).

$$\hat{f}(s) = k_{cat} \hat{P}_{E_1S}(s) = \frac{k_{cat}(k_{on}[S]s^2 + \xi_8 s + \xi_9)}{s^4 + \xi_4 s^3 + \xi_5 s^2 + \xi_6 s + \xi_7}. \quad (3.12)$$

Here, $\xi_1 = \mu + \varepsilon + \xi$, $\xi_2 = \alpha(\xi + \varepsilon) + \beta_2(k_{on}[S] + k_{off}^{(1)} + k_{cat}) + \xi(k_{on}[S] + k_{off}^{(2)})$,

$$\xi_3 = \beta_2(k_{off}^{(1)} + k_{cat})\mu + \alpha\xi k_{off}^{(2)}, \quad \xi_4 = \mu + \xi_1,$$

$$\xi_5 = 2\alpha(\xi + \varepsilon) + k_{on}[S](2\alpha + \beta_1 + \beta_2 + k_{cat}) + \beta_2(k_{on}[S] + k_{off}^{(1)} + k_{cat}) +$$

$$(\xi + k_{on}[S])(k_{on}[S] + k_{off}^{(2)}),$$

$$\xi_6 = 2\alpha(\beta_1 k_{off}^{(2)} + (k_{off}^{(1)} + k_{cat})(\beta_2 + k_{off}^{(2)})) + \alpha k_{on}[S](\varepsilon + \xi + \beta_1 + \beta_2 + k_{cat}) +$$

$$k_{on}[S](\beta_2(k_{on}[S] + k_{off}^{(1)} + 2k_{cat}) + (\beta_1 + k_{cat})(k_{on}[S] + k_{off}^{(2)})),$$

$$\xi_7 = k_{on}[S]k_{cat}(\alpha(\varepsilon + \beta_2) + k_{on}[S]\beta_2), \quad \xi_8 = k_{on}[S](\mu + \varepsilon),$$

$$\xi_9 = k_{on}[S](\alpha\beta_2 - k_{on}[S]k_{off}^{(2)} + \varepsilon\mu), \quad \xi_{10} = \alpha(\xi + \varepsilon),$$

$$\varepsilon_1 = \alpha(\beta_1 k_{off}^{(2)} + \varepsilon(k_{off}^{(1)} + k_{cat})) + \beta_1 k_{off}^{(2)} k_{on}[S], \quad \varepsilon_2 = k_{on}[S](\alpha + \beta_1) \text{ and}$$

$$\varepsilon_3 = k_{on}[S](\alpha\xi + \beta_1\mu).$$

In order to satisfy the detailed balance condition, the following relation must be satisfied $\beta_1 k_{off}^{(2)} = k_{off}^{(1)} \beta_2$. We use this relation to eliminate $k_{off}^{(2)}$ from the velocity expression

$$v_2 = \frac{k_{on}[S]\beta_2 k_{cat} (\alpha(2\beta_1 + k_{off}^{(1)}) + \beta_1 k_{on}[S])}{2\alpha\beta_2 (k_{off}^{(1)}(k_{cat} + k_{off}^{(1)}) + \beta_1(k_{cat} + 2k_{off}^{(1)})) + \alpha k_{on}[S] (\beta_1(2(\beta_1 + \beta_2) + k_{cat}) + (\beta_1 + \beta_2)k_{off}^{(1)}) + \beta_1 k_{on}[S] (\beta_2(k_{cat} + 2k_{off}^{(1)}) + (\beta_1 + \beta_2)k_{on}[S])} \quad (3.13)$$

Eq. 14 represents the normalized reaction velocity.

$$v_{ratio} = \frac{v_2}{v_2(k_{off} \rightarrow 0)} = \frac{(\alpha(2\beta_1 + k_{off}^{(1)}) + \beta_1 k_{on}[S]) (2\alpha\beta_2 k_{cat} + \alpha k_{on}[S] (2(\beta_1 + \beta_2) + k_{cat}) + k_{on}[S] (\beta_2 k_{cat} + (\beta_1 + \beta_2) k_{on}[S]))}{(2\alpha + k_{on}[S]) (2\alpha\beta_2 (k_{off}^{(1)}(k_{cat} + k_{off}^{(1)}) + \beta_1(k_{cat} + 2k_{off}^{(1)})) + \alpha k_{on}[S] (\beta_1(2(\beta_1 + \beta_2) + k_{cat}) + (\beta_1 + \beta_2)k_{off}^{(1)}) + \beta_1 k_{on}[S] (\beta_2(k_{cat} + 2k_{off}^{(1)}) + (\beta_1 + \beta_2)k_{on}[S]))} \quad (3.14)$$

In Figures 3.2 and 3.3, we plot the normalized velocity given in Eq. 8 and Eq. 14, respectively at various $[S]$ with the assumption of zero substrate fluctuations. In order to examine the effect of substrate fluctuations, we have performed a few sets of Gillespie stochastic simulations²⁰ and compared our theoretical expressions for the normalized velocity. It shows that when there are no fluctuations in the $[S]$ our theoretical and simulation results are in excellent agreement. In the presence of substrate fluctuations, the average rate of product formation is found to be less than that predicted at a constant substrate concentration.²¹

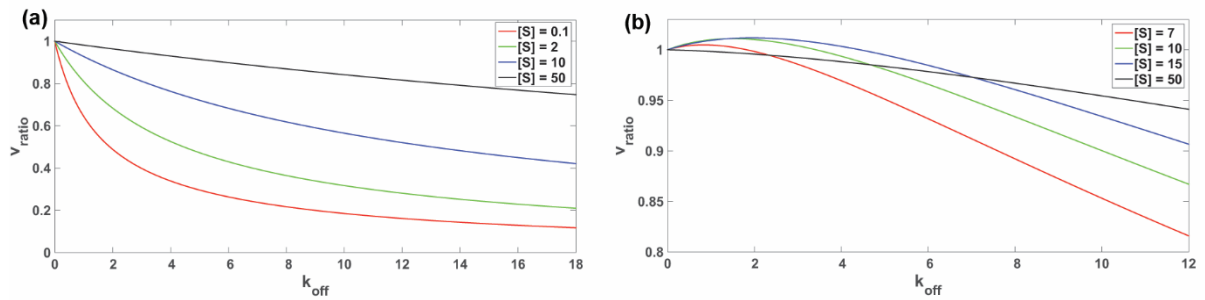


Figure 3.2: (a) Normalized reaction velocity (Eq. 4.8) showing a monotonic behaviour when plotted as a function of k_{off} for the reaction scheme represented in Figure 3.1(a) at different values of substrate concentrations 0.1, 2, 10 and 50 represented by red, green, blue and black solid lines, respectively. The common set of reaction rate constants are $k_{on} = 1$, $\alpha = 1$, $\beta = 2$, and $k_{cat} = 5$. (b) Normalized reaction velocity showing a non-monotonic behavior under the specified limits ($k_{cat} > \frac{16\alpha\beta^2}{(\alpha-\beta)^2}$, $\alpha > \beta$) when plotted as a function of k_{off} for the reaction scheme represented in Figure 3.1(a) at different substrate concentrations 7, 10 and 15 represented by red, green, and blue solid lines, respectively. Beyond this determined range of substrate concentration the non-monotonicity vanishes which is represented by the black solid line at $[S] = 50$. The common set of reaction rate constants are $k_{on} = 1$, $\alpha = 3$, $\beta = 1$, and $k_{cat} = 20$.

As shown in Figure 3.2(a) the enzymatic velocity (Eq. 8) for the kinetic scheme described in Figure 3.1(a) decreases with an increase in the off dissociation rate k_{off} . On differentiating Eq. 8 with respect to k_{off} and equating it to zero, we obtain a quadratic relation of $[S]$. The velocity is a non-monotonic function of k_{off} only when the rate constants satisfy the following inequality

$$\alpha^2 k_{cat} k_{on} [S] > 2\alpha^2 \beta (4\beta + k_{cat}) + \alpha\beta (8\beta + k_{cat}) k_{on} [S] + 2\beta^2 k_{on}^2 [S]^2. \quad (3.15)$$

At low substrate concentration, the terms $\alpha\beta (8\beta + k_{cat}) k_{on} [S]$ and $2\beta^2 k_{on}^2 [S]^2$ on RHS of the inequality are very small compared to $2\alpha^2 \beta (4\beta + k_{cat})$. For standard values of all other kinetic rate constants, the LHS of Eq. 15 will always be smaller than $2\alpha^2 \beta (4\beta + k_{cat})$. At intermediate to high substrate concentrations, we look for a certain region in the parameter space in which the inequality in Eq. 15 is satisfied. Solving this inequality gives the following roots:

$$[S_1] = \frac{\alpha(\alpha k_{cat} - \beta(8\beta + k_{cat}) + \sqrt{-k_{cat}} \sqrt{16\alpha\beta^2 - (\alpha - \beta)^2 k_{cat}})}{4\beta^2 k_{on}}$$

$$[S_2] = \frac{\alpha(\alpha k_{cat} - \beta(8\beta + k_{cat}) - \sqrt{-k_{cat}} \sqrt{16\alpha\beta^2 - (\alpha - \beta)^2 k_{cat}})}{4\beta^2 k_{on}}$$

Thus, these two roots represent a range of substrate concentration within which one can observe non-monotonicity. For these two roots to be real and positive, the following conditions need to be satisfied.

$$\text{Limit 1: } k_{cat} > \frac{16\alpha\beta^2}{(\alpha - \beta)^2} \quad (\text{for the roots to be real}) \quad (3.16a)$$

$$\text{Limit 2: } k_{cat} > \frac{8\beta^2}{\alpha - \beta} \quad (\text{for the roots to be positive}). \quad (3.16b)$$

Figure 3.2(b) shows the non-monotonic behaviour of the enzymatic velocity as a function of k_{off} within a range of $[S]$ for a certain set of parameter values. At higher $[S]$, the third term on the RHS of Eq. 16 that is quadratic in the substrate concentration $[S]$ will always dominate.

Hence, the inequality does not hold. Thus, the normalized velocity will always decrease with the increase in k_{off} .

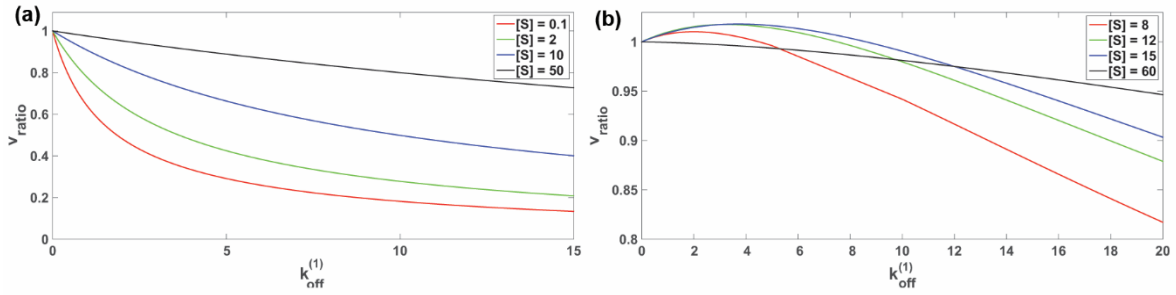


Figure 3.3: (a) Normalized reaction velocity (from Eq. 14) showing a monotonic behaviour when plotted as a function of $k_{off}^{(1)}$ for the reaction scheme represented in Figure 3.1(b) at different values of substrate concentrations 0.1, 2, 10 and 50 represented by red, green, blue and black solid lines, respectively. The common set of reaction rate constants are $k_{on} = 1$, $\alpha = 1$, $\beta_1 = 2$, $\beta_2 = 4$, and $k_{cat} = 5$. (b) Normalized reaction velocity showing a non-monotonic behavior under specified limits ($k_{cat} > \frac{16\alpha\beta_1\beta_2}{(\alpha-\beta_2)^2}$, $\alpha > \beta_2$) when plotted as a function of $k_{off}^{(1)}$ for the reaction scheme represented in Figure 3.1(b) at different substrate concentrations 8, 12 and 15 represented by red, green, and blue solid lines, respectively. Beyond this determined range of substrate concentration the non-monotonicity vanishes which is represented by the black solid line at $[S] = 60$. The common set of reaction rate constants are $k_{on} = 1$, $\alpha = 4$, $\beta_1 = 2$, $\beta_2 = 1$ and $k_{cat} = 25$.

Figure 3.3(a) describes the behaviour of the enzymatic velocity as obtained in Eq. 14 for the kinetic scheme described in Figure 3.1(b). The velocity will show a non-monotonic behaviour with respect to $k_{off}^{(1)}$ only when the following inequality is satisfied.

$$\alpha^2 k_{cat} k_{on} [S] > 2\alpha^2 \beta_2 (4\beta_1 + k_{cat}) + \alpha\beta_2 (8\beta_1 + k_{cat}) k_{on} [S] + 2\beta_1 \beta_2 k_{on}^2 [S]^2 \quad (3.17)$$

At low $[S]$, the contribution of the last two terms on RHS of the inequality is insignificant as compared to $2\alpha^2 \beta_2 (4\beta_1 + k_{cat})$. At intermediate to high substrate concentrations, by solving the quadratic inequality we can obtain a range of substrate concentration within which the non-monotonic behaviour would be observed. The inequality gives the following roots

$$[S_1] = \frac{\alpha(\alpha k_{cat} - \beta_2(8\beta_1 + k_{cat}) + \sqrt{-k_{cat}\sqrt{-16\alpha\beta_1\beta_2 + (\alpha - \beta_2)^2 k_{cat}}})}{4\beta_1\beta_2 k_{on}}$$

$$[S_2] = \frac{\alpha(\alpha k_{cat} - \beta_2(8\beta_1 + k_{cat}) - \sqrt{-k_{cat}\sqrt{-16\alpha\beta_1\beta_2 + (\alpha - \beta_2)^2 k_{cat}}})}{4\beta_1\beta_2 k_{on}}$$

Since the roots represent substrate concentration, they should be real and positive.

$$\text{Limit 1: } k_{cat} > \frac{16 \alpha \beta_1 \beta_2}{(\alpha - \beta_2)^2} \text{ (for real values)} \quad (3.18a)$$

$$\text{Limit 2: } k_{cat} > \frac{8 \beta_1 \beta_2}{\alpha - \beta_2}, \alpha > \beta_2 \text{ (for positive values).} \quad (3.18b)$$

We have compared our theoretical results plotted in Figure 3.2(b) and 3.3(b) showing the non-monotonic behaviour with stochastic simulations at zero substrate fluctuations as shown in Figure 2 of Ref 21.²¹ As studied by Cao and co-workers²² we have also constructed a phase diagram (Figure 3 of Ref 21) for the reaction scheme represented in Figure 3.1(a) and 3.1(b) that identify the regimes of the monotonic and the conditional non-monotonic behaviours of the reaction velocity as a function of the dissociation rate constant.²¹

To measure the temporal fluctuations we compute the randomness parameter.²³ For single-molecule fluorescence measurements, dynamic disorder was reported at high substrate concentrations.² For the kinetic scheme shown in Figure 3.1(a) and 3.1(b), from the higher moments of the distribution, we can calculate the randomness parameter. Eq. 19 shows the randomness expression for the reaction scheme shown in Figure 3.1(a).

$$R = \frac{4\alpha^2 k_{off}^4 + A k_{off}^3 + B k_{off}^2 + C k_{off} + D}{4\alpha^2 k_{off}^4 + 4\alpha E k_{off}^3 + G k_{off}^2 + 2EF k_{off} + F^2} \quad (3.19)$$

$$\text{Here, } \Omega = (k_{cat} + 2\beta), \lambda = k_{cat} + k_{on}[S], A = 2\alpha(4\Omega\alpha + (4(\alpha + \beta) + k_{cat})k_{on}[S]),$$

$$B = 2 \left(\beta \Omega k_{on}^2 [S]^2 + \alpha k_{on} [S] (8\beta(\lambda + \beta) + k_{cat}(\lambda + k_{on}[S])) + 2\alpha^2 (4\beta^2 + \lambda^2 + \beta(6\lambda + 2k_{on}[S])) \right),$$

$$C = 4\beta k_{on}^2 [S]^2 (k_{on}[S]\Omega + \beta k_{cat}) + 4\alpha^2 (2\beta + k_{on}[S]) (k_{cat}\Omega + (\Omega + 2\beta)k_{on}[S]) + 2\alpha k_{on}[S] ((k_{cat} + \lambda)k_{cat}k_{on}[S] + 8\beta^2(\lambda + k_{on}[S]) + \beta(\lambda + k_{on}[S])(2\lambda + k_{cat})),$$

$$D = 4\alpha^2 \beta^2 k_{cat}^2 \mu + 4\alpha \beta^2 k_{cat}^2 k_{on}[S] + k_{on}^2 [S]^2 (16\alpha^2 \beta^2 + 8\alpha^2 \beta k_{cat} + (3\alpha^2 + 2\alpha\beta + \beta^2)k_{cat}^2) + 2\alpha k_{on}^3 [S]^3 (8\beta^2 + 4\beta k_{cat} + k_{cat}^2) + 2\beta \Omega k_{on}^4 [S]^4,$$

$$E = 2(\alpha\Omega + (\alpha + \beta)k_{on}[S]), F = 2\alpha\beta k_{cat} + \alpha k_{on}[S](\Omega + 2\beta) + \beta k_{on}[S](\lambda + k_{on}[S]) \text{ and} \\ G = E^2 + 4\alpha F.$$

For the reaction scheme shown in Figure 3.1(b), Eq. 20 represents the analytical form of R .

$$R = \frac{4\alpha^2\beta_2^2(k_{off}^{(1)})^4 + H(k_{off}^{(1)})^3 + I(k_{off}^{(1)})^2 + J k_{off}^{(1)} + L}{4\alpha^2\beta_2^2(k_{off}^{(1)})^4 + 4\alpha\beta_2 M(k_{off}^{(1)})^3 + P(k_{off}^{(1)})^2 + 2MN k_{off}^{(1)} + N^2} \quad (3.20)$$

$$\text{Here, } \chi = k_{cat} + 2\beta_1, \theta = \beta_1 + \beta_2, \rho = 2\beta_1 + \chi, \Lambda = 2\beta_2 + \chi,$$

$$H = 2\alpha\beta_2(4\alpha\beta_2\chi + (2\alpha\theta + \beta_2\rho)k_{on}[S]),$$

$$I = 4\alpha^2\beta_2^2(2\beta_1(\chi + 2k_{cat}) + k_{cat}^2) + 2\alpha\beta_2 k_{on}[S](4\alpha\beta_1\Lambda + \beta_2(8\beta_1(\beta_1 + k_{cat}) + k_{cat}^2)) + k_{on}^2[S]^2(\alpha^2\theta^2 + 2\beta_1\beta_2^2\chi + 4\alpha\beta_1\beta_2\Lambda),$$

$$J = 2\beta_1(4\alpha^2\beta_2^2 k_{cat}\chi + \alpha\beta_2 k_{on}[S](8\beta_1(\alpha\theta + (\alpha + \beta_2)k_{cat}) + (2\alpha + 3\beta_2)k_{cat}^2) + 2k_{on}^2[S]^2(\alpha\theta(4\beta_1\beta_2 + \alpha\theta) + \beta_1 k_{cat}(\alpha^2 + 4\alpha\beta_2 + \beta_2^2) + \alpha\beta_2 k_{cat}^2) + k_{on}^3[S]^3(2\beta_1\beta_2(\theta + k_{cat}) + \alpha(\theta^2 + \beta_1 k_{cat}))),$$

$$L = \beta_1^2(4\alpha\beta_2^2 k_{cat}^2\mu + k_{on}^2[S]^2(4\alpha^2\theta^2 + 8\alpha^2\beta_1 k_{cat} + (3\alpha^2 + 2\alpha\beta_2 + \beta_2^2)k_{cat}^2) + 2\alpha k_{on}^3[S]^3(2\theta^2 + 4\beta_1 k_{cat} + k_{cat}^2) + k_{on}^4[S]^4(\theta^2 + 2\beta_1 k_{cat})),$$

$$M = 2\alpha\beta_2(k_{cat} + 2\beta_1) + k_{on}[S](\alpha\theta + 2\beta_1\beta_2),$$

$$N = 2\alpha\beta_1\beta_2 k_{cat} + \beta_1 k_{on}[S](\mu + \alpha)\theta + (\alpha + \beta_2)k_{cat} \text{ and } P = M^2 + 4\alpha\beta_2 N.$$

Eq. 3.19 and Eq. 3.20 show that the randomness parameter is equal to unity at low substrate concentration and deviates from one at high substrate concentration. The value of R is a measure of the dynamic disorder present in the system. In Figure 3.4(a) and 3.4(b) we study the dependence of the randomness parameter on the off dissociation rate, k_{off} . At moderate to high

substrate concentration, mostly the enzyme exists in the substrate-bound state E_1S or E_2S . As k_{off} increases, and when it is comparable to k_{cat} , the enzymatic reaction follows a multistep process and the waiting time distribution is a multiexponential distribution. The E_2S state can dissociate to E_2 and undergo a conformational change to E_1 but can again quickly get converted to the E_1S complex. Such multiple reaction pathways lead to an increase in randomness in the system and reach a peak at a certain value of k_{off} . When k_{off} is very high, the unbinding of the substrate from the enzyme-substrate complex is highly favorable and the product formation step is the rate-determining step. This leads to a decrease in the value of R since the reaction switches to a single-pathway mechanism and the randomness parameter finally saturates to unity at very high values of k_{off} . This is also evident from Eq. 19 and Eq. 20. In both cases, R saturates to one at high values of k_{off} .

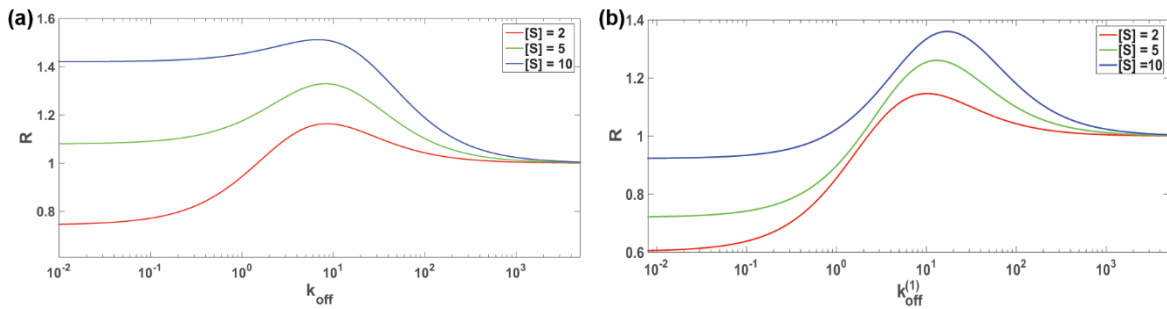


Figure 3.4: (a) Randomness parameter (from Eq. 3.19) plotted as a function of k_{off} for the reaction scheme represented in Figure 3.1(a) at different values of substrate concentrations 2, 5 and 10 represented by red, green, and blue solid lines, respectively. The common set of reaction rate constants are $k_{on} = 1$, $\alpha = 1$, $\beta = 2$, and $k_{cat} = 5$. (b) Randomness parameter (from Eq. 20) plotted as a function of $k_{off}^{(1)}$ for the reaction scheme represented in Figure 3.1(b) at different values of substrate concentrations 2, 5 and 10 represented by red, green, and blue solid lines, respectively. The common set of reaction rate constants are $k_{on} = 1$, $\alpha = 1$, $\beta_1 = 2$, $\beta_2 = 4$, and $k_{cat} = 5$.

3.3 Conclusions:

In this chapter, we calculate the velocity of a single enzyme using the chemical master equation approach. We consider two discrete conformations of the free enzyme and the enzyme-substrate

complex. The rate equation does not follow the MM law. When the reaction rate is studied as a function of k_{off} , an increase in the off dissociation rate assists the system to escape from the unproductive E_2S state. The non-monotonic dependence of the enzymatic velocity on the off dissociation rate is observed only within a certain concentration range of $[S]$ and this range is defined by a specific parameter space that satisfies a set of limiting conditions. From our enzymatic velocity expression, we can calculate these limiting conditions for both the cases when the off-rate constants are identical as well as different. The randomness parameter computed for different models indicates the time-dependent fluctuations in the catalytic rates and its dependence on the off rate at high substrate concentrations.

3.4 References:

- (1) Lu, H. P.; Xun, L.; Xie, X. S. *Science* **1998**, *282*, 1877.
- (2) English, B. P.; Min, W.; van Oijen, A. M.; Lee, K. T.; Luo, G.; Sun, H.; Cherayil, B. J.; Kou, S. C.; Xie, X. S. *Nat. Chem. Biol.* **2006**, *2*, 87.
- (3) Min, W.; Gopich, I. V.; English, B. P.; Kou, S. C.; Xie, X. S.; Szabo, A. J. *Phys. Chem. B. Lett.* **2006**, *110*, 20093.
- (4) Kolomeisky, A. B. *J. Chem. Phys.* **2011**, *134*, 155101.
- (5) Kou, S. C.; Cherayil, B. J.; Min, W.; English, B. P.; Xie, X. S. *J. Phys. Chem. B* **2005**, *109*, 19068.
- (6) Reuveni, S.; Urbakh, M.; Klafter, J. *Proc. Natl. Acad. Sci. U. S. A.* **2014**, *111*, 4391.
- (7) Berezhkovskii, A. M.; Szabo, A.; Rotbart, T.; Urbakh, M.; Kolomeisky, A. B. *J. Phys. Chem. B* **2017**, *121*, 3437.
- (8) Gopich, I. V.; Szabo, A. J. *Chem. Phys.* **2006**, *124*, 154712.
- (9) Kumar, A.; Maity, H.; Dua, A. J. *Phys. Chem. B* **2015**, *119*, 8490.
- (10) Singh, D.; Chaudhury, S. J. *Chem. Phys.* **2017**, *146*, 145103.
- (11) Qian, H. *Biophys. J.* **2008**, *95*, 10.
- (12) Chaudhury, S.; Cao, J.; Sinitzyn, N. A. *J. Phys. Chem. B* **2013**, *117*, 503.
- (13) Chaudhury, S. J. *Phys. Chem. B* **2014**, *118*, 10405.
- (14) Gardiner, C. W. *Handbook of Stochastic Methods: for Physics, Chemistry, and the Natural Sciences*; Springer: New York, 1996.
- (15) Qian, H.; Bishop, L. M. *Int. J. Mol. Sci.* **2010**, *11*, 3472.
- (16) Grima, R.; Leier, A. J. *Phys. Chem. B* **2016**, *121*, 13.
- (17) Grima, R.; Walter, N. G.; Schnell, S. *FEBS J.* **2014**, *281*, 518.
- (18) Stéfanini, M. O.; McKane, A. J.; Newman, T. J. *Nonlinearity* **2005**, *18*, 1575.
- (19) Van Kampen, N. G. *Stochastic Processes in Physics and Chemistry*; 3rd Edition ed.; Elseiver: North Holland, 2007.
- (20) Gillespie, D. T. *J. Phys. Chem.* **1977**, *81*, 2340.
- (21) Singh, D.; Chaudhury, S. *Data in Brief* **2019**, *25*, 104211.
- (22) Piephoff, D. E.; Wu, J.; Cao, J. J. *Phys. Chem. Lett.* **2017**, *8*, 3619.
- (23) Moffitt, J. R.; Bustamante, C. *FEBS J.* **2014**, *281*, 498.

4. Single molecule kinetics of an enzyme in the presence of multiple substrates

Reprinted from “Singh, D.; Chaudhury, S., ChemBioChem 2018, 19, 842-850.” with the permission from the John Wiley and Sons publishing.

© 2018 Wiley-VCH Verlag GmbH & Co. KGaA, Weinheim

4.1 Introduction:

In our previous thesis chapters (2 and 3), we have considered different enzymatic models where a single enzyme exists in multiple free and bound states. These reaction mechanisms have only one kind of substrate, which can reversibly bind with any of the existing free enzyme conformers and form the enzyme-substrate complexes. For the classical MM reaction model also, there is a single type of the substrate-binding event.¹ However, there are biochemical reactions involving different types of substrates. Various substrate-binding events complicate the network and affect the overall dynamics of the catalytic process. For the multi-substrate reactions, the mechanism is complex since it depends on the binding site specifications as well as on the sequence of binding.² Based on these factors, the multiple substrate reactions are broadly classified into the sequential and the non-sequential pathways.^{3,4} For a reaction involving two substrates, in the sequential mechanism, both the substrates bind to the enzyme either in a random or ordered manner to form a ternary complex which forms the product. In the random mechanism, the order of binding of the two substrates is unimportant. In the non-sequential mechanism, commonly known as ping-pong mechanism, both the substrates do not bind before the release of the product.

At the deterministic level, using the quasi-steady state approximation (QSSA), one can obtain the initial rate of product formation. The functional form of the reaction velocity follows the MM type of equation. By measuring the initial rate as a function of $[S_1]$ and varying the concentration of $[S_2]$, the Lineweaver-Burk plot ($1/v$ versus $1/[S_1]$) enables one to distinguish between the sequential and ping-pong mechanisms. Though the rate equation follows a MM form, for a sequential reaction, change in the concentration of substrate $[S_2]$, changes the slope and intercept of the Lineweaver-Burk plot, whereas, in the non-sequential (ping-pong) reaction, there is a change in the intercept but not the slope of the plot.⁴ Using a stochastic chemical master equation approach involving substrate number changes (attributed to limiting $[S]$),

Grima and Leier have also studied single enzyme kinetics for multiple substrate bindings.⁵ Although in SM experiments, excess substrate availability is approximately justified because here an enzyme is immobilized on a surface and there is a steady flow of substrate.^{6,7}

In this chapter, we study the stochastic single molecule enzyme kinetics for the multi-substrate reactions under the excess substrate availability.⁸ We ask the following questions. Can we get any further information about the kinetics of multi substrate reactions by measuring the higher moments of the waiting time distribution? Can we differentiate between different bisubstrate binding mechanisms at the single molecule level? In previous theoretical studies, the stochastic SM reaction kinetics have been described for different type of chain and branching reactions⁹ and a first passage time distribution formalism¹⁰ for generic reaction schemes. Here, we consider a chemical master equation approach¹¹ to obtain the probability for the enzyme to exist in one or more substrate bound states for bisubstrate binding reaction mechanisms.

Provided, the detailed balance condition holds, the MM behaviour would be followed even for complex reaction systems.^{12,13} Therefore, one needs to quantify the temporal fluctuations in the reaction rates. For probing the noise, we calculate the randomness parameter from the higher moments of the probability distribution function.

4.2 Reaction Models and Analyses:

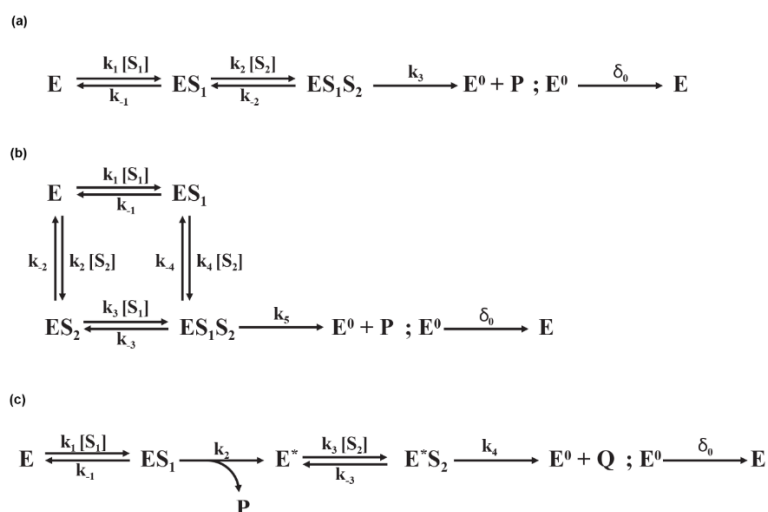


Figure 4.1: Schemes for bisubstrate binding in enzyme catalysis (a) ordered (b) random (c) ping-pong mechanism.

As shown in Fig. 4.1(a), in the ordered mechanism, the substrate S_1 binds first to the enzyme E to form the ES_1 complex followed by the binding of substrate S_2 to form the ternary complex, ES_1S_2 . In the random sequential mechanism as shown in Fig. 4.1b, there is no preference for binding of S_1 and S_2 to the enzyme, E . The formation of the same ternary complex ES_1S_2 occurs irrespective of the order in which the substrate binds. In Fig. 4.1(c), first substrate S_1 binds to E , followed by product release P and along with a new form of the enzyme, E^* . Then the second substrate S_2 binds reversibly to E^* and the reaction takes place to form the product Q with the regeneration of the free enzyme.

For an ordered sequential substrate binding mechanism, if $n_E, n_{ES_1}, n_{ES_1S_2}, n_{E^0}, n_P$ are the number of enzyme, enzyme-substrate complex, ternary complex, regenerated enzyme, and products at any time t , the chemical master equation can be written as¹⁴

$$\begin{aligned}
& \partial_t P(n_E, n_{ES_1}, n_{ES_1S_2}, n_{E^0}, n_P; t) \\
&= k_1[S_1](n_E + 1)P(n_E + 1, n_{ES_1} - 1, n_{ES_1S_2}, n_{E^0}, n_P; t) \\
&+ k_{-1}(n_{ES_1} + 1)P(n_E - 1, n_{ES_1} + 1, n_{ES_1S_2}, n_{E^0}, n_P; t) \\
&+ k_2[S_2](n_{ES_1} + 1)P(n_E, n_{ES_1} + 1, n_{ES_1S_2} - 1, n_{E^0}, n_P; t) \\
&+ k_{-2}(n_{ES_1S_2} + 1)P(n_E, n_{ES_1} - 1, n_{ES_1S_2} + 1, n_{E^0}, n_P; t) \\
&+ k_3(n_{ES_1S_2} + 1)P(n_E, n_{ES_1}, n_{ES_1S_2} + 1, n_{E^0} - 1, n_P - 1; t) \\
&- (k_1[S_1]n_E + (k_{-1} + k_2[S_2])n_{ES_1} \\
&+ (k_{-2} + k_3)n_{ES_1S_2})P(n_E, n_{ES_1}, n_{ES_1S_2}, n_{E^0}, n_P; t).
\end{aligned} \tag{4.1}$$

Because of the mutually exclusive of different enzymatic states, the CME reduces to the following set of coupled differential equations.

$$\frac{\partial P_E(t)}{\partial t} = -k_1[S_1]P_E(t) + k_{-1}P_{ES_1}(t) + \delta_0 P_{E^0}(t) \quad (4.2.a)$$

$$\frac{\partial P_{ES_1}(t)}{\partial t} = k_1[S_1]P_E(t) - (k_{-1} + k_2[S_2])P_{ES_1}(t) + k_{-2}P_{ES_1S_2}(t) \quad (4.2.b)$$

$$\frac{\partial P_{ES_1S_2}(t)}{\partial t} = k_2[S_2]P_{ES_1}(t) - (k_{-2} + k_3)P_{ES_1S_2}(t) \quad (4.2.c)$$

$$\frac{\partial P_{E^0}(t)}{\partial t} = k_3P_{ES_1S_2}(t) - \delta_0 P_{E^0}(t) \quad (4.2.d)$$

We solve these differential equations by taking their Laplace transforms. At $t = 0$, $P_E(0) = 1$, $P_{ES_1}(0) = 0$, $P_{ES_1S_2}(0) = 0$, and $P_{E^0}(0) = 0$ holds and at any time sum of all the probability densities should be giving unity. Chapter I of the thesis describes all other details of the waiting-time distribution formalism.

$$(s + k_1[S_1])\hat{P}_E(s) - k_{-1}\hat{P}_{ES_1}(s) - \delta_0\hat{P}_{E^0}(s) = 1 \quad (4.3a)$$

$$-k_1[S_1]\hat{P}_E(s) + (s + k_{-1} + k_2[S_2])\hat{P}_{ES_1}(s) - k_{-2}\hat{P}_{ES_1S_2}(s) = 0 \quad (4.3b)$$

$$-k_2[S_2]\hat{P}_{ES_1}(s) + (s + k_{-2} + k_3)\hat{P}_{ES_1S_2}(s) = 0 \quad (4.3c)$$

$$s\hat{P}_{E^0}(s) = 0 \quad (4.3d)$$

Arranging in the form of matrix and simplifying gives Eq.4.

$$\begin{bmatrix} \hat{P}_E(s) \\ \hat{P}_{ES_1}(s) \\ \hat{P}_{ES_1S_2}(s) \\ \hat{P}_{E^0}(s) \end{bmatrix} = \begin{bmatrix} \frac{s^2+as+b}{s^3+es^2+fs+g} \\ \frac{os+h}{s^3+es^2+fs+g} \\ \frac{j}{s^3+es^2+fs+g} \\ 0 \end{bmatrix} \quad (4.4)$$

Here $a = k_{-1} + k_{-2} + k_3 + k_2[S_2]$, $b = k_{-1}k_{-2} + k_{-1}k_3 + k_2k_3[S_2]$, $e = a + k_1[S_1]$,

$j = k_1k_2[S_1][S_2]$, $f = (k_{-2} + k_3)(k_{-1} + k_1[S_1] + k_2[S_2]) + j$, $g = (k_{-2} + k_3)j$,

$h = (k_{-2} + k_3)o$ and $o = k_1[S_1]$.

Eq.5 represents the waiting-time distribution function $\hat{f}(s)$ for the sequential ordered pathway.

$$\hat{f}(s) = k_3 \hat{P}_{ES_1 S_2}(s) = \frac{k_3 j}{s^3 + e s^2 + f s + g} \quad (4.5)$$

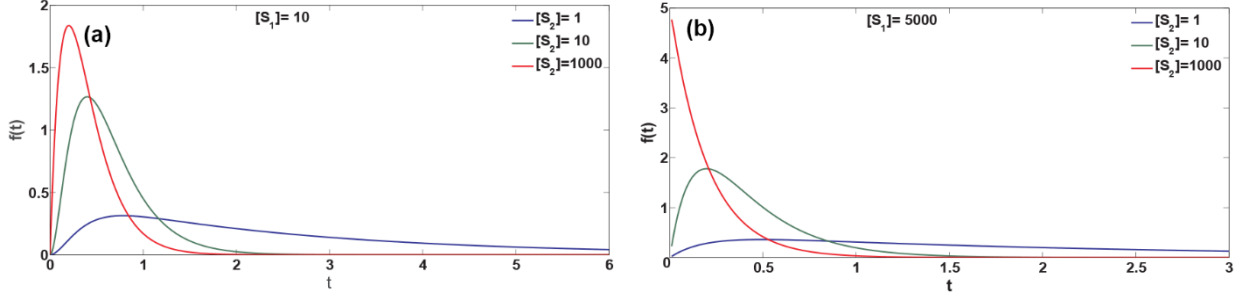


Figure 4.2: Plot of the dimensionless waiting time distribution as a function of the dimensionless time for the ordered sequential mechanism at (a) moderate concentration $[S_1] = 10$ and (b) high concentration $[S_1] = 5000$ at three concentrations of the second substrate, $[S_2] = 1$ (blue line), $[S_2] = 10$ (green line), and $[S_2] = 1000$ (red line). Parameter values chosen are $k_1 = k_{-1} = k_2 = k_{-2} = 0.5$ and $k_3 = 5$.

The first moment of Eq. 4.5 gives the mean waiting time.

$$\langle t \rangle_{ordered} = \frac{A}{[S_1][S_2]} + \frac{B}{[S_2]} + \frac{C}{[S_1]} + D \quad (4.6)$$

Here, $A = \frac{Bk_{-1}}{k_1}$, $B = \frac{(k_{-2} + k_3)}{k_2 k_3}$, $C = \frac{1}{k_1}$ and $D = \frac{1}{k_3}$. From Eq. 4.6, at a constant $[S_2]$, the

expression for average time reduces to a MM type equation.

$$\langle t \rangle_{ordered} = F + \frac{E}{[S_1]} \quad (4.7)$$

Here, $F = \left(\frac{B}{[S_2]} + D \right)$, $E = \left(\frac{A}{[S_2]} + C \right)$. Similarly, for a random substrate binding mechanism

(Figure 4.1b) the CME can be written as

$$\begin{aligned}
& \partial_t P(n_E, n_{ES_1}, n_{ES_2}, n_{ES_1S_2}, n_{E^0}, n_P; t) \\
&= k_1[S_1](n_E + 1)P(n_E + 1, n_{ES_1} - 1, n_{ES_2}, n_{ES_1S_2}, n_{E^0}, n_P; t) \\
&+ k_{-1}(n_{ES_1} + 1)P(n_E - 1, n_{ES_1} + 1, n_{ES_2}, n_{ES_1S_2}, n_{E^0}, n_P; t) \\
&+ k_2[S_2](n_E + 1)P(n_E + 1, n_{ES_1}, n_{ES_2} - 1, n_{ES_1S_2}, n_{E^0}, n_P; t) \\
&+ k_{-2}(n_{ES_2} + 1)P(n_E - 1, n_{ES_1}, n_{ES_2} + 1, n_{ES_1S_2}, n_{E^0}, n_P; t) \\
&+ k_3[S_1](n_{ES_2} + 1)P(n_E, n_{ES_1}, n_{ES_2} + 1, n_{ES_1S_2} - 1, n_{E^0}, n_P; t) \\
&+ k_{-3}(n_{ES_1S_2} + 1)P(n_E, n_{ES_1}, n_{ES_2} - 1, n_{ES_1S_2} + 1, n_{E^0}, n_P; t) \\
&+ k_4[S_2](n_{ES_1} + 1)P(n_E, n_{ES_1} + 1, n_{ES_2}, n_{ES_1S_2} - 1, n_{E^0}, n_P; t) \\
&+ k_{-4}(n_{ES_1S_2} + 1)P(n_E, n_{ES_1} - 1, n_{ES_2}, n_{ES_1S_2} + 1, n_{E^0}, n_P; t) \\
&+ k_5(n_{ES_1S_2} + 1)P(n_E, n_{ES_1}, n_{ES_2}, n_{ES_1S_2} + 1, n_{E^0} - 1, n_P - 1; t) \\
&- [(k_1[S_1] + k_2[S_2])n_E + (k_{-1} + k_4[S_2])n_{ES_1} + (k_{-2} + k_3[S_1])n_{ES_2} + (k_{-3} \\
&+ k_{-4} + k_5)n_{ES_1S_2}]P(n_E, n_{ES_1}, n_{ES_2}, n_{ES_1S_2}, n_{E^0}, n_P; t).
\end{aligned} \tag{4.8}$$

Following the same mathematical procedure as used for the sequential ordered pathway, we can obtain the following set of equations.

$$\frac{\partial P_E(t)}{\partial t} = -(k_1[S_1] + k_2[S_2])P_E(t) + k_{-1}P_{ES_1}(t) + k_{-2}P_{ES_2}(t) - \delta_0 P_{E^0}(t) \tag{4.9.a}$$

$$\frac{\partial P_{ES_1}(t)}{\partial t} = k_1[S_1]P_E(t) - (k_{-1} + k_4[S_2])P_{ES_1}(t) + k_{-4}P_{ES_1S_2}(t) \tag{4.9.b}$$

$$\frac{\partial P_{ES_2}(t)}{\partial t} = k_2[S_2]P_E(t) - (k_{-2} + k_3[S_1])P_{ES_2}(t) + k_{-3}P_{ES_1S_2}(t) \tag{4.9.c}$$

$$\frac{\partial P_{ES_1S_2}(t)}{\partial t} = k_4[S_2]P_{ES_1}(t) + k_3[S_1]P_{ES_2}(t) - (k_{-3} + k_{-4} + k_5)P_{ES_1S_2}(t) \tag{4.9.d}$$

$$\frac{\partial P_{E^0}(t)}{\partial t} = k_5P_{ES_1S_2}(t) - \delta_0 P_{E^0}(t) \tag{4.9.e}$$

Taking the Laplace transform and performing the matrix algebra gives Eq. 4.10.

$$\begin{bmatrix} \hat{P}_E(s) \\ \hat{P}_{ES_1}(s) \\ \hat{P}_{ES_2}(s) \\ \hat{P}_{ES_1S_2}(s) \\ \hat{P}_{E^0}(s) \end{bmatrix} = \begin{bmatrix} \frac{s^3 + \mu_1 s^2 + \mu_2 s + \mu_3}{s^4 + \theta_5 s^3 + \theta_9 s^2 + \theta_{10} s + \theta_{11}} \\ \frac{\sigma_1 s^2 + \sigma_2 s + \sigma_4}{s^4 + \theta_5 s^3 + \theta_9 s^2 + \theta_{10} s + \theta_{11}} \\ \frac{\sigma_5 s^2 + \sigma_6 s + \sigma_7}{s^4 + \theta_5 s^3 + \theta_9 s^2 + \theta_{10} s + \theta_{11}} \\ \frac{\sigma_8 s + \sigma_9}{s^4 + \theta_5 s^3 + \theta_9 s^2 + \theta_{10} s + \theta_{11}} \\ 0 \end{bmatrix} \quad (4.10)$$

Here, $\epsilon_1 = k_1[S_1] + k_2[S_2]$, $\epsilon_2 = k_{-1} + k_4[S_2]$, $\epsilon_3 = k_{-2} + k_3[S_1]$, $\epsilon_4 = k_{-3} + k_{-4} + k_5$,

$\mu_1 = \epsilon_2 + \epsilon_3 + \epsilon_4$, $\mu_2 = k_3 k_4 [S_2]^2 + k_3 (k_{-4} + k_5) [S_1] + (k_4 (k_{-2} + k_{-3} + k_5) + k_{-1} k_3) [S_2] + \epsilon_4 (k_{-1} + k_{-2}) + k_{-1} k_5$,

$\mu_3 = k_3 (-k_3 k_{-4} + k_4 k_{-4} + k_4 k_5) [S_1] [S_2] + (k_{-1} \epsilon_4 - k_3 k_{-3} k_4) [S_1] + k_{-2} (k_{-4} (k_4 - k_3) + k_4 (k_{-4} + k_5)) [S_2] + k_{-1} k_{-2} \epsilon_4$,

$\theta_5 = \mu_1 + \epsilon_1$, $\theta_9 = k_2 (k_{-1} - k_2) [S_2] + k_4 \epsilon_1 [S_2] + (\mu_1 - \epsilon_2) (1 + \epsilon_2 + \epsilon_1)$, $\rho_1 = \epsilon_3 \epsilon_4$,

$\theta_{10} = -k_1 k_{-1} [S_1] (\mu_1 - \epsilon_2 + \rho_1) - k_2 k_{-2} [S_2] (\mu_1 - \epsilon_3) + (\rho_1 + \mu_1 - \epsilon_2) (\epsilon_2 + \epsilon_1)$,

$\rho_2 = \epsilon_2 \epsilon_4$, $\theta_{11} = -k_2 k_{-2} [S_2] \rho_2 + \rho_1 \epsilon_1 \epsilon_2$, $\sigma_1 = k_1 [S_1]$, $\sigma_3 = \sigma_1 (\mu_1 - \epsilon_2)$, $\sigma_4 =$

$\sigma_1 [k_{-2} \epsilon_4 + k_3 [S_1] (k_{-4} + k_5)] + k_2 k_3 k_4 [S_1] [S_2]$, $\sigma_5 = k_2 [S_2]$,

$\sigma_6 = \sigma_5 (\mu_1 - \epsilon_3)$, $\sigma_7 = \sigma_5 \rho_2 + k_4 [S_2] (k_1 k_{-3} [S_1] - k_2 k_{-4} [S_2])$, $\sigma_8 = [S_1] (k_1 k_4 + k_2 k_3 [S_2])$,

$\sigma_9 = k_1 k_4 \epsilon_3 [S_1] + k_2 k_3 [S_1] [S_2] (k_{-1} + k_3 [S_1])$.

Eq. 4.11 represents the waiting time distribution for the random sequential mechanism.

$$\hat{f}(s) = k_5 * \hat{P}_{ES_1S_2}(s) = \frac{k_5 (\sigma_8 s + \sigma_9)}{s^4 + \theta_5 s^3 + \theta_9 s^2 + \theta_{10} s + \theta_{11}} \quad (4.11)$$

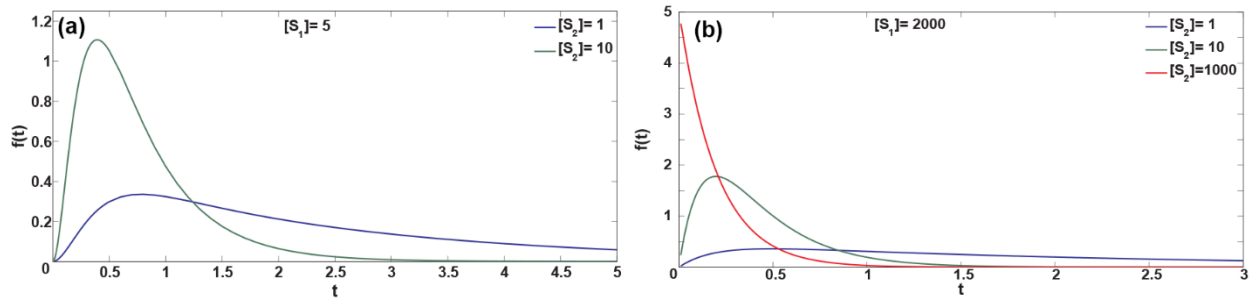


Figure 4.3: Plot of the dimensionless waiting time distribution as a function of the dimensionless time for the random mechanism at (a) moderate concentration $[S_1] = 5$, $[S_2] = 1$ (blue line), $[S_2] = 10$ (green line) and (b) high concentration $[S_1] = 2000$ at $[S_2] = 1$ (blue line), $[S_2] =$

10 (green line), and $[S_2] = 1000$ (red line). Parameter values chosen are $k_1 = k_{-1} = k_2 = k_{-2} = k_3 = k_{-3} = k_4 = k_{-4} = 0.5$ and $k_5 = 5$.

Figures 4.2 and 4.3 show the temporal variation of the waiting time distribution for the ordered and the random mechanism of bisubstrate reaction respectively as a function of the substrate concentration, $[S_1]$. At low $[S_1]$, the binding of the substrate to the free enzyme E is the rate-determining step and the waiting time shows a mono-exponential decay irrespective of the concentration of the second substrate, $[S_2]$. At intermediate concentration $[S_1]$, the distribution is multi-exponential, an exponential rise followed by an exponential decay at a constant value of $[S_2]$. As shown in Figures 4.2(a) and 4.3(a), at an intermediate $[S_1]$, the distribution becomes increasingly narrower, with increasing value of $[S_2]$. At high $[S_1]$, the distribution of the waiting times decays multi-exponentially (Figures 4.2(b) and 4.3(b)), but finally becomes steeper and mono-exponential at very high $[S_2]$ (red line in Figures 4.2(b) and 4.3(b)). The increase in the substrate concentration $[S_2]$ leads to only one rate-determining step, which corresponds to the product formation step. Thus in both the sequential reaction pathways the distribution is characterized by multiple relaxation time scales, arising due to the presence of multiple competing chemical steps.

Eq. 4.12 represents the mean waiting time (first moment of Eq. 4.11) for the random mechanism.

$$\langle t \rangle_{random} = \frac{a_0 + e_0[S_1] + l_0[S_2] + d_0[S_1]^2 + n_0[S_2]^2 + m_0[S_1][S_2] + k_0[S_1]^2[S_2] + p_0[S_1][S_2]^2}{x_0[S_1][S_2] + v_0[S_1]^2[S_2] + w_0[S_1][S_2]^2} \quad (4.12)$$

Here, $a_0 = k_{-1}k_{-2}\epsilon_4$, $e_0 = (k_{-1}k_3 + k_1k_{-2})(k_{-4} + k_5) + k_1k_{-2}k_{-3}$,

$l_0 = (k_{-2}k_4 + k_{-1}k_2)(k_{-3} + k_5) + k_{-1}k_2k_{-4}$, $d_0 = k_1k_3(k_{-4} + k_5)$, $n_0 = k_2k_4(k_{-3} + k_5)$,

$m_0 = k_1k_4(k_{-2} + k_{-3}) + k_2k_3(k_{-1} + k_{-4}) + k_3k_4k_5$, $k_0 = k_1k_3k_4$, $p_0 = k_2k_3k_4$,

$x_0 = k_5(k_{-1}k_2k_3 + k_1k_{-2}k_4)$, $v_0 = k_1k_3k_4k_5$ and $w_0 = k_2k_3k_4k_5$.

At a constant $[S_2]$, Eq. 4.12 reduces to

$$\langle t \rangle_{random} = \frac{d_0'}{v_0'} + \frac{\left(\frac{v_0'e_0' - A'd_0'}{v_0'} \right) [S_1] + R'}{A'[S_1] + v_0'[S_1]^2}. \quad (4.13)$$

Here, $A' = x_0[S_2] + w_0[S_2]^2$, $v'_0 = v_0[S_2]$, $d'_0 = d_0 + k_0[S_2]$, $R' = a_0 + l_0[S_2] + n_0[S_2]^2$,
 $e'_0 = e_0 + m_0[S_2] + p_0[S_2]^2$.

Thus, the behaviour of the mean waiting time is not the same as observed for the ordered sequential mechanism. In the limit when $k_2 \rightarrow 0$ and $k_{-2} \rightarrow 0$, there is only one initial substrate binding step as a result of which Eq. 4.13 reduces to

$$\langle t \rangle_{random} = \xi + \frac{\mu}{[S_1]} \quad (4.14)$$

Here, $\xi = \frac{k_4[S_2] + k_{-4} + k_5}{k_4 k_5 [S_2]}$ and $\mu = \frac{k_{-1} k_3 (k_{-4} + k_5) + k_4 [S_2] (k_1 k_{-3} + k_3 k_5)}{k_1 k_3 k_4 [S_2] k_5}$. This resembles the classical

MM equation. The mean waiting time $\langle t \rangle_{random}$ behaves non-linearly as a function of the concentration of S_1 for a fixed $[S_2]$ (Eq. 4.13). The non-MM behaviour of the enzyme corresponds to a cooperative effect.¹⁵ Chapter 2 of the thesis covers cooperativity and its effects for enzymatic models with different types of conformational interconversions. A MM type of behaviour recovers when one considers only a single substrate binding to the free enzyme (Eq. 4.14). Thus, the non-MM behaviour of the initial rate of product formation as a function of the substrate concentration S_1 can distinguish between the ordered and the random sequential mechanisms.

$$\begin{aligned} \partial_t P(n_E, n_{ES_1}, n_{E^*}, n_P, n_{E^*S_2}, n_{E^0}, n_Q; t) &= k_1 [S_1] (n_E + 1) P(n_E + 1, n_{ES_1} - 1, n_{E^*}, n_P, n_{E^*S_2}, n_{E^0}, n_Q; t) \\ &+ k_{-1} (n_{ES_1} + 1) P(n_E - 1, n_{ES_1} + 1, n_{E^*}, n_P, n_{E^*S_2}, n_{E^0}, n_Q; t) \\ &+ k_2 (n_{ES_1} + 1) P(n_E, n_{ES_1} + 1, n_{E^*} - 1, n_P - 1, n_{E^*S_2}, n_{E^0}, n_Q; t) \\ &+ k_3 [S_2] (n_{E^*} + 1) P(n_E, n_{ES_1}, n_{E^*} + 1, n_P, n_{E^*S_2} - 1, n_{E^0}, n_Q; t) \\ &+ k_{-3} (n_{E^*S_2} + 1) P(n_E, n_{ES_1}, n_{E^*} - 1, n_P, n_{E^*S_2} + 1, n_{E^0}, n_Q; t) \\ &+ k_4 (n_{E^*S_2} + 1) P(n_E, n_{ES_1}, n_{E^*}, n_P, n_{E^*S_2} + 1, n_{E^0} - 1, n_Q - 1; t) \\ &- (k_1 [S_1] n_E + (k_{-1} + k_2) n_{ES_1} + k_3 [S_2] n_{E^*} + (k_{-3} \\ &+ k_4) n_{E^*S_2}) P(n_E, n_{ES_1}, n_{E^*}, n_P, n_{E^*S_2}, n_{E^0}, n_Q; t) \end{aligned}$$

(4.15)

Eq. 4.15 shown above represents the CME for the ping-pong mechanism as given in Figure 4.1(c). The joint probability distribution shown in Eq. 4.15 reduces to the following set of coupled ordinary differential equations.

$$\frac{\partial P_E(t)}{\partial t} = -k_1[S_1]P_E(t) + k_{-1}P_{ES_1}(t) + \delta_0 P_{E^0}(t) \quad (4.16.a)$$

$$\frac{\partial P_{ES_1}(t)}{\partial t} = k_1[S_1]P_E(t) - (k_{-1} + k_2)P_{ES_1}(t) \quad (4.16.b)$$

$$\frac{\partial P_{E^*}(t)}{\partial t} = k_2P_{ES_1}(t) - k_3[S_2]P_{E^*}(t) + k_{-3}P_{E^*S_2}(t) \quad (4.16.c)$$

$$\frac{\partial P_{E^*S_2}(t)}{\partial t} = k_3[S_2]P_{E^*}(t) - (k_{-3} + k_4)P_{E^*S_2}(t) \quad (4.16.d)$$

$$\frac{\partial P_{E^0}(t)}{\partial t} = k_4P_{E^*S_2}(t) - \delta_0 P_{E^0}(t) \quad (4.16.e)$$

Solving the above set of differential equations gives Eq. 4.17.

$$\begin{bmatrix} \hat{P}_E(s) \\ \hat{P}_{ES_1}(s) \\ \hat{P}_{E^*}(s) \\ \hat{P}_{E^*S_2}(s) \\ \hat{P}_{E^0}(s) \end{bmatrix} = \begin{bmatrix} \frac{s^3 + \alpha_1 s^2 + \alpha_2 s + \alpha_3}{s^4 + \gamma_1 s^3 + \delta_1 s^2 + \delta_2 s + \delta_3} \\ \frac{\alpha_4 s^2 + \alpha_5 s + \alpha_6}{s^4 + \gamma_1 s^3 + \delta_1 s^2 + \delta_2 s + \delta_3} \\ \frac{\alpha_8 s + \alpha_7}{s^4 + \gamma_1 s^3 + \delta_1 s^2 + \delta_2 s + \delta_3} \\ \frac{\alpha_9}{s^4 + \gamma_1 s^3 + \delta_1 s^2 + \delta_2 s + \delta_3} \\ 0 \end{bmatrix} \quad (4.17)$$

Here $\vartheta_1 = k_{-1} + k_2$, $\vartheta_2 = k_{-3} + k_4$, $\alpha_1 = \vartheta_1 + \vartheta_2 + k_3[S_2]$, $\alpha_2 = \vartheta_1(\vartheta_2 + k_3[S_2]) + k_3 k_4[S_2]$, $\alpha_3 = \vartheta_1 k_3 k_4[S_2]$, $\gamma_1 = \alpha_1 + k_1[S_1]$, $\alpha_4 = k_1[S_1]$, $\alpha_5 = \alpha_4(\vartheta_2 + k_3 k_4[S_2])$,

$\alpha_6 = k_1 k_3[S_1][S_2]$, $\alpha_7 = k_1 k_2[S_1]$, $\alpha_8 = k_1 k_2(k_{-3} + k_4)[S_1]$, $\alpha_9 = k_1 k_2 k_3[S_1][S_2]$,

$\delta_1 = (\vartheta_1 + k_1[S_1])(\vartheta_2 + k_3[S_2]) + k_1 k_2[S_1] + k_3 k_4[S_2]$, $\delta_3 = k_1 k_2 k_3 k_4[S_1][S_2]$ and

$\delta_2 = (\vartheta_2 + k_3[S_2])k_1 k_2[S_1] + k_{-1} k_3 k_4[S_2] + k_2 k_3 k_4[S_2] + k_1 k_3 k_4[S_1][S_2]$.

From the obtained solution, calculating waiting time distribution function $\hat{f}(s)$ as

$$\hat{f}(s) = k_4 \hat{P}_{E^* S_2}(s) = \frac{k_4 \alpha_9}{s^4 + \gamma_1 s^3 + \delta_1 s^2 + \delta_2 s + \delta_3}. \quad (4.18)$$

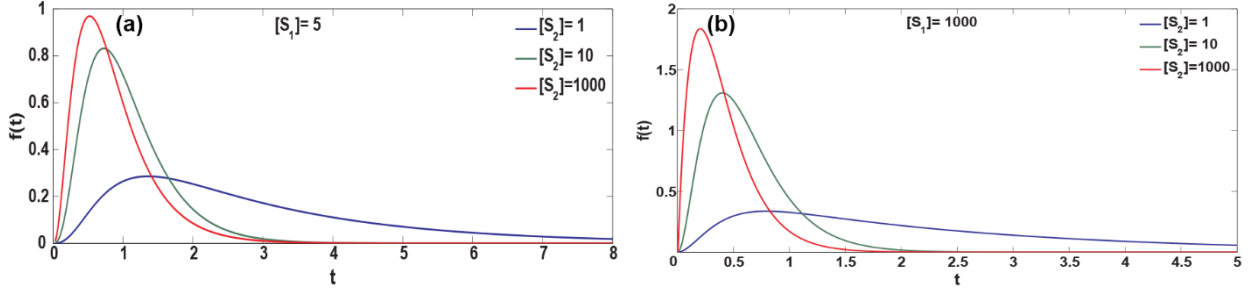


Figure 4.4: Plot of the dimensionless waiting time distribution as a function of the dimensionless time for the non-sequential ping-pong mechanism at (a) moderate concentration $[S_1] = 5$ and (b) high concentration $[S_1] = 1000$ at three concentrations of the second substrate, $[S_2] = 1$ (blue line), $[S_2] = 10$ (green line), and $[S_2] = 1000$ (red line). Parameter values chosen are $k_1 = k_{-1} = k_3 = k_{-3} = 0.5$ and $k_2 = k_4 = 5$.

The waiting time distribution behaves similarly to the sequential mechanism at low and intermediate substrate concentration, $[S_1]$. However, the distribution of the waiting times behaves differently at high $[S_1]$. Unlike the sequential pathways, the distribution decays multi-exponentially at high $[S_1]$, irrespective of the concentration $[S_2]$. The distribution becomes steeper and narrower with increasing $[S_2]$ at large values of $[S_1]$ but never follows an exponential decay pattern (Figure 3(b)). In the ping-pong mechanism, at high concentrations of S_1 and S_2 , there exists a competition between the two product formation timescales. Our theoretical results are validated against stochastic simulations based on the Gillespie algorithm.¹⁶ The difference in the distribution profiles at high concentrations can distinguish between the sequential and the ping-pong mechanism at the SM level.

The first moment of Eq. 4.18 gives the average turnover time.

$$\langle t \rangle_{ping\ pong} = \frac{A_0}{[S_1]} + \frac{B_0}{[S_2]} + C_0 \quad (4.19)$$

Here, $A_0 = \frac{(k_{-1} + k_2)}{k_1 k_2}$, $B_0 = \frac{(k_{-3} + k_4)}{k_3 k_4}$ and $C_0 = \frac{1}{k_2} + \frac{1}{k_4}$. If $[S_2]$ is constant then the expression

for average turnover time reduces to MM type of equation given as

$$\langle t \rangle_{ping-pong} = D_0 + \frac{A_0}{[S_1]}. \quad (4.20)$$

Here, $D_0 = \frac{B_0}{[S_2]} + C_0$.

To quantify the time dependent fluctuations present in different bisubstrate mechanisms, we evaluate the randomness parameter. Eq. 4.21 represents R , for the sequential ordered pathway.

$$R_{ordered} = 1 - \frac{[S_1][S_2](J+I[S_1]+L[S_2])}{[M+N[S_1]+P[S_2]+Q[S_1][S_2]]^2} \quad (4.21)$$

Here, $J = 2k_1k_2k_3(k_{-1} + k_{-2} + k_3)$, $I = 2k_1^2k_2k_3$, $L = 2k_1k_2^2k_3$, $M = (k_{-2} + k_3)k_{-1}$, $N = (k_{-2} + k_3)k_1$, $P = k_2k_3$ and $Q = k_1k_2$.

From the above expression, it is clear that the randomness parameter is not equal to unity at high substrate concentration. However, when $[S_1] \rightarrow 0$, the value of $R_{ordered}$ is equal to unity irrespective of the concentration of the second substrate ($[S_2]$). For the physical scenario, when $[S_1]$ is very large and $[S_2]$ has low to intermediate values, Eq. 4.21 reduces to Eq. 4.22.

$$R_{ordered} = \frac{N^2+U[S_2]+Q^2[S_2]^2}{N^2+V[S_2]+Q^2[S_2]^2} \quad (4.22)$$

Here, $U = 2k_1^2k_2k_{-2}$, and $V = 2k_1^2k_2(k_{-2} + k_3)$. Further, if $[S_2] \rightarrow 0$ or $[S_2]$ is very large then the value of $R_{ordered}$ (Eq. 4.22) will be unity.

Figure 4.5(a) graphically depicts the randomness parameter (Eq. 4.21) for the ordered sequential mechanism. At intermediate concentrations of $[S_1]$ and $[S_2]$, the probability of transitions between different intermediate states increases. Such a multi-step cascade leads to a non-monotonic variation of the randomness parameter. At high substrate concentration of $[S_1]$, and an intermediate $[S_2]$, R saturates to a value other than unity indicating transitions between the intermediate steps in the reaction pathway (Eq. 4.22). At high $[S_2]$, the product formation step is the rate-determining step, and R saturates to unity (solid black line). The sequential random mechanism also shows similar observations represented in Figure 4.5(b).

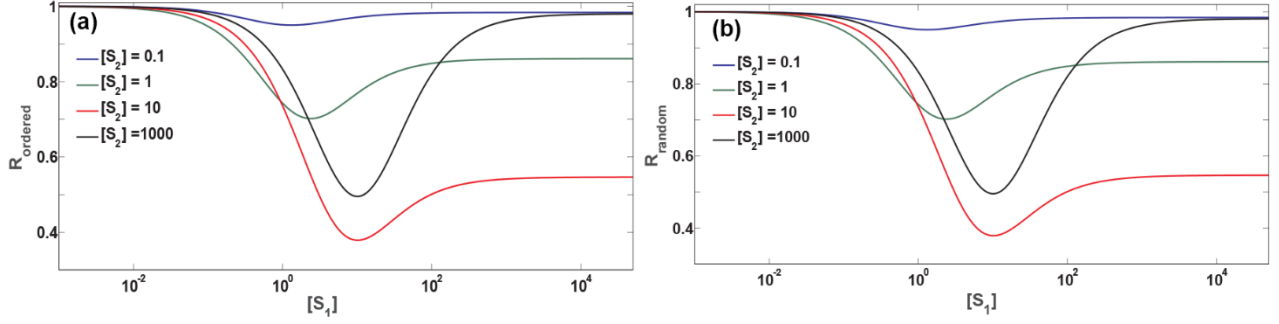


Figure 4.5: Variation of the randomness parameter as a function of the substrate concentration $[S_1]$ (in dimensionless units) at different values of $[S_2]$ for the (a) ordered and (b) random pathway. The randomness parameter deviates from unity at high concentration of $[S_1]$ and at an intermediate concentration of S_2 , ($[S_2 = 1]$: green line and $[S_2] = 10$: red line). At high concentration of S_2 , the randomness parameter is unity for both ordered and random mechanisms ($[S_2] = 1000$, black line). Kinetic parameter values for ordered and random mechanisms are same as in Figures 4.2 and 4.3 respectively.

Eq. 4.23 represents the randomness parameter for the ping-pong mechanism.

$$R_{ping-pong} = 1 - \frac{G_0[S_1]^2[S_2]^2 + H_0[S_1]^2[S_2] + F_0[S_1][S_2]^2 + E_0[S_1][S_2]}{[J_0[S_1][S_2] + K_0[S_1] + L_0[S_2]]^2} \quad (4.23)$$

Here, $E_0 = 2k_1k_2k_3k_4(k_{-1} + k_2)(k_{-3} + k_4)$, $F_0 = 2k_1k_2k_3^2k_4(k_{-1} + k_2 + k_4)$, $G_0 = 2k_1^2k_2k_3^2k_4$, $H_0 = 2k_1^2k_2k_3k_4(k_2 + k_{-3} + k_4)$, $J_0 = k_1k_3(k_2 + k_4)$, $K_0 = k_1k_2(k_{-3} + k_4)$ and $L_0 = k_3k_4(k_{-1} + k_2)$.

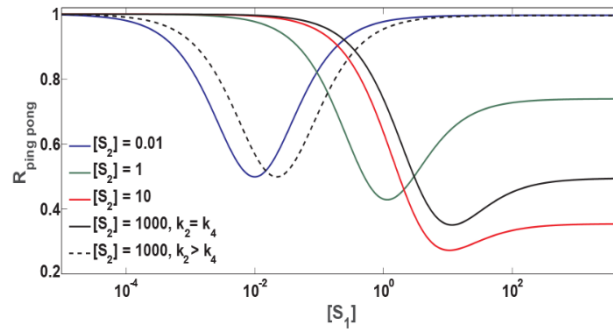


Figure 4.6: Variation of the randomness parameter as a function of the substrate concentration $[S_1]$ (in dimensionless units) at different values of $[S_2]$ for ping-pong mechanism. The randomness parameter does not saturate to unity at high concentration of $[S_1]$ and at intermediate to a high concentration of S_2 ($[S_2=1]$: green line, $[S_2] = 10$: red line and $[S_2] = 1000$: black line). At high concentration of S_2 , when $k_2 > k_4$, the randomness parameter reduces to unity (black dashed line). Kinetic parameter values are same as in Figure 4.4.

Thus, unlike the sequential kinetic mechanism of bi-substrate binding, the randomness parameter for the ping-pong mechanism attains a constant value other than unity when both

substrates S_1 and S_2 are present in excess. The randomness parameter saturates at a value different from unity at high concentration of $[S_1]$ irrespective of $[S_2]$ (black solid line). The interconversions between multiple intermediate states affect the timescale of the product formation and thus leading to dynamic disorder. When k_2 is much larger than k_4 , then k_4 is the rate-determining step and the randomness parameter decays to unity (black dashed line) at high $[S_1]$ and $[S_2]$. Thus, the magnitude of the temporal fluctuations depends on the type of the bisubstrate binding mechanism at various concentrations of the substrates.

4.3 Conclusions:

In this chapter, we use the chemical master equation approach to study the kinetics of a single enzyme binding to multiple substrates either in a sequential or a non-sequential manner under the substrate abundance assumption at short times.^{17,18} We obtain closed-form analytical expressions for the waiting time distribution from which the mean waiting time and the randomness parameter are calculated. We fix one substrate concentration at some low to moderate value, the waiting time distribution is multi-exponential and the randomness parameter deviates from unity at high concentration of the other substrate. For the sequential mechanisms (Figures 4.1(a) and 4.1(b)), the waiting time distribution becomes single-exponential and the randomness parameter saturates to unity at high concentrations of both the substrates. The distribution profile and the randomness parameter is same for both the sequential mechanisms. This is not the case for non-sequential binding, where the waiting time distribution remains multi-exponential and the randomness parameter is not equal to unity at high substrate concentrations.

At a quasi-statically fixed concentration of one substrate, the mean waiting time recovers a MM type reaction, *i.e.* it has a linear dependence on the inverse of the concentration of the other substrate for the ordered and the ping-pong mechanism. However, there are deviations from this linear behaviour when one considers the random mechanism. Here one

can observe a non-MM behaviour as the binding of one of the substrate influences the simultaneous binding of the other substrate to the single enzyme. Thus, such stochastic analysis of the rate of product formation can distinguish the two pathways of sequential bisubstrate binding.

4.4 References:

- (1) Michaelis, L.; Menten, M. L. *Biochem. Z.* **1913**, *49*, 333.
- (2) Cleland, W. W. *Biochim. Biophys. Acta* **1963**, *67*, 104.
- (3) Marangoni, A. G. *Substrate Reactions, in Enzyme Kinetics: A Modern Approach*; John Wiley & Sons, Inc.: Hoboken, NJ, USA., 2002; Vol. 10.1002/0471267295.ch7.
- (4) Segel, I. H. *Enzyme Kinetics: Behaviour and Analysis of Rapid Equilibrium and Steady State Enzymes Systems*; Wiley: New York, 1993.
- (5) Grima, R.; Leier, A. *J. Phys. Chem. B* **2016**, *121*, 13.
- (6) Lu, H. P.; Xun, L.; Xie, X. S. *Science* **1998**, *282*, 1877.
- (7) English, B. P.; Min, W.; van Oijen, A. M.; Lee, K. T.; Luo, G.; Sun, H.; Cherayil, B. J.; Kou, S. C.; Xie, X. S. *Nat. Chem. Biol.* **2006**, *2*, 87.
- (8) Schwabe, A.; Maarleveld, T. R.; Bruggeman, F. J. *FEBS Lett.* **2013**, *587*, 2744.
- (9) Avila, T. R.; Piephoff, D. E.; Cao, J. *J. Phys. Chem. B* **2017**, *121*, 7750.
- (10) Chaudhury, S.; Cao, J.; Sinitsyn, N. A. *J. Phys. Chem. B* **2013**, *117*, 503.
- (11) Gardiner, C. W. *Handbook of Stochastic Methods: for Physics, Chemistry, and the Natural Sciences*; Springer: New York, 1996.
- (12) Kolomeisky, A. B. *J. Chem. Phys.* **2011**, *134*, 155101.
- (13) Cao, J. *J. Phys. Chem. B* **2011**, *115*, 5493.
- (14) Qian, H.; Bishop, L. M. *Int. J. Mol. Sci.* **2010**, *11*, 3472.
- (15) Cornish-Bowden, A. *Fundamentals of Enzyme Kinetics*,; 3rd ed.; Portland Press: London, 2004.
- (16) Gillespie, D. T. *J. Phys. Chem.* **1977**, *81*, 2340.
- (17) Kou, S. C.; Cherayil, B. J.; Min, W.; English, B. P.; Xie, X. S. *J. Phys. Chem. B* **2005**, *109*, 19068.
- (18) Chaudhury, S. *J. Phys. Chem. B* **2014**, *118*, 10405.

5. Effect of substrate number fluctuations in stochastic enzyme kinetics

Reprinted from “Singh, D.; Chaudhury, S., ACS Omega 2018, 3, 5574-5583.” with the permission from the ACS publishing.

<https://pubs.acs.org/doi/10.1021/acsomega.8b00611>

Readers please note that further permissions related to the material excerpted should be directed to the ACS.

© 2018 American Chemical Society

5.1 Introduction:

In our previous thesis chapters (2, 3 and 4), we have modelled enzymatic chemical reactions involving single and multiple type of substrates at the SM level. For determining the reaction velocity, one applies the steady state approximation, which ensures excess substrate availability for the initial phase of reaction. That is why in the application of the probabilistic treatments, substrate number changes are not present in the time evolution equations. However, the consumption of the substrate molecules with the reaction progression will consequently decrease its number. At the SM level, following the chemical master equation approach, it has been shown that if the substrate is present in abundance and the conformational detailed balance is satisfied, the average rate follows the MM form.^{1,2} However, there are many chemical systems where the substrate concentration is comparable or limiting to that of the catalyst. For instance, in the living cells, the assumption that the substrate is present in abundance may not be always valid.³ Recently Grima and Leier have used the chemical master equation technique to study a wide range of enzymatic reaction mechanisms and obtain the average rate of product formation without including the substrate abundance assumption.⁴ This study confirmed that at long times, the rate attains a logarithmically corrected MM type of equation.

In this chapter, we study a more realistic situation using the CME approach. The main objective of this chapter is to model the catalytic activity of an enzyme in an intracellular environment. Here the substrate molecules enter into a compartment, and on the completion of the catalytic cycle, the product molecules leave the compartment. To account for the substrate fluctuations, one must explicitly include the number of substrate molecules as a variable in the joint probability distribution. Here we consider two examples: an enzymatic reaction with one intermediate enzyme-substrate complex that corresponds to a MM mechanism and a reaction scheme with two intermediate enzyme-substrate complexes. Our model demonstrates

that the effect of the substrate fluctuations across the compartment membrane in one (influx) or both directions (influx and out-flux). The processing of the substrate units by the single enzyme will lead to the product formation (turnover rate). For these model systems, the functional form of the reaction velocity does not follow the MM relation.

In order to study the stochastic noise present in the system, one can calculate the higher moments of the PDF. Grima has also studied the role of noise in multi-subunit enzymes where one can obtain an expression for protein fluctuations.^{5,6} One can measure the stochastic fluctuations through a dimensionless quantity, known as the coefficient of variation. Eq. 1 represents its mathematical form.

$$\sigma = \frac{\sqrt{\langle n^2 \rangle - \langle n \rangle^2}}{\langle n \rangle} \quad (5.1)$$

Here n is the number of substrate molecules present in the compartment at some definite time.

5.2 Reaction Models and Analyses:

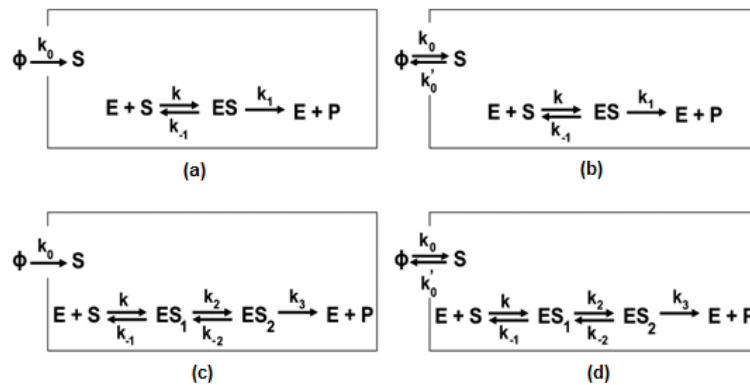


Figure 5.1: Schematic representation of catalytic reaction schemes associated with (a) an irreversible substrate flow with one intermediate, (b) a reversible substrate flow with one intermediate, (c) an irreversible substrate flow with two intermediates, and (d) a reversible substrate flow with two intermediates.

We consider four examples in which a single enzyme catalyses the formation of the product in an intercellular environment, where substrate molecules are fed in at a constant rate k_0 . In the first two cases, the enzymatic reaction involves a single intermediate complex ES (Figures 5.1(a) and 5.1(b)). Such unidirectional transport mechanisms are common inside cells.⁷ For the

case with a bidirectional substrate flow, along with influx, we consider an additional backward reaction for the substrate out-flux in the reaction scheme with an average rate equal to k'_0 . Next, we consider two other schemes that involve two intermediate complexes, ES_1 and ES_2 . For all these different models, we describe the system by $P[p, n, J, t]$, the probability that when the enzyme is in state J , p molecules are processed and n substrate molecules are present in the compartment at time t . $J = 0$ represents the free enzyme and $J = 1$ corresponds to the bound enzyme such that $P[p, n, J = 0, t] = P_0[p, n, t]$ and $P[p, n, J = 1, t] = P_1[p, n, t]$. We use the steady state approximation which allows us to write these master equations as a set of reduced distributions that can be solved for the turnover rate and also derive the moments of the distribution.⁸ Eq. 5.2 represents the chemical master equations for the probability distributions for the scheme shown in Figure 5.1(a).

$$\begin{aligned} \frac{\partial P_0[p, n, t]}{\partial t} = & -nkP_0[p, n, t] + k_{-1}P_1[p + 1, n - 1, t] + k_1P_1[p, n, t] - k_0P_0[p, n, t] \\ & + k_0P_0[p, n - 1, t] \end{aligned} \quad (5.2a)$$

$$\begin{aligned} \frac{\partial P_1[p, n, t]}{\partial t} = & (n + 1)kP_0[p - 1, n + 1, t] - (k_{-1} + k_1)P_1[p, n, t] - k_0P_1[p, n, t] \\ & + k_0P_1[p, n - 1, t] \end{aligned} \quad (5.2b)$$

On rescaling, $\tau = kt$, $\epsilon_{-1} = \frac{k_{-1}}{k}$, $\epsilon_1 = \frac{k_1}{k}$ and $\theta = \frac{k_0}{k}$, Eq. 5.2 takes the following form.

$$\begin{aligned} \frac{\partial P_0[p, n, \tau]}{\partial \tau} = & -nP_0[p, n, \tau] + \epsilon_{-1}P_1[p + 1, n - 1, \tau] + \epsilon_1P_1[p, n, \tau] - \theta P_0[p, n, \tau] \\ & + \theta P_0[p, n - 1, \tau] \end{aligned} \quad (5.3a)$$

$$\begin{aligned}\frac{\partial P_1[p, n, \tau]}{\partial \tau} &= (n+1)P_0[p-1, n+1, \tau] - (\epsilon_1 + \epsilon_{-1})P_1[p, n, \tau] - \theta P_1[p, n, \tau] \\ &\quad + \theta P_1[p, n-1, \tau]\end{aligned}\tag{5.3b}$$

The normalization condition $\sum_{p,n}(P_0[p, n, \tau] + P_1[p, n, \tau]) = 1$ must be satisfied at all times.

Eq. 5.4 represents the turnover rate under the steady state approximation.

$$V = \frac{\partial \langle p \rangle}{\partial \tau} = \sum_{p,n} p(P_0[p, n, \tau] + P_1[p, n, \tau]) \quad . \tag{5.4}$$

For Figure 5.1(a), we can reduce the distributions in the form mentioned below.

$$\sum_p P_0[p, n, \tau] = Q_0[n, \tau]$$

$$\sum_p P_1[p, n, \tau] = Q_1[n, \tau]$$

Following the reduced form of the distributions, Eq. 5.3 becomes

$$\frac{\partial Q_0[n, \tau]}{\partial \tau} = -nQ_0[n, \tau] + \epsilon_{-1}Q_1[n-1, \tau] + \epsilon_1Q_1[n, \tau] - \theta Q_0[n, \tau] + \theta Q_0[n-1, \tau] \tag{5.5a}$$

$$\frac{\partial Q_1[n, \tau]}{\partial \tau} = (n+1)Q_0[n+1, \tau] - (\epsilon_1 + \epsilon_{-1})Q_1[n, \tau] - \theta Q_1[n, \tau] + \theta Q_1[n-1, \tau] \tag{5.5b}$$

Similarly, the velocity equation takes the form

$$V = \sum_n nQ_0[n, \tau] - \epsilon_{-1} \sum_n Q_1[n, \tau]. \tag{5.6}$$

Eq. 5.7 defines the N^{th} moment of the distribution corresponding to any particular state.

$$\sum_n n^q Q_0[n, \tau] = \mu_q^{(0)} \tag{5.7a}$$

$$\sum_n n^q Q_1[n, \tau] = \mu_q^{(1)} \tag{5.7b}$$

Following Eq. 5.7, the velocity expression in Eq. 5.6 reduces to Eq. 5.8.

$$V = \mu_1^{(0)} - \epsilon_{-1}\mu_0^{(1)} \tag{5.8}$$

In the steady state approximation, $\frac{\partial Q_0[n, \tau]}{\partial \tau} = 0$ and $\frac{\partial Q_1[n, \tau]}{\partial \tau} = 0$ which give the following set.

$$(n+\theta)Q_0[n, \tau] = \epsilon_{-1}Q_1[n-1, \tau] + \epsilon_1Q_1[n, \tau] + \theta Q_0[n-1, \tau] \tag{5.9a}$$

$$(\epsilon_1 + \epsilon_{-1} + \theta)Q_1[n, \tau] = (n+1)Q_0[n+1, \tau] + \theta Q_1[n-1, \tau] \tag{5.9b}$$

Summing Eq. 5.9a over n we get

$$\mu_1^{(0)} = (\epsilon_1 + \epsilon_{-1})\mu_0^{(1)}. \quad (5.10a)$$

Summing Eq. 5.9a over n and weighting it by n gives

$$\mu_2^{(0)} = (\epsilon_1 + \epsilon_{-1})\mu_1^{(1)} + \epsilon_{-1}\mu_0^{(1)} + \theta\mu_0^{(0)}. \quad (5.10b)$$

Summing Eq. 5.9a over n and weighting it by n^2 leads to

$$\mu_3^{(0)} = (\epsilon_1 + \epsilon_{-1})\mu_2^{(1)} + \epsilon_{-1}\mu_0^{(1)} + 2\epsilon_{-1}\mu_0^{(1)} + \theta\mu_0^{(0)} + 2\theta\mu_1^{(0)}. \quad (5.10c)$$

Summing Eq. 5.9a over n and weighting it by n^3 yields

$$\mu_4^{(0)} = (\epsilon_1 + \epsilon_{-1})\mu_3^{(1)} + \epsilon_{-1}\mu_0^{(1)} + 3\epsilon_{-1}\mu_2^{(1)} + 3\epsilon_{-1}\mu_1^{(1)} + \theta\mu_0^{(0)} + 3\theta\mu_2^{(0)} + 3\theta\mu_1^{(0)}. \quad (5.10d)$$

Similarly, summing Eq. 5.9b over n we get

$$\mu_1^{(0)} = (\epsilon_1 + \epsilon_{-1})\mu_0^{(1)} \quad (5.11a)$$

Summing Eq. 5.9b over n and weighting it by n one can find

$$\mu_2^{(0)} = (\epsilon_1 + \epsilon_{-1})\mu_1^{(1)} + \mu_1^{(0)} - \theta\mu_0^{(1)}. \quad (5.11b)$$

Summing Eq. 5.9b over n and weighting it by n^2 yields

$$\mu_3^{(0)} = (\epsilon_1 + \epsilon_{-1})\mu_2^{(1)} - \mu_1^{(0)} + 2\mu_2^{(0)} - \theta\mu_0^{(1)} - 2\theta\mu_1^{(1)} \quad (5.11c)$$

Summing Eq. 5.9b over n and weighting it by n^3 will give

$$\mu_4^{(0)} = (\epsilon_1 + \epsilon_{-1})\mu_3^{(1)} + \mu_1^{(0)} + 3\mu_3^{(0)} - 3\mu_2^{(0)} - \theta\mu_0^{(1)} - 3\theta\mu_2^{(1)} - 3\theta\mu_1^{(1)}. \quad (5.11d)$$

Equating 5.10b and 5.11b and using the normalization condition, $\mu_0^{(0)} + \mu_0^{(1)} = 1$, we get

$$V = \theta = \mu_1^{(0)} - \epsilon_{-1}\mu_0^{(1)} \quad (5.12)$$

Equating 5.10c and 5.11c one can deduce

$$\mu_2^{(0)} = \left(\frac{\theta + \epsilon_{-1}}{2}\right)\mu_0^{(1)} + (\theta + \epsilon_{-1})\mu_1^{(1)} + \frac{\theta}{2}\mu_0^{(0)} + \left(\theta + \frac{1}{2}\right)\mu_1^{(0)}. \quad (5.13)$$

Equating 5.10d and 5.11d one can obtain Eq. 5.14.

$$\begin{aligned} \mu_3^{(0)} = & \left(\frac{\theta + \epsilon_{-1}}{3}\right)\mu_0^{(1)} + (\theta + \epsilon_{-1})\mu_2^{(1)} + (\theta + \epsilon_{-1})\mu_1^{(1)} + (\theta + 1)\mu_2^{(0)} + \frac{\theta}{3}\mu_0^{(0)} \\ & + \left(\theta - \frac{1}{3}\right)\mu_1^{(0)} \end{aligned} \quad (5.14)$$

From Eq. 5.13 and Eq. 5.9b we get the desired equation to be solved for θ

$$\left(\frac{\theta - \epsilon_{-1}}{23}\right)\mu_0^{(1)} + (\theta - \epsilon_1)\mu_1^{(1)} - \frac{\theta}{2}\mu_0^{(0)} + \left(\theta + \frac{1}{2}\right)\mu_1^{(0)} = 0 \quad (5.15)$$

For obtaining an equation in terms of the variable θ that represents the reaction velocity, we need the moments of respective states present in Eq. 5.15 in terms of reaction rate constants.

From normalization condition and definition of $\langle n \rangle$ we have

$$\mu_0^{(0)} + \mu_0^{(1)} = 1 \text{ and } \mu_1^{(0)} + \mu_1^{(1)} = \langle n \rangle.$$

Putting Eq. 5.10a into Eq. 5.12 we get

$$\mu_0^{(1)} = \frac{\theta}{\epsilon_1} \quad (5.16)$$

Putting Eq. 5.16 in Eq. 5.10a we obtain

$$\mu_1^{(0)} = \theta + \frac{\epsilon_{-1}}{\epsilon_1}\theta \quad (5.17)$$

From the definition of $\langle n \rangle$ we get

$$\mu_1^{(1)} = \langle n \rangle - \theta - \frac{\epsilon_{-1}}{\epsilon_1}\theta \quad (5.18)$$

From normalization we get

$$\mu_0^{(0)} = 1 - \frac{\theta}{\epsilon_1} \quad (5.19)$$

Substituting Eq. 5.16 to Eq. 5.19 into Eq. 5.15, followed by some rearrangements we obtain a quadratic equation in terms of variable θ .

$$\frac{\theta^2}{\epsilon_1} + \theta(\langle n \rangle + z) - \langle n \rangle \epsilon_1 = 0 \quad (5.20)$$

Eq. 5.21 represents the solution of Eq. 5.20.

$$V = \theta = \frac{\epsilon_1}{2}(\langle n \rangle + z) \left[\sqrt{1 + \frac{4\langle n \rangle}{(\langle n \rangle + z)^2}} - 1 \right] \quad (5.21)$$

Here, $z = \epsilon_1 + \epsilon_{-1}$. When $\langle n \rangle + z \gg 2\sqrt{n}$, which is true at high substrate concentration, or at large values of z , Eq. 5.21 can be binomially expanded as

$$V = \theta = \frac{\epsilon_1}{2} (\langle n \rangle + z) \left[1 + \left(\frac{1}{2}\right) \frac{4\langle n \rangle}{(\langle n \rangle + z)^2} - \left(\frac{1}{4}\right) \frac{\left(\frac{4\langle n \rangle}{(\langle n \rangle + z)^2}\right)^2}{2!} + \dots - 1 \right].$$

Neglecting the higher order terms and simplifying, the above equation reduces to a MM form.

$$V_{MM} = \theta = \frac{\epsilon_1 \langle n \rangle}{\langle n \rangle + z} \quad (5.22)$$

Thus at higher substrate concentrations and higher values of z (at a given value of $\langle n \rangle$), the velocity equation behaves as MM type equation. As shown in Figures 5.2 (a) and 5.2(b), we compare Eq. 5.21 with the MM relation (Eq. 22) and different values of z by varying ϵ_1 . The difference between the two curves is more at lower values of ϵ_1 . Also at a higher value of z , the two curves come closer at higher substrate concentrations where the effect of fluctuations is less prominent.

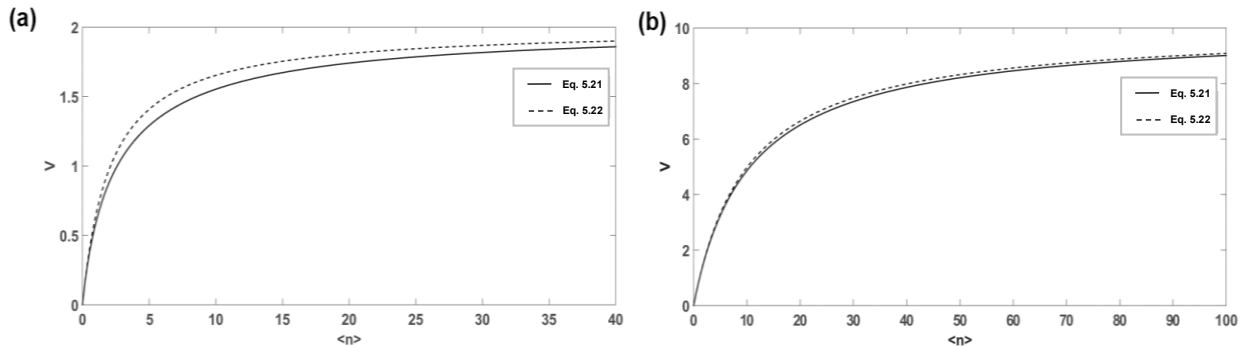


Figure 5.2: Variation of reaction velocity V as a function of average number of substrate molecules $\langle n \rangle$ for the scheme with one intermediate and irreversible substrate flow at (a) $\epsilon_1 = 2$, $\epsilon_{-1} = 0.1$ and (b) $\epsilon_1 = 10$, $\epsilon_{-1} = 0.1$. Solid line represents the velocity expression (Eq. 5.21) and dashed line is the velocity in the MM limit (Eq. 5.22).

For deducing $\langle n^2 \rangle$, analytical forms of $\mu_2^{(0)}$ and $\mu_2^{(1)}$ are required.

Substituting 5.16, 5.18 and 5.19 in Eq. 5.10b we get Eq. 5.23.

$$\mu_2^{(0)} = -\frac{\theta^2}{\epsilon_1} + \theta \left[\frac{z(1-z)}{\epsilon_1} \right] + z\langle n \rangle \quad (5.23)$$

Equating Eq. 5.14 and 5.11c we obtain

$$\mu_2^{(1)} = \frac{\theta^3 + \theta^2 z(1+z) + \theta(\epsilon_1 z - \epsilon_1(1+z)\langle n \rangle) - \epsilon_1^2 \langle n \rangle}{\epsilon_1(\theta - \epsilon_1)}. \quad (5.24)$$

Substituting Eq. 5.23 and 5.24 in Eq. 5.22 gives the required expression of $\langle n^2 \rangle$ for Figure 5.1(a).

$$\langle n^2 \rangle = \mu_2^{(0)} + \mu_2^{(1)} = \frac{\theta^2(2z+\epsilon_1)+\theta(\epsilon_1z^2-(n)\epsilon_1)-\langle n \rangle\epsilon_1^2(1+z)}{\epsilon_1(\theta-\epsilon_1)} \quad (5.25)$$

Using Eq. 5.25, we calculate the coefficient of variation σ as defined in Eq. 5.1.

For the catalytic reaction scheme described in Figure 5.1(b) with an additional backward reaction at an average rate equal to k'_0 , Eq. 5.26 represents the master equations

$$\begin{aligned} \frac{\partial P_0[p, n, t]}{\partial t} = & -nkP_0[p, n, t] + k_{-1}P_1[p + 1, n - 1, t] + k_1P_1[p, n, t] + k_0P_0[p, n - 1, t] \\ & + k'_0P_0[p, n + 1, t] - (k_0 + k'_0)P_0[p, n, t] \end{aligned} \quad (5.26a)$$

$$\begin{aligned} \frac{\partial P_1[p, n, t]}{\partial t} = & (n + 1)kP_0[p - 1, n + 1, t] - (k_{-1} + k_1)P_1[p, n, t] + k_0P_1[p, n - 1, t] \\ & + k'_0P_1[p, n + 1, t] - (k_0 + k'_0)P_1[p, n, t] \end{aligned} \quad (5.26b)$$

and satisfies the normalization condition $\sum_{p,n}(P_0[p, n, \tau] + P_1[p, n, \tau])$. Following the

rescaling as $\epsilon_{-1} = \frac{k_{-1}}{k}$, $\epsilon_1 = \frac{k_1}{k}$, $\eta = \frac{k'_0}{k}$ and $\theta = \frac{k_0}{k}$, the master equations reduce to Eq. 5.27.

$$\begin{aligned} \frac{\partial Q_0[n, \tau]}{\partial \tau} = & -nQ_0[n, \tau] + \epsilon_{-1}Q_1[n - 1, \tau] + \epsilon_1Q_1[n, \tau] + \theta Q_0[n - 1, \tau] + \eta Q_0[n + 1, \tau] \\ & - (\theta + \eta)Q_0[n, \tau] \end{aligned} \quad (5.27a)$$

$$\begin{aligned} \frac{\partial Q_1[n, \tau]}{\partial \tau} = & (n + 1)Q_0[n + 1, \tau] - (\epsilon_1 + \epsilon_{-1})Q_1[n, \tau] + \theta Q_1[n - 1, \tau] + \eta Q_1[n + 1, \tau] \\ & - (\theta + \eta)Q_1[n, \tau] \end{aligned} \quad (5.27b)$$

For the given model, in the steady state the turnover has the following form.

$$V = \mu_1^{(0)} - \epsilon_{-1}\mu_0^{(1)} \quad (5.28)$$

Using the steady-state approximation, $\frac{\partial Q_0[n,\tau]}{\partial \tau} = 0$ and $\frac{\partial Q_1[n,\tau]}{\partial \tau} = 0$, gives the following set of equations.

$$(n + \theta + \eta)Q_0[n, \tau] = \epsilon_{-1}Q_1[n - 1, \tau] + \epsilon_1Q_1[n, \tau] + \theta Q_0[n - 1, \tau] + \eta Q_0[n + 1, \tau] \quad (5.29a)$$

$$(\epsilon_1 + \epsilon_{-1} + \theta + \eta)Q_1[n, \tau] = (n + 1)Q_0[n + 1, \tau] + \theta Q_1[n - 1, \tau] + \eta Q_1[n + 1, \tau] \quad (5.29b)$$

Summing 5.29a over n, weighting it by n, n^2, n^3

$$\mu_1^{(0)} = (\epsilon_1 + \epsilon_{-1})\mu_0^{(1)} \quad (5.30a)$$

$$\mu_2^{(0)} = (\epsilon_1 + \epsilon_{-1})\mu_1^{(1)} + \epsilon_{-1}\mu_0^{(1)} + (\theta - \eta)\mu_0^{(0)} \quad (5.30b)$$

$$\mu_3^{(0)} = (\epsilon_1 + \epsilon_{-1})\mu_2^{(1)} + \epsilon_{-1}\mu_0^{(1)} + 2\epsilon_{-1}\mu_1^{(1)} + (\theta + \eta)\mu_0^{(0)} + 2(\theta - \eta)\mu_1^{(0)} \quad (5.30c)$$

$$\begin{aligned} \mu_4^{(0)} = & (\epsilon_1 + \epsilon_{-1})\mu_3^{(1)} + \epsilon_{-1}\mu_0^{(1)} \\ & + 3\epsilon_{-1}\mu_2^{(1)} + 3\epsilon_{-1}\mu_1^{(1)} + (\theta - \eta)\mu_0^{(0)} + 3(\theta - \eta)\mu_2^{(0)} + 3(\theta + \eta)\mu_1^{(0)} \end{aligned} \quad (5.30d)$$

Summing 5.29b over n, weighting it by n, n^2, n^3

$$\mu_1^{(0)} = (\epsilon_1 + \epsilon_{-1})\mu_0^{(1)} \quad (5.31a)$$

$$\mu_2^{(0)} = (\epsilon_1 + \epsilon_{-1})\mu_1^{(1)} + \mu_1^{(0)} - (\theta - \eta)\mu_0^{(1)} \quad (5.31b)$$

$$\mu_3^{(0)} = (\epsilon_1 + \epsilon_{-1})\mu_2^{(1)} - \mu_1^{(0)} + 2\mu_2^{(0)} - (\theta + \eta)\mu_0^{(1)} - 2(\theta - \eta)\mu_1^{(1)} \quad (5.31c)$$

$$\begin{aligned} \mu_4^{(0)} = & (\epsilon_1 + \epsilon_{-1})\mu_3^{(1)} + \mu_1^{(0)} + 3\mu_3^{(0)} - 3\mu_2^{(0)} - (\theta - \eta)\mu_0^{(1)} - 3(\theta - \eta)\mu_2^{(1)} - 3(\theta + \eta)\mu_1^{(1)} \end{aligned} \quad (5.31d)$$

Equating 5.30b and 5.31b and using the normalization condition, we get

$$V = \theta = \mu_1^{(0)} - \epsilon_{-1}\mu_0^{(1)} + \eta \quad (5.32)$$

Equating 5.30c and 5.31c we get

$$\mu_2^{(0)} = \left(\frac{\theta + \eta + \epsilon_{-1}}{2}\right)\mu_0^{(1)} + (\theta - \eta + \epsilon_{-1})\mu_1^{(1)} + \frac{(\theta + \eta)}{2}\mu_0^{(0)} + \left(\theta - \eta + \frac{1}{2}\right)\mu_1^{(0)} \quad (5.33)$$

Equating 5.30d and 5.31d we get

$$\begin{aligned} \mu_3^{(0)} = & \left(\frac{\theta-\eta+\epsilon_{-1}}{3}\right)\mu_0^{(1)} + (\theta - \eta + \epsilon_{-1})\mu_2^{(1)} + (\theta + \eta + \epsilon_{-1})\mu_1^{(1)} + (\theta - \eta + 1)\mu_2^{(0)} + \\ & \frac{(\theta-\eta)}{3}\mu_0^{(0)} + \left(\theta + \eta - \frac{1}{3}\right)\mu_1^{(0)} \end{aligned} \quad (5.34)$$

From equations 5.33 and 5.30b we get the desired equation to be solved for θ

$$\frac{(\theta+\eta)}{2} + (\theta - \eta)\langle n \rangle - \frac{\epsilon_{-1}}{2}\mu_0^{(1)} - \epsilon_1\mu_1^{(1)} - (\theta - \eta)\mu_0^{(0)} + \frac{1}{2}\mu_1^{(0)} = 0 \quad (5.35)$$

To obtain an equation in terms of the variable θ that represents the reaction velocity, we need to calculate the moments in Eq. 5.35 in terms of reaction rate constants by using the above set of relations. As shown for Figure 5.1(a), by using the above equations, the normalization condition, and definition of $\langle n \rangle$, we get

$$\mu_0^{(1)} = \frac{(\theta-\eta)}{\epsilon_1} \quad (5.36)$$

$$\mu_1^{(0)} = (\theta - \eta) \left(\frac{\epsilon_1+\epsilon_{-1}}{\epsilon_1}\right) \quad (5.37)$$

$$\mu_1^{(1)} = \langle n \rangle - (\theta - \eta) \left(\frac{\epsilon_1+\epsilon_{-1}}{\epsilon_1}\right) \quad (5.38)$$

$$\mu_0^{(0)} = 1 - \frac{(\theta-\eta)}{\epsilon_1} \quad (5.39)$$

After substituting equations 5.36 to 5.39 in Eq. 5.35 and performing some rearrangement, we get a quadratic equation in terms of the reaction variable θ .

$$\frac{\theta^2}{\epsilon_1} + \theta \left(z + \langle n \rangle - \frac{2\eta}{\epsilon_1} \right) - \left[\epsilon_1 \langle n \rangle + \eta(z + \langle n \rangle - 1) - \frac{\eta^2}{\epsilon_1} \right] = 0 \quad (5.40)$$

Eq.5.41 represents the solution of Eq. 5.40.

$$V = \theta = \frac{\epsilon_1}{2} \left(\langle n \rangle + z - \frac{2\eta}{\epsilon_1} \right) \left[\sqrt{1 + \frac{4(\langle n \rangle(\epsilon_1+\eta) + \eta(z-1-\eta))}{\epsilon_1(\langle n \rangle + z - \frac{2\eta}{\epsilon_1})^2}} - 1 \right] \quad (5.41)$$

Thus, the functional form of the turnover rate equation changes when we include the reverse outflow reaction. For the velocity function to exist over the entire range substrate concentration, $\eta \ll \frac{\epsilon_1(\langle n \rangle + z)}{2}$ at given value of z and at a given substrate concentration $\langle n \rangle$. In Figure 5.3(a) we plot the velocity as function of average substrate concentration. We show that in the limit

when $\eta = 0$, Eq. 5.41 reduces to Eq. 5.21 (the dotted line and the black circles coincide with each other).

In the limit when $\langle n \rangle + z - \frac{2\eta}{\epsilon_1} \gg 2 \sqrt{\frac{\langle n \rangle(\epsilon_1 + \eta) + \eta(z-1-\eta)}{\epsilon_1}}$ which is true at high substrate concentration, or at large values of z and small values of η (at a given substrate concentration), Eq. 5.41 can be binomially expanded and neglecting the higher order terms and simplifying we get Eq. 5.42.

$$V = \frac{\langle n \rangle(\epsilon_1 + \eta) + \eta(z-1) - \eta^2}{\langle n \rangle + z - \frac{2\eta}{\epsilon_1}} \quad (5.42)$$

Further, in the limit when $z \gg \eta$, the above equation reduces the MM velocity expression.

$$V_{MM} = \frac{\langle n \rangle(\epsilon_1 + \eta)}{\langle n \rangle + z - \frac{2\eta}{\epsilon_1}} \quad (5.43)$$

In order to take the limit of $z \gg \eta$ in Eq. 5.43, we need not take very small values of η . The effect of adding the condition of substrate export out of the compartment vanishes when η is very small. Thus the condition of $z \gg \eta$ can be achieved by making z significantly higher than the rate of substrate output out of the compartment. In Figures 5.3(b) and 5.3(c) we compare the velocity expressions obtained from Eq. 5.41 and 5.43 at different values of z and η . For higher values of z (i.e. by increasing the value of ϵ_1), the expression in Eq. 5.41 agrees with MM form (Eq. 5.43).

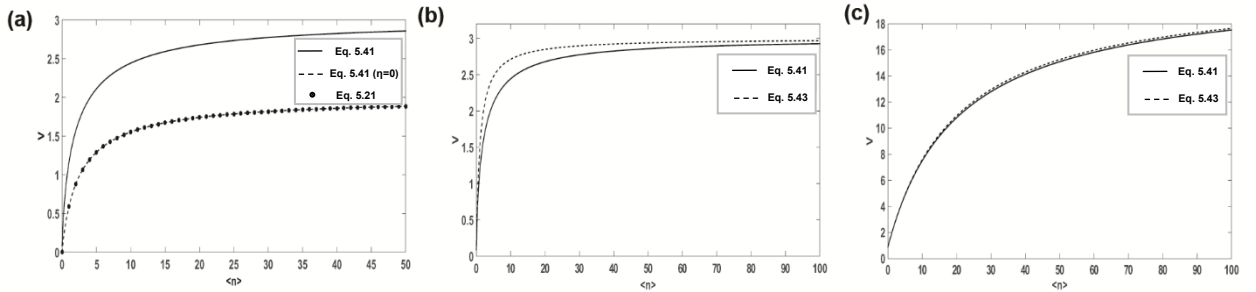


Figure 5.3: Variation of reaction velocity V as a function of average number of substrate molecules $\langle n \rangle$ for the scheme with one intermediate and reversible substrate flow (influx and out flux). (a) Solid line represents the velocity expression (Eq. 5.41) at $\epsilon_1 = 2$, $\epsilon_{-1} = 0.1$, $\eta = 1$. The black circles represent the velocity expression obtained when the limit $\eta \rightarrow 0$ is applied to Eq. 5.41 and dashed line represents velocity in Eq. 5.21. Comparison of the reaction velocity (Eq. 5.41, solid line) with the MM equation (Eq. 5.43, dashed line) at (b) $\epsilon_1 = 2$, $\epsilon_{-1} = 0.1$, $\eta = 1$ (c) $\epsilon_1 = 20$, $\epsilon_{-1} = 0.1$, $\eta = 1$.

Eq. 5.44 represents the second moment $\langle n^2 \rangle$.

$$\langle n^2 \rangle =$$

$$\frac{\theta^2(\epsilon_1 + 2z) + \theta(z(\epsilon_1 z - 4\eta) - 2\eta(1 + \epsilon_1) - \langle n \rangle \epsilon_1) - \langle n \rangle \left(\eta \epsilon_1 + \epsilon_1^2 (1 + z) \right) + \eta z \left(\frac{1}{3} + \epsilon_{-1} (2 - z) \right) + \eta^2 (2 - \epsilon_{-1} - z^2) + \frac{4\eta \epsilon_1 - 2\eta \epsilon_{-1}}{3}}{\epsilon_1 (\theta - \eta - \epsilon_1)} \quad (5.44)$$

If we put the limit, $\eta \rightarrow 0$, Eq. 5.44 reduces to Eq. 5.25. In Figure 5.4, we compare the coefficient of variation for enzyme-catalysed reaction with and without substrate molecules.

As the concentration of the substrate increases, the noise strength decreases.

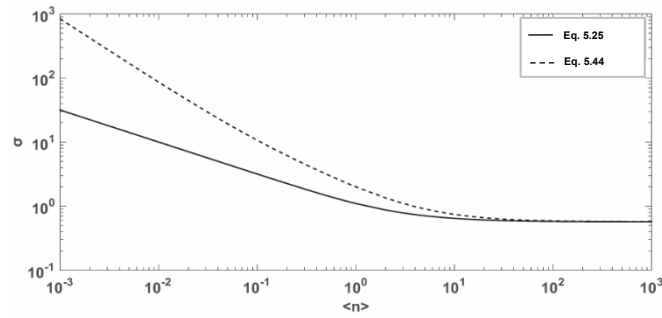


Figure 5.4: Plot of the coefficient of variation, σ versus the mean substrate concentration $\langle n \rangle$ for the catalytic reaction scheme with one intermediate complex in the (a) absence of substrate outflow (solid line) obtained from Eq. 5.25 and (b) in the presence of substrate outflow (dashed line) obtained from Eq. 5.44. Parameter values are $\epsilon_1 = 2$, $\epsilon_{-1} = 0.1$, $\eta = 1$.

Next, we consider an enzymatic reaction where two intermediate enzyme-substrate complexes are formed before the product is released out of the compartment as shown in Figure 5.1(c). Instead of two values of J , one needs to consider the number of substrate molecules present and number of product molecules formed in the ES_2 state ($J = 2$) such that $P[p, n, J = 2, t] = P_2[p, n, t]$. the master equations for this model are described below.

$$\begin{aligned} \frac{\partial P_0[p, n, t]}{\partial t} = & -nkP_0[p, n, t] + k_{-1}P_1[p + 1, n - 1, t] + k_3P_2[p, n, t] - k_0P_0[p, n, t] \\ & + k_0P_0[p, n - 1, t] \end{aligned} \quad (5.45a)$$

$$\begin{aligned} \frac{\partial P_1[p, n, t]}{\partial t} = & (n + 1)kP_0[p - 1, n + 1, t] - (k_{-1} + k_2)P_1[p, n, t] + k_{-2}P_2[p, n, t] \\ & + -k_0P_1[p, n, t] + k_0P_1[p, n - 1, t] \end{aligned}$$

(5.45b)

$$\frac{\partial P_2[p, n, t]}{\partial t} = k_2 P_1[p, n, t] - (k_{-2} + k_3) P_2[p, n, t] - k_0 P_2[p, n, t] + k_0 P_2[p, n - 1, t]$$

(5.45c)

The normalization condition $\sum_{p,n} (P_0[p, n, \tau] + P_1[p, n, \tau] + P_2[p, n, \tau]) = 1$ is satisfied at all times, $= kt$.

Eq. 5.46 shows the turnover rate.

$$V = \frac{\partial \langle p \rangle}{\partial \tau} = \frac{\partial}{\partial \tau} \sum_{n,p} p (P_0[p, n, \tau] + P_1[p, n, \tau] + P_2[p, n, \tau]). \quad (5.46)$$

Following the same mathematical procedure, one can derive the reaction velocity as

$$V = \theta = \frac{(B'' + \langle n \rangle)}{2A''} \left[\sqrt{1 + \frac{4A''\epsilon_2\epsilon_3\langle n \rangle}{(\epsilon_2 + \Omega_2)(B'' + \langle n \rangle)^2}} - 1 \right]. \quad (5.47)$$

$$\text{Here } A'' = \frac{(\epsilon_2 + \Omega_2)^2 - \epsilon_2\epsilon_3}{\epsilon_2\epsilon_3(\epsilon_2 + \Omega_2)}, B'' = \frac{\epsilon_{-1}\Omega_2 + \epsilon_2\epsilon_3}{(\epsilon_2 + \Omega_2)}, \Omega_1 = \epsilon_{-1} + \epsilon_2, \Omega_2 = \epsilon_{-2} + \epsilon_3.$$

The functional form of the turnover rate relation with only the substrate input does not change by including an additional intermediate state in the catalysis reaction (Eq. 5.21).

In the limit, when $B'' + \langle n \rangle \gg 2 \sqrt{\frac{A''\epsilon_2\epsilon_3\langle n \rangle}{\epsilon_2 + \Omega_2}}$, carrying out the binomial expansion we obtain

the velocity expression in the MM form as shown in Eq. 5.48.

$$V_{MM} = \theta = \frac{\epsilon_2\epsilon_3\langle n \rangle}{(B'' + \langle n \rangle)(\epsilon_2 + \Omega_2)} \quad (5.48)$$

This condition is satisfied either at very high substrate concentration or at high values of ϵ_2 and ϵ_3 for a given value of $\langle n \rangle$. Eq. 5.47 when considered in these limits, gives the MM form as described in Figures 5.5(a) and 5.5(b).

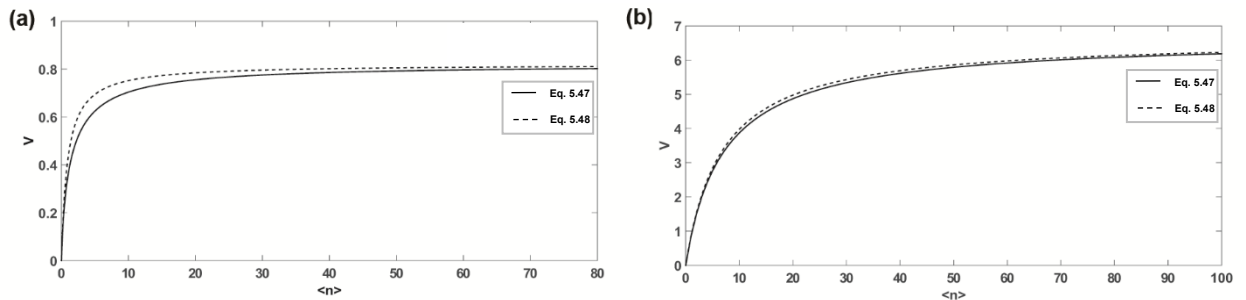


Figure 5.5: Variation of reaction velocity V as a function of average number of substrate molecules $\langle n \rangle$ for the scheme with two intermediates and irreversible substrate flow at (a) $\epsilon_2 = 1$, $\epsilon_{-1} = 0.1$, $\epsilon_3 = 5$, $\epsilon_{-2} = 0.1$ and (b) $\epsilon_2 = 10$, $\epsilon_{-1} = 0.1$, $\epsilon_3 = 20$, $\epsilon_{-2} = 0.1$. Solid line represents the velocity expression (Eq. 5.47) and dashed line is the velocity in the MM limit (Eq. 5.48).

For the model shown in Figure 5.1 (c), Eq. 5.19 represents the $\langle n^2 \rangle$ expression.

$$\langle n^2 \rangle = \mu_2^{(0)} + \mu_2^{(1)} + \mu_2^{(2)} = a_4 + a_5 \langle n \rangle \quad (5.49)$$

$$\text{Here } C = \frac{\epsilon_2(\epsilon_3 - \epsilon_{-1}) - (\Omega_2 + \epsilon_2)^2}{\epsilon_2 \epsilon_3 (\Omega_2 + \epsilon_2)}, D = 1 + \frac{\epsilon_{-1} \Omega_2 (1 - \epsilon_{-1}) - \epsilon_2 \epsilon_3 \epsilon_{-1}}{\epsilon_2 \epsilon_3} + \left(\frac{\epsilon_{-1}^2 \Omega_2 + \epsilon_{-1} \epsilon_3 (\epsilon_2 - \epsilon_{-2}) - \epsilon_3^2 \Omega_1}{\epsilon_3 (\Omega_2 + \epsilon_2)} \right),$$

$$E = \frac{\epsilon_{-1} \Omega_2 + \epsilon_2 \epsilon_3}{\Omega_2 + \epsilon_2}, F = \frac{2}{\epsilon_3 (\Omega_2 + \epsilon_2)}, M = -F, G = \frac{\epsilon_2 (\epsilon_{-1} - \epsilon_3)}{\epsilon_3 (\Omega_2 + \epsilon_2)} - \frac{2E}{\epsilon_3} + \frac{\Omega_2 + \epsilon_2 + 1}{\epsilon_3},$$

$$O = \frac{G \Omega_2}{\epsilon_2} + \frac{2}{(\Omega_2 + \epsilon_2)} + \frac{(2\epsilon_{-1} - 1) \Omega_2 + \epsilon_2 (2\epsilon_3 - 1)}{\epsilon_2 \epsilon_3}, H = -\frac{I}{2} - D \epsilon_2 + \frac{2\epsilon_{-1} \Omega_2}{\epsilon_3} + 2\epsilon_2,$$

$$P = \frac{H \Omega_2}{\epsilon_2} - 2E + 1, I = \frac{2\epsilon_2}{\Omega_2 + \epsilon_2}, J = \frac{\Omega_2 (2 + \epsilon_{-1})}{3\epsilon_3} - \frac{\epsilon_{-1} \Omega_2}{\epsilon_3} + \frac{\epsilon_{-1} \epsilon_2 \epsilon_{-2} + \epsilon_2 \epsilon_3 \Omega_1}{\Omega_2 + \epsilon_2}, K = -\epsilon_2 (1 +$$

$$E), Q = -\Omega_2 (1 + E) + I \epsilon_3, L = -\frac{\epsilon_2^2 \epsilon_3}{\Omega_2 + \epsilon_2},$$

$$a_1 = \frac{2}{(\Omega_2 + \epsilon_2)} \theta^3 + (H + P - C \epsilon_2 \epsilon_3 + D (\Omega_2 + \epsilon_2)) \theta^2 + J \left(1 + \frac{\Omega_2}{\epsilon_2} \right) \theta, a_2 = (-\epsilon_2 - \Omega_2 +$$

$$\epsilon_3 I) \theta + L \left(1 + \frac{\Omega_2}{\epsilon_2} \right) - E \epsilon_2 \epsilon_3, a_3 = \theta (\Omega_2 + \epsilon_2) - \epsilon_2 \epsilon_3, a_4 = \frac{a_1}{a_3} \text{ and } a_5 = \frac{a_2}{a_3}.$$

Next, we consider the same enzymatic reaction as described in Figure 5.1(d) with a reversible substrate influx and out-flux. Eq. 5.50 represents the master equations for the same.

$$\begin{aligned} \frac{\partial P_0[p, n, t]}{\partial t} = & -nkP_0[p, n, t] + k_{-1}P_1[p + 1, n - 1, t] + k_3P_2[p, n, t] + k_0P_0[p, n - 1, t] \\ & + k_0'P_0[p, n + 1, t] - (k_0 + k_0')P_0[p, n, t] \end{aligned} \quad (5.50a)$$

$$\begin{aligned} \frac{\partial P_1[p, n, t]}{\partial t} = & (n + 1)kP_0[p - 1, n + 1, t] - (k_{-1} + k_2)P_1[p, n, t] + k_{-2}P_2[p, n, t] \\ & + k_0P_1[p, n - 1, t] + k_0'P_1[p, n + 1, t] - (k_0 + k_0')P_1[p, n, t] \end{aligned} \quad (5.50b)$$

$$\frac{\partial P_2[p, n, t]}{\partial t} = k_2 P_1[p, n, t] - (k_{-2} + k_3) P_2[p, n, t] + k_0 P_2[p, n - 1, t] + k_0' P_2[p, n + 1, t] - (k_0 + k_0') P_2[p, n, t] \quad (5.50c)$$

The normalization condition $\sum_{p,n} (P_0[p, n, \tau] + P_1[p, n, \tau] + P_2[p, n, \tau]) = 1$ is satisfied at all times, where $\tau = kt$.

Eq. 5.51 gives the turnover rate.

$$V = \theta = \frac{(B'' - 2\eta + \langle n \rangle)}{2A''} \left[\sqrt{1 + \frac{4A'' \left(\left(\frac{\epsilon_2 \epsilon_3}{\epsilon_2 + \Omega_2} + \eta \right) \langle n \rangle + \eta(B'' - 1) - \eta^2 A'' \right)}{(B'' - 2\eta + \langle n \rangle)^2}} - 1 \right] \quad (5.51)$$

In the limit when $\eta \rightarrow 0$ Eq. 5.51 reduces to Eq. 5.47. Figure 5.6(a) graphically depicts the same.

In the limit, when $(B'' - 2\eta + \langle n \rangle) \gg 2 \sqrt{A'' \left(\left(\frac{\epsilon_2 \epsilon_3}{\epsilon_2 + \Omega_2} + \eta \right) \langle n \rangle + \eta(B'' - 1) - \eta^2 A'' \right)}$,

carrying out the binomial expansion we get Eq. 5.52.

$$V = \theta = \frac{\left(\frac{\epsilon_2 \epsilon_3}{\epsilon_2 + \Omega_2} + \eta \right) \langle n \rangle + \eta(B'' - 1) - \eta^2 A''}{(B'' - 2\eta + \langle n \rangle)} \quad (5.52)$$

In the limit when ϵ_2 and ϵ_3 are much higher than η , Eq. 5.52 reduces to a MM form of velocity as shown in Figures 5.6(b) and 5.6(c).

$$V_{MM} = \theta = \frac{\left(\frac{\epsilon_2 \epsilon_3}{\epsilon_2 + \Omega_2} + \eta \right) \langle n \rangle}{(B'' - 2\eta + \langle n \rangle)}. \quad (5.53)$$

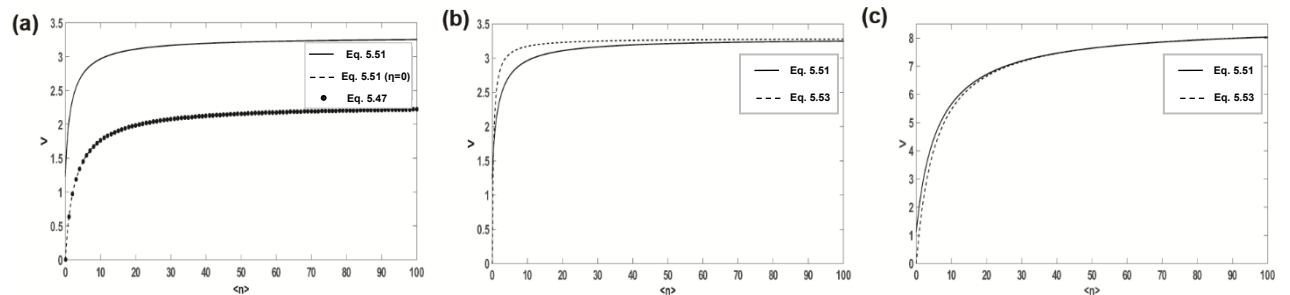


Figure 5.6: Variation of reaction velocity V as a function of average number of substrate molecules $\langle n \rangle$ for the scheme with two intermediate and reversible substrate flow (influx and out)

flux). (a) Solid line represents the velocity expression (Eq. 5.51) at $\epsilon_2 = 3, \epsilon_{-1} = \epsilon_{-2} = 0.1, \epsilon_3 = 10, \eta = 1$. The black circle represents the velocity expression obtained when the limit $\eta \rightarrow 0$ is applied to Eq. 5.51 and dashed line represents velocity in Eq. 5.47. Comparison of the reaction velocity (Eq. 5.51, solid line) with the MM equation (Eq. 5.53, dashed line) at (b) $\epsilon_2 = 3, \epsilon_{-1} = \epsilon_{-2} = 0.1, \epsilon_3 = 10, \eta = 1$. (c) $\epsilon_2 = 30, \epsilon_{-1} = \epsilon_{-2} = 0.1, \epsilon_3 = 10, \eta = 1$

Eq. 5.54 represents the expression for the second moment for the model shown in Figure 5.1

(d).

$$\langle n^2 \rangle = a_9 + a_{10} \langle n \rangle \quad (5.54)$$

$$a_6 = \frac{2}{(\Omega_2 + \epsilon_2)} (\theta - \eta)^3 + \left(H + P - C\epsilon_2\epsilon_3 + D(\Omega_2 + \epsilon_2) + \frac{(\Omega_2 + \epsilon_2)^2}{\epsilon_2\epsilon_3} - 1 \right) (\theta - \eta)^2$$

$$+ \left(J \left(1 + \frac{\Omega_2}{\epsilon_2} \right) - D\epsilon_2\epsilon_3 - \Omega_2 - \epsilon_2 \right) (\theta - \eta) + (\theta + \eta)(\Omega_2 + \epsilon_2)$$

$$+ (\theta^2 - \eta^2) \left(1 - \frac{(\Omega_2 + \epsilon_2)^2}{\epsilon_2\epsilon_3} \right),$$

$$a_7 = \epsilon_3 I (\theta - \eta) - (\theta + \eta)(\Omega_2 + \epsilon_2) + L \left(1 + \frac{\Omega_2}{\epsilon_2} \right) - E\epsilon_2\epsilon_3,$$

$$a_8 = (\theta - \eta)(\Omega_2 + \epsilon_2) - \epsilon_2\epsilon_3, a_9 = \frac{a_6}{a_8} \text{ and } a_{10} = \frac{a_7}{a_8}.$$

Similar to Figure 5.4, in Figure 5.7 we plot σ as a function of the mean substrate concentration for the two intermediate enzyme catalyzed reaction in the absence and presence of substrate outflux. The fluctuations decrease with the increase in substrate molecules. This implies that at high substrate concentrations the removal of substrate molecules during the catalytic reaction decreases and substrate is present in excess within the compartment. Also the out-flux rate is small and does not change during the course of the reaction. As a result, the size of the fluctuations remains constant with increasing substrate concentration.

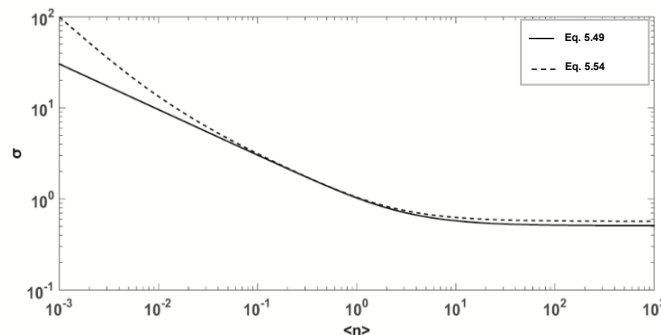


Figure 5.7: Plot of the coefficient of variation, σ of fluctuations in substrate concentration versus the mean substrate concentration $\langle n \rangle$ for the catalytic reaction scheme with two intermediate steps in the absence of substrate outflow (solid line) obtained from Eq. 5.49 and in the presence of substrate outflow (dashed line) obtained from Eq. 5.54. Parameter values are $\epsilon_2 = 3$, $\epsilon_{-1} = \epsilon_{-2} = 0.1$, $\epsilon_3 = 10$, $\eta = 1$.

We have also compared the noise for the reaction models with one and two intermediate states. For both the models, the noise level decreases as we move from low to moderate substrate concentrations. At high substrate number, σ remains the same with an increase in the mean substrate concentration. At high substrate concentration, when most of the enzyme is in the substrate bound state, the presence of slow fluctuations between the two enzyme-substrate conformers lead to higher noise levels in the two state model.

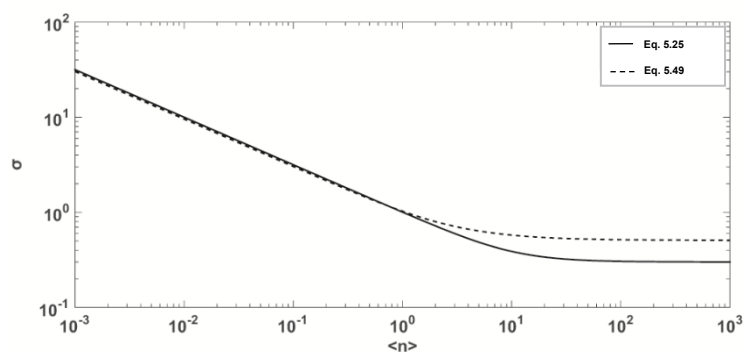


Figure 5.8: Plot of the coefficient of variation versus the mean substrate concentration $\langle n \rangle$ for the catalytic reaction scheme in the absence of substrate outflow for the one intermediate scheme, (solid line) at $\epsilon_1 = 10$, $\epsilon_{-1} = 0.1$ and the two intermediate scheme (dashed line) at parameter values are $\epsilon_3 = 10$, $\epsilon_{-1} = 0.1$, $\epsilon_2 = 3$, $\epsilon_{-2} = 0.1$.

5.4 Conclusions:

In this chapter, we study the role of noise in enzymatic reactions that take place in intracellular environments. One can obtain the stochastic description of the system by solving the chemical master equation under the steady state approximation. Our results show that irrespective of the number of intermediates present in the reaction scheme, substrate fluctuations can lead to deviation from the classical MM equation. This is in contrary to the studies performed under the substrate abundance assumption. The velocity expressions have a different functional form when there is a unidirectional or bidirectional transport of substrate

molecules into the intracellular compartment. For unidirectional as well as bidirectional transport, the velocity equation cannot distinguish between single and multiple intermediate states. At high substrate concentration, all these velocity equations reduce to the classical MM type equation.

We also study the fluctuations in the substrate concentration by measuring the coefficient of variation, σ . For a catalytic reaction with one intermediate or more number of intermediate states, σ decreases with the increase in the mean substrate number and reaches a constant value at high substrate concentrations. We observe that the fluctuations are larger in the presence of both substrate influx and out-flux at low substrate concentrations as compared to reactions where there is only unidirectional flow of the substrate into the compartment. On comparing systems with different number of intermediates with a unidirectional substrate flow, system with more internal states undergoes more fluctuations at higher substrate concentrations. Therefore, noise plays an important role in cellular compartments.

5.5 References:

- (1) Cao, J. *J. Phys. Chem. B* **2011**, *115*, 5493.
- (2) Gardiner, C. W. *Handbook of Stochastic Methods: for Physics, Chemistry, and the Natural Sciences*; Springer: New York, 1996.
- (3) Holwerda, E. K.; Lynd, L. R. *Biotechnol. Bioeng.* **2013**, *110*, 2389.
- (4) Grima, R.; Leier, A. *J. Phys. Chem. B* **2016**, *121*, 13.
- (5) Grima, R. *Phys. Rev. E* **2014**, *89*, 012710.
- (6) Kampen, N. G. V. *Stochastic Processes in Physics and Chemistry*; 4th ed.; Elsevier: North-Holland, 2007.
- (7) Alberts, B.; Watson, J.; Bray, D.; Lewis, J. *Molecular Biology of the Cell*; 4 ed.; Garland Science: New York, 2008.
- (8) Stefanimo, M. O.; McKane, A. K.; Newman, T. J. *Nonlinearity* **2005**, *18*, 1575.

6. Single-Molecule Kinetics of an Enzyme in the phosphorylation-dephosphorylation cycle

6.1 Introduction:

In the previous chapters, we have discussed many enzymatic models with different free and bound conformers mutually interconverting among themselves in the absence or presence of substrate number fluctuations. The processing of a substrate molecule by the free (already in the active state) enzyme leads to the completion of one catalytic cycle and marks the beginning of the next. However, in certain biological networks for performing the catalytic turnovers some enzymes need a prior activation. Mitogen-activated protein kinase ERK2 also known as extracellular signal regulatory kinase works at the integration of several biochemical signals assisting various cellular processes like cell proliferation, transcription control and development.¹ Most of the physiological enzymatic actions involve phosphorylation and de-phosphorylation cycle (PdPC). ERK2 activation requires phosphorylation carried out by MAP/ERK kinases (MEK).² For the substrate phosphorylation, the phosphorylated/activated enzyme³ goes into the nucleus of the stimulated cell and phosphorylates the target. The corresponding de-phosphorylation is the detachment of phosphoric ester or anhydride through reversible hydrolysis catalysed by phosphatases, which leads to the deactivation of the activated enzyme. This PdPC⁴ is very common in post-translational modification occurring in proteins.

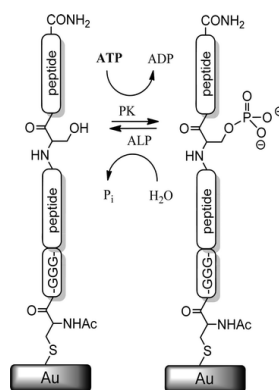


Figure 6.1: Schematic representation showing the Phosphorylation-dephosphorylation cycle catalysed by pyruvate kinase on a Gold surface-immobilized peptide monolayer.⁵

Experimental and theoretical investigations on the mechanistic action of ERK2 enzyme have shed light on how the initial occupancy of the docking site introduces conformational modifications, followed by the specific substrate-binding happening at the active site.⁶⁻⁸ Recently, Kolomeisky and co-workers have provided a quantitative network model⁹ for theoretically investigating an unexpected enhanced activity caused by the mutations¹⁰ in the D-site of ERK2 enzyme. As per the proposed mechanism firstly, the inactive ERK2 enzyme binds with an activator (MEK). The activator bound enzymatic state irreversibly dissociates leading to the formation of the activated/phosphorylated ERK2. The phosphorylated enzyme can execute the substrate phosphorylation or it can simply follow the deactivation route. This biochemical network has three coupled Michaelis-Menten (MM) reactions associated with each of the reaction routes namely, the phosphorylation of the inactive ERK2 (activation), dephosphorylation of the active ERK2 (deactivation) and phosphorylation of the substrate by the active ERK2. The average rate of the substrate phosphorylation by the active (phosphorylated) ERK2 shows the MM behaviour.⁹

We ask the following questions: although the average rate of substrate phosphorylation catalysed by the active ERK2 enzyme shows the hyperbolic dependence with the substrate concentration, what is the form of the corresponding waiting-time distribution? Is dynamic disorder present in such PdPC reaction networks? If so, how does the randomness change under different physical scenarios subjected to changes in the magnitude of the rate constants constituting the parameter space and concentrations of the activator, deactivator, and substrate? How the introduction of one more activator-bound internal state affects the functional form of the reaction velocity and system randomness?

In this chapter, we have considered three different types of PdPC networks and applied the CME (Chemical Master Equation)¹¹ approach. The formulated waiting time distribution focuses on the substrate phosphorylation catalysed by the active ERK2 enzyme. In different

physical scenarios depending on the magnitudes of the rate constants and concentrations of the activator, deactivator, and substrate, the rate determining step changes. We obtain the analytical expression for the waiting time distribution and the mean turnover time. In order to quantify the temporal fluctuations in the reactions rates, we calculate the randomness parameter.^{12,13}

6.2 Reaction Models and Analysis:

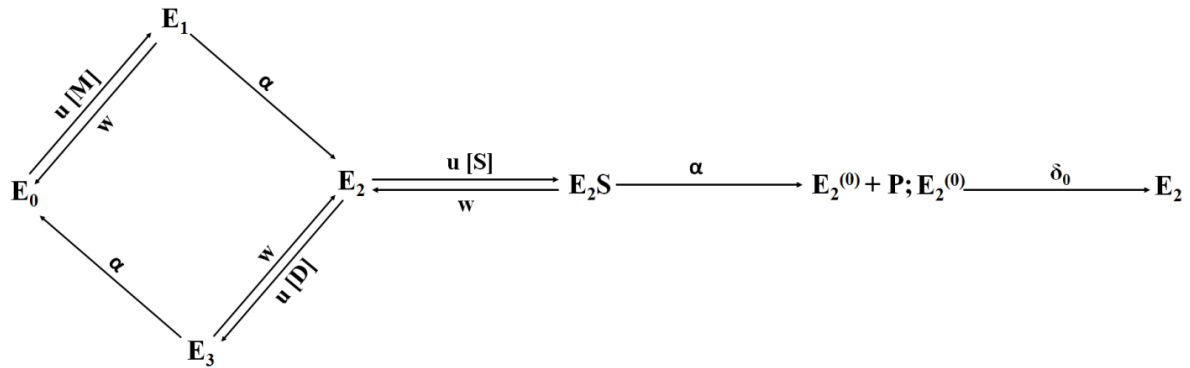


Figure 6.2: Schematic representation showing the activation/phosphorylation of the inactive ERK2, deactivation/de-phosphorylation of the active ERK2 and substrate phosphorylation carried out by the activated ERK2 enzyme.

In the above schematic, there are three reaction routes namely, the activator (MEK) assisted activation/phosphorylation, the deactivator (phosphatases) involved deactivation/de-phosphorylation and the substrate phosphorylation pathway catalysed by the active ERK2 enzyme. Firstly, the inactive free enzyme (E_0) binds reversibly with an activator (M) to form an activator bound enzymatic state (E_1). Further, E_1 can irreversibly dissociate to give the phosphorylated/activated state (E_2). Now, this phosphorylated enzyme (E_2) can access the two probable pathways. Following the deactivation route, E_2 can bind reversibly with the deactivator (D) to form the deactivator bound enzymatic state (E_3) which can irreversibly regenerate the starting non-phosphorylated free enzyme state, E_0 . Following the substrate phosphorylation pathway, E_2 can reversibly bind with the substrate (S) forming the enzyme-substrate complex (E_2S). Further, E_2S irreversibly dissociates to give the product and regenerated enzyme, $E_2^{(0)}$. The enzymatic state $E_2^{(0)}$ instantaneously converts to E_2 through

a transition characterized by the rate constant δ_0 . In the given reaction mechanism, all binding events associated with the three routes namely, the phosphorylation of the inactive ERK2, the de-phosphorylation of the active ERK2 and the substrate phosphorylation catalysed by the active ERK2 are characterized by the rate constant u . All the unbinding processes, beginning from the enzymatic bound states (E_1, E_3, E_2S) are designated by the rate constant w . Similarly, all the irreversible rate processes are designated by the rate constant α . For this reaction mechanism, the reaction rate statistics in terms of the time evolution of the joint probability of the number of each species involved in the chemical reaction is described by the chemical master equation (CME) approach. The variables constituting the probability distributions are $n_{E_0}, n_{E_1}, n_{E_2}, n_{E_3}, n_{E_2S}, n_{E_2^{(0)}}$ and n_P representing the number of enzyme molecules present in the state $E_0, E_1, E_2, E_3, E_2S, E_2^{(0)}$, and P respectively and n_P is the number of product molecules formed at a time t .

$$\begin{aligned}
& \partial_t P \left[n_{E_0}, n_{E_1}, n_{E_2}, n_{E_3}, n_{E_2S}, n_{E_2^{(0)}}, n_P; t \right] \\
&= \left(u[M](n_{E_0} + 1)Y_{E_0}Y_{E_1}^{-1} + w(n_{E_1} + 1)Y_{E_0}^{-1}Y_{E_1} + \alpha(n_{E_1} + 1)Y_{E_1}Y_{E_2}^{-1} \right. \\
&+ u[D](n_{E_2} + 1)Y_{E_2}Y_{E_3}^{-1} + w(n_{E_3} + 1)Y_{E_2}^{-1}Y_{E_3} + \alpha(n_{E_3} + 1)Y_{E_0}^{-1}Y_{E_3} \\
&+ u[S](n_{E_2} + 1)Y_{E_2}Y_{E_2S}^{-1} + w(n_{E_2S} + 1)Y_{E_2}^{-1}Y_{E_2S} + \alpha(n_{E_2S} + 1)Y_{E_2S}Y_{E_2^{(0)}}^{-1}Y_P^{-1} \\
&- \left(u([M]n_{E_0} + ([D] + [S])n_{E_2}) \right. \\
&\left. \left. + (w + \alpha)(n_{E_1} + n_{E_3} + n_{E_2S}) \right) \right) P \left[n_{E_0}, n_{E_1}, n_{E_2}, n_{E_3}, n_{E_2S}, n_{E_2^{(0)}}, n_P; t \right]
\end{aligned} \tag{6.1}$$

Owing to the mutual exclusivity of different enzymatic states, Eq. 6.1 reduces to Eq. 6.2.

$$\frac{\partial P_{E_0}(t)}{\partial t} = -u[M]P_{E_0}(t) + wP_{E_1}(t) + \alpha P_{E_3}(t) \tag{6.2.a}$$

$$\frac{\partial P_{E_1}(t)}{\partial t} = u[M]P_{E_0}(t) - (w + \alpha)P_{E_1}(t) \quad (6.2.b)$$

$$\frac{\partial P_{E_2}(t)}{\partial t} = \alpha P_{E_1}(t) - u([D] + [S])P_{E_2}(t) + wP_{E_3}(t) + wP_{E_2S}(t) + \delta_0 P_{E_2^{(0)}}(t) \quad (6.2.c)$$

$$\frac{\partial P_{E_3}(t)}{\partial t} = u[D]P_{E_2}(t) - (w + \alpha)P_{E_3}(t) \quad (6.2.d)$$

$$\frac{\partial P_{E_2S}(t)}{\partial t} = u[S]P_{E_2}(t) - (w + \alpha)P_{E_2S}(t) \quad (6.2.e)$$

$$\frac{\partial P_{E_2^{(0)}}(t)}{\partial t} = \alpha P_{E_2S}(t) - \delta_0 P_{E_2^{(0)}}(t) \quad (6.2.f)$$

For the given model, Eq. 6.3 represents the turnover time distribution.

$$f(t) = \frac{\partial P_P(t)}{\partial t} = \alpha P_{E_2S}(t) \quad (6.3)$$

At the beginning of the reaction, the enzyme exists in the free-state conformer E_0 such that $P_{E_0}(0) = 1, P_{E_1}(0) = 0, P_{E_2}(0) = 0, P_{E_3}(0) = 0, P_{E_2S}(0) = 0, P_{E_2^{(0)}}(0) = 0$ and $P_P(0) = 0$.

At any instant of time, the condition $P_{E_0}(t) + P_{E_1}(t) + P_{E_2}(t) + P_{E_3}(t) + P_{E_2S}(t) = 1$ must be satisfied. Thus, the above set of coupled differential equations can be solved by taking the Laplace transform and applying appropriate initial conditions and normalization constraints we get the following matrix

$$\begin{bmatrix} s + [M]u & -w & 0 & -\alpha & 0 & 0 & 0 \\ -[M]u & s + w + \alpha & 0 & 0 & 0 & 0 & 0 \\ 0 & -\alpha & s + u([D] + [S]) & -w & -w & -\delta_0 & 0 \\ 0 & 0 & -u[D] & s + \alpha + w & 0 & 0 & 0 \\ 0 & 0 & -u[S] & 0 & s + w + \alpha & 0 & 0 \\ 0 & 0 & 0 & 0 & 0 & s & 0 \end{bmatrix} \begin{bmatrix} \hat{P}_{E_0}(s) \\ \hat{P}_{E_1}(s) \\ \hat{P}_{E_2}(s) \\ \hat{P}_{E_3}(s) \\ \hat{P}_{E_2S}(s) \\ \hat{P}_{E_2^{(0)}}(s) \end{bmatrix} = \begin{bmatrix} 1 \\ 0 \\ 0 \\ 0 \\ 0 \\ 0 \end{bmatrix} \quad (6.4)$$

Solving this matrix by taking an inverse gives Eq. 6.5.

$$\begin{bmatrix} \hat{P}_{E_0}(s) \\ \hat{P}_{E_1}(s) \\ \hat{P}_{E_2}(s) \\ \hat{P}_{E_3}(s) \\ \hat{P}_{E_2S}(s) \\ \hat{P}_{E_2^{(0)}}(s) \end{bmatrix} = \begin{bmatrix} \frac{s^3 + A s^2 + B s + C}{s^4 + E s^3 + F s^2 + G s + H} \\ \frac{[M]u s^2 + I s + J}{s^4 + E s^3 + F s^2 + G s + H} \\ \frac{\alpha[M]u s + K}{s^4 + E s^3 + F s^2 + G s + H} \\ \frac{\alpha[D][M]u^2}{s^4 + E s^3 + F s^2 + G s + H} \\ \frac{\alpha[M][S]u^2}{s^4 + E s^3 + F s^2 + G s + H} \\ 0 \end{bmatrix} \quad (6.5)$$

Here $A = ([D] + [S])u + 2(\alpha + w)$, $B = \alpha([D] + [S])u + (\alpha + w)(\alpha + ([D] + [S])u + w)$,

$C = \alpha([D] + [S])u(\alpha + w)$, $E = A + [M]u$,

$F = \alpha^2 + 2\alpha([D] + [S])u + ([M]u + w)(2\alpha + ([D] + [S])u + w)$, $G = 2J + C + K$,

$H = \alpha^2[M][S]u^2$, $I = [M]u(\alpha + ([D] + [S])u + w)$, $J = \alpha[M]([D] + [S])u^2$, and

$K = \alpha[M]u(\alpha + w)$.

Eq. 6.6 represents the waiting-time distribution function for the scheme shown in Figure 6.2.

$$\hat{f}(s) = \alpha \hat{P}_{E_2S}(s) = \frac{\alpha^2[M][S]u^2}{s^4 + E s^3 + F s^2 + G s + H} \quad (6.6)$$

From Eq.6.6, we obtain the corresponding mean waiting-time.

$$\langle t \rangle = \frac{(\alpha+w)([D]+[M])+2[M][D]u}{\alpha[M][S]u} + \frac{\alpha+2[M]u+w}{\alpha[M]u} \quad (6.7)$$

For the reaction scheme represented in Figure 6.2, the average waiting-time for the substrate phosphorylation shows a linear relationship with the inverse of the substrate concentration.

To quantify the temporal fluctuations, we calculate the randomness, represented by Eq. 6.8.

$$R = 1 - \frac{2[M][S]\xi_1}{\xi_2} \quad (6.8)$$

Here $\xi_1 = \left(\alpha^2 + ([M]u + w)([D] + [S])u + w \right) + 2\alpha([D] + [M] + [S])u + w$, and

$\xi_2 = ((\alpha + w)([D] + [M] + [S]) + 2[M]([D] + [S])u)^2$.

If we apply, the limit $[M] \rightarrow 0$ in Eq. 6.8 then R attains the value to be unity since the phosphorylation of the enzyme via E_1 formation becomes the slowest step. The substrate phosphorylation would happen only after the activation of the enzyme. In Eq. 8 if we consider

the limit $[S] \rightarrow 0$, R goes to unity. In this physical scenario, the binding of the substrate with the active ERK2 enzyme becomes the rate-determining step.

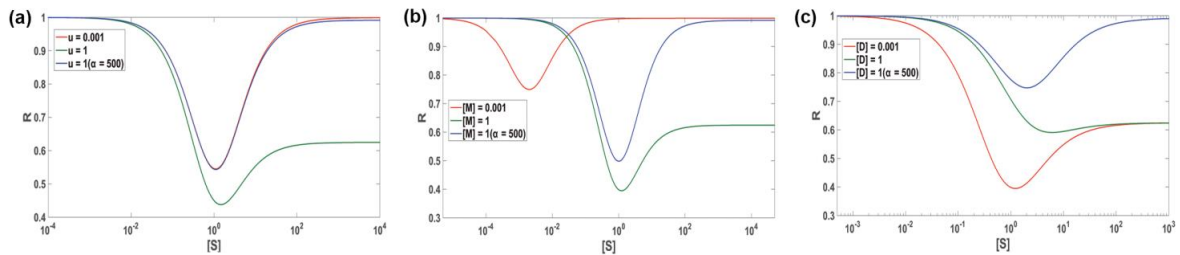


Figure 6.3: The plots showing the variation of the randomness parameter (R) as a function of the substrate-concentration ($[S]$) for Figure 6.2, to analyse the effect of (a) the binding rate constant (u) with the common set of reaction parameters: $w = 1$, $\alpha = 5$, $[M] = 1$ and $[D] = 0.1$, (b) the activator concentration ($[M]$) in the common parameter space: $u = 1$, $w = 1$, $\alpha = 5$, and $[D] = 0.001$ and (c) the deactivator concentration ($[D]$) for the given set of reaction rate constants: $u = 1$, $w = 1$, $\alpha = 5$ and $[M] = 1$. The red and green solid lines represent the obtained behaviour at two values 0.001 and 1, respectively for $u/[M]/[D]$ for the plots labelled as (a), (b) and (c), respectively. The blue solid line in each plot represents the response for the case when $\alpha = 500$ and the corresponding values of $u/[M]/[D]$ are taken to be unity for the plots labelled as (a), (b) and (c), respectively.

We plot the randomness parameter R (Eq. 6.8) as a function of $[S]$ for a given set of kinetic parameters to analyze the effects of u , $[M]$ and $[D]$ as shown in Figure 6.2. For all the cases, at low $[S]$, the substrate binding event is the rate-determining step and there is no dynamic disorder. At higher $[S]$, the enzyme is present in the substrate-bound E_2S state and there is a competition between the product formation event and the dissociation of E_2S back to E_2 . For comparable values of α and w , there is competition between these two events contributing to the randomness of the system and R deviates from unity. The competition reduces when one of the rate constant involved in the competition is considerably higher than the other constant, assuring the presence of a single rate-determining step. For example, at high values of α , the product formation event occurs readily and the value of randomness parameter approaches to unity irrespective of changes in any other system parameters.

At higher $[S]$, when the enzyme is present in the substrate-bound E_2S state, at low values of u , the conversion of E_2 into E_2S is the slowest step and $R = 1$. With an increase in

the value of u , the substrate-binding event is no longer the slowest step. There is a competition between the events starting from E_2S state, which can lead to deviation in the value of R from unity.

For a given set of kinetic parameters at low $[S]$, $R = 1$ irrespective of $[M]$. At high $[S]$, when $[M]$ is low, the formation of E_1 from E_0 is the rate governing step and R approaches unity. With an increase in $[M]$, a sufficient amount of the activated enzyme E_2 would be formed which will be readily converted to E_2S at moderate to high $[S]$ and R deviates from unity due to competing reaction time scales.

For a given parameter space, at low $[S]$, there is no dynamic disorder irrespective of $[D]$. For higher values of $[M]$, the free enzyme E_0 will go to the E_2 state, which can participate either in the substrate phosphorylation or the deactivation route, when $[S]$ and $[D]$ are of comparable order. This leads to deviation in the value R from unity. At higher $[S]$, and low to moderate values of $[D]$, the substrate phosphorylation would be favoured over the deactivation route and R is independent of $[D]$. The enzyme will be now in the E_2S state from which product formation and dissociation can happen on comparable timescales and the randomness parameter attains a constant non-unity value irrespective of the value of $[D]$. Considering a physical scenario where the magnitudes of $[D]$ and $[S]$ are considerably high, we find that irrespective of $[D]$, at low $[S]$, $R = 1$. At higher $[S]$ and $[D]$, sufficient amount of E_2S and as well as E_3 would be formed which increases the probabilities of the transitions from these bound enzymatic states and thus, $R \neq 1$. Further, at high $[S]$ and at extremely high values of $[D]$, the dephosphorylation route will be favored over the product formation step and thus, the value of R approaches to unity.

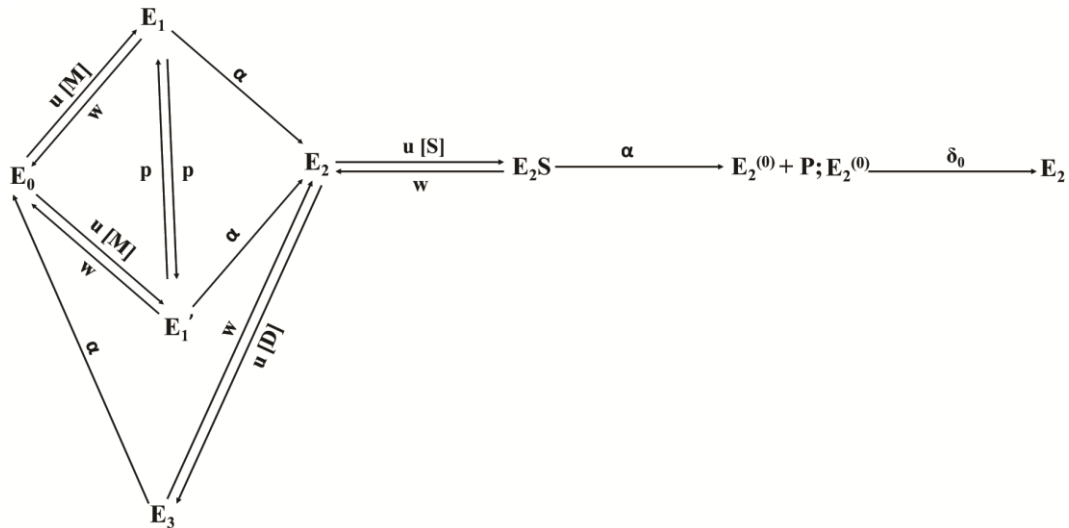


Figure 6.4: Schematic representation showing the activation/phosphorylation of the inactive ERK2 assisted by the two different activator-bound enzymatic states (E_1 and E_1' both can directly access the phosphorylated state of the ERK2), deactivation/de-phosphorylation of the active ERK2 and substrate phosphorylation carried out by the activated ERK2 enzyme.

Next, we consider another reaction route where there is one additional internal state (E_1'). E_1' formation occurs, when the starting enzyme conformer E_0 reversibly binds with the activator. To form to the activated/phosphorylated enzyme (E_2), E_1' dissociates irreversibly. We also consider the conformational fluctuations between these two activator bound enzymatic conformers E_1 and E_1' characterized by the rate constant, p . The variables constituting the probability distributions are $n_{E_0}, n_{E_1}, n_{E_1'}, n_{E_2}, n_{E_3}, n_{E_2S}, n_{E_2^{(0)}}$ and n_p representing the number of enzyme molecules present in the state $E_0, E_1, E_1', E_2, E_3, E_2S$, and $E_2^{(0)}$, respectively and n_p is the number of product molecules formed at a time t .

$$\begin{aligned}
& \partial_t P \left[n_{E_0}, n_{E_1}, n_{E_1'}, n_{E_2}, n_{E_3}, n_{E_2S}, n_{E_2^{(0)}}, n_P; t \right] \\
&= \left(u[M](n_{E_0} + 1)Y_{E_0}Y_{E_1}^{-1} + w(n_{E_1} + 1)Y_{E_0}^{-1}Y_{E_1} + \alpha(n_{E_1} + 1)Y_{E_1}Y_{E_2}^{-1} \right. \\
&+ u[M](n_{E_0} + 1)Y_{E_0}Y_{E_1'}^{-1} + w(n_{E_1'} + 1)Y_{E_0}^{-1}Y_{E_1'} + \alpha(n_{E_1'} + 1)Y_{E_1'}Y_{E_2}^{-1} \\
&+ p(n_{E_1} + 1)Y_{E_1}Y_{E_1'}^{-1} + p(n_{E_1'} + 1)Y_{E_1}^{-1}Y_{E_1'} + u[D](n_{E_2} + 1)Y_{E_2}Y_{E_3}^{-1} \\
&+ w(n_{E_3} + 1)Y_{E_2}^{-1}Y_{E_3} + \alpha(n_{E_3} + 1)Y_{E_0}^{-1}Y_{E_3} + u[S](n_{E_2} + 1)Y_{E_2}Y_{E_2S}^{-1} \\
&+ w(n_{E_2S} + 1)Y_{E_2}^{-1}Y_{E_2S} + \alpha(n_{E_2S} + 1)Y_{E_2S}Y_{E_2^{(0)}}^{-1}Y_P^{-1} \\
&- (2u[M]n_{E_0} + (w + p + \alpha)n_{E_1} + (w + p + \alpha)n_{E_1'} + u([D] + [S])n_{E_2S} \\
&+ (\alpha + w)n_{E_3} + (\alpha + w)n_{E_2S}) \left. \right) P \left[n_{E_0}, n_{E_1}, n_{E_1'}, n_{E_2}, n_{E_3}, n_{E_2S}, n_{E_2^{(0)}}, n_P; t \right]
\end{aligned} \tag{6.9}$$

To solve Eq. 6.9, we use the mutual exclusivity of different enzymatic states, which gives the following set of coupled differential equations.

$$\frac{\partial P_{E_0}(t)}{\partial t} = -2u[M]P_{E_0}(t) + wP_{E_1}(t) + wP_{E_1'}(t) + \alpha P_{E_3}(t) \tag{6.10.a}$$

$$\frac{\partial P_{E_1}(t)}{\partial t} = u[M]P_{E_0}(t) - (w + p + \alpha)P_{E_1}(t) + pP_{E_1'}(t) \tag{6.10.b}$$

$$\frac{\partial P_{E_1'}(t)}{\partial t} = u[M]P_{E_0}(t) + pP_{E_1}(t) - (w + p + \alpha)P_{E_1'}(t) \tag{6.10.c}$$

$$\frac{\partial P_{E_2}(t)}{\partial t} = \alpha P_{E_1}(t) + \alpha P_{E_1'}(t) - u([D] + [S])P_{E_2}(t) + wP_{E_3}(t) + wP_{E_2S}(t) + \delta_0 P_{E_2^{(0)}}(t) \tag{6.10.d}$$

$$\frac{\partial P_{E_3}(t)}{\partial t} = u[D]P_{E_2}(t) - (w + \alpha)P_{E_3}(t) \tag{6.10.e}$$

$$\frac{\partial P_{E_2S}(t)}{\partial t} = u[S]P_{E_2}(t) - (w + \alpha)P_{E_2S}(t) \tag{6.10.f}$$

$$\frac{\partial P_{E_2^{(0)}}(t)}{\partial t} = \alpha P_{E_2 S}(t) - \delta_0 P_{E_2^{(0)}}(t) \quad (6.10.g)$$

As explained for the previous model, for the scheme shown in Figure 6.4 we have

$$\begin{bmatrix} \hat{P}_{E_0}(s) \\ \hat{P}_{E_1}(s) \\ \hat{P}_{E_1'}(s) \\ \hat{P}_{E_2}(s) \\ \hat{P}_{E_3}(s) \\ \hat{P}_{E_2 S}(s) \\ \hat{P}_{E_2^{(0)}}(s) \end{bmatrix} = \begin{bmatrix} s^3 + L s^2 + N s + Q \\ \frac{s^4 + X s^3 + Y s^2 + Z s + b}{[M]u s^2 + e s + f} \\ \frac{s^4 + X s^3 + Y s^2 + Z s + b}{[M]u s^2 + e s + f} \\ \frac{s^4 + X s^3 + Y s^2 + Z s + b}{2\alpha[M]u s + g} \\ \frac{s^4 + X s^3 + Y s^2 + Z s + b}{2\alpha[D][M]u^2} \\ \frac{s^4 + X s^3 + Y s^2 + Z s + b}{2\alpha[M][S]u^2} \\ \frac{s^4 + X s^3 + Y s^2 + Z s + b}{0} \end{bmatrix}. \quad (6.11)$$

Here $L = ([D] + [S])u + 2(\alpha + w)$, $N = \alpha([D] + [S])u + (\alpha + w)(\alpha + ([D] + [S])u + w)$,
 $Q = \alpha([D] + [S])u(\alpha + w)$, $X = 2\alpha + ([D] + 2[M] + [S])u + 2w$,
 $Y = \alpha^2 + (2[M]u + w)(([D] + [S])u + w) + 2\alpha(([D] + 2[M] + [S])u + w)$,
 $Z = \alpha u(\alpha([D] + 2[M] + [S]) + 4[M]([D] + [S])u + ([D] + 2[M] + [S])w)$,
 $b = \alpha^2[M][S]u^2$, $e = [M]u[\alpha + ([D] + [S])u + w]$, $f = \alpha[M]([D] + [S])u^2$, and
 $g = 2\alpha[M]u(\alpha + w)$.

Eq. 6.12 represents the waiting-time distribution for Figure 6.4.

$$\hat{f}(s) = \alpha \hat{P}_{E_2 S}(s) = \frac{2\alpha^2[M][S]u^2}{s^4 + X s^3 + Y s^2 + Z s + 2H}. \quad (6.12)$$

Using the above equation, we get the mean reaction time.

$$\langle t \rangle = \frac{\alpha + 4[M]u + w}{2\alpha[M]u} + \frac{(\alpha + w)([D] + 2M) + 4[M][D]u}{2\alpha[M][S]u} \quad (6.13)$$

Thus, the mean time for the substrate phosphorylation follows the MM equation. Eq.6.14 represents the analytical expression for the randomness parameter for Figure 6.4.

$$R = 1 - \frac{4[M][S]\xi_3}{\xi_4} \quad (6.14)$$

Here $\xi_3 = (\alpha^2 + w + 2\alpha(([D] + 2[M] + [S])u + w) + u(2[M]([D] + [S])u + ([D] + 2[M] + [S])w))$, and $\xi_4 = ((\alpha + w)([D] + 2[M] + [S]) + 4[M]([D] + [S])u)^2$.

In Eq. 14, in the limit $[S] \rightarrow 0$, R attains the value unity, as the substrate-binding event becomes the rate-determining step. In the limit, $[M] \rightarrow 0$, the activation of ERK2 enzyme becomes the slowest step so $R = 1$.

Based on the data listed in Table 1 shown below, the dependence of the randomness parameter on u , $[M]$ and $[D]$ for model shown in Figure 6.4 is same as that of Figure 6.2. Also based on the expression of the randomness parameter as given in Eq.14, the randomness parameter is independent of the conformational fluctuation rate p for Figure 6.4. When the rate of conformational fluctuations between E_1 and E'_1 and the rate of formation of the phosphorylated enzyme from E_1 and E'_1 are same, there is no competition among reaction timescales, and the randomness parameter is independent of the conformational fluctuations at a given concentration of $[M]$ and $[D]$.

Table 6.1:

6.1(a) Effect of the binding rate constant u at high $[S]$ for Figure 6.4:

Kinetic Parameters	u	R
$w = 1, \alpha = 5, [M] = 1, [D] = 0.1, [S] = 5 * 10^4$	0.001	~ 1
	0.5	0.6250
	1	0.4800
	5	0.3786
$w = 1, \alpha = 500, [M] = 1, [D] = 0.1, [S] = 5 * 10^4$	1 (fixed)	~ 1

6.1(b) Effect of the activator concentration $[M]$ at high $[S]$ Figure 6.4:

Kinetic Parameters	$[M]$	R
$u = 1, w = 1, \alpha = 5, [D] = 0.001, [S] = 5 * 10^4$	0.001	~ 1
	0.1	0.8906
	1	0.4800
	10	0.4140
$u = 1, w = 1, \alpha = 500, [D] = 0.001, [S] = 5 * 10^4$	1 (fixed)	~ 1

6.1(c) Effect of the deactivator concentration $[D]$ for Figure 6.4:

Kinetic Parameters	[D]	R
$u = 1, \omega = 1, \alpha = 5, [M] = 1, [S] = 5 * 10^4$	0.001	0.4800
	1	0.4800
	$1 * 10^3$	0.4902
	$5 * 10^6$	~ 1
$u = 1, \omega = 1, \alpha = 500, [M] = 1, [S] = 5 * 10^4$	1 (fixed)	~ 1

In the next schematic, the activator bound state E_1' , cannot directly undergo an irreversible transition leading to the activated state E_2 . E_1' can make a conformational flip to E_1 , followed by reaching E_2 . The rest of Figure 6.5 is same as that of the reaction model shown in Figure 6.4. The variables constituting the probability distributions are $n_{E_0}, n_{E_1}, n_{E_1'}, n_{E_2}, n_{E_3}, n_{E_2S}, n_{E_2^{(0)}}$ and n_P representing the number of enzyme molecules present in the state $E_0, E_1, E_1', E_2, E_3, E_2S$, and $E_2^{(0)}$, respectively. n_P is the number of product molecules formed at a time t .

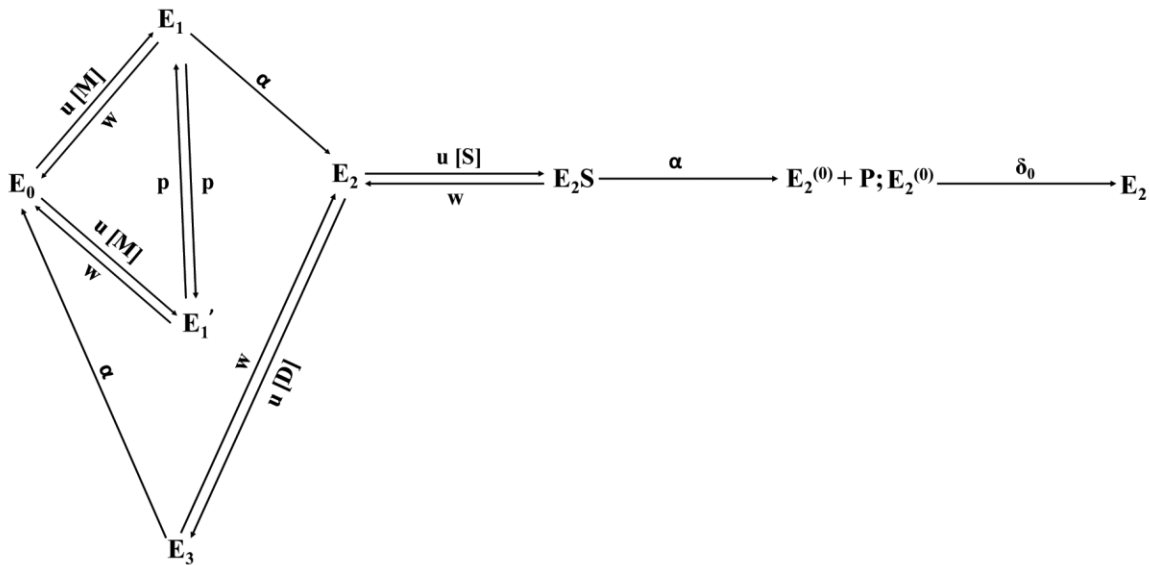


Figure 6.5: Schematic representation showing the activation/phosphorylation of the inactive ERK2 assisted by the two different activator-bound enzymatic states (E_1' cannot directly reach the phosphorylated state of the ERK2), deactivation of the active ERK2 and substrate phosphorylation carried out by the activated ERK2 enzyme.

$$\begin{aligned}
& \partial_t P \left[n_{E_0}, n_{E_1}, n_{E_1'}, n_{E_2}, n_{E_3}, n_{E_2S}, n_{E_2^{(0)}}, n_P; t \right] \\
&= \left(u[M](n_{E_0} + 1)Y_{E_0}Y_{E_1}^{-1} + w(n_{E_1} + 1)Y_{E_0}^{-1}Y_{E_1} + \alpha(n_{E_1} + 1)Y_{E_1}Y_{E_2}^{-1} \right. \\
&+ u[M](n_{E_0} + 1)Y_{E_0}Y_{E_1'}^{-1} + w(n_{E_1'} + 1)Y_{E_0}^{-1}Y_{E_1'} + p(n_{E_1} + 1)Y_{E_1}Y_{E_1'}^{-1} \\
&+ p(n_{E_1'} + 1)Y_{E_1}^{-1}Y_{E_1'} + u[D](n_{E_2} + 1)Y_{E_2}Y_{E_3}^{-1} + w(n_{E_3} + 1)Y_{E_2}^{-1}Y_{E_3} \\
&+ \alpha(n_{E_3} + 1)Y_{E_0}^{-1}Y_{E_3} + u[S](n_{E_2} + 1)Y_{E_2}Y_{E_2S}^{-1} + w(n_{E_2S} + 1)Y_{E_2}^{-1}Y_{E_2S} \\
&+ \alpha(n_{E_2S} + 1)Y_{E_2S}Y_{E_2^{(0)}}^{-1}Y_P^{-1} \\
&- (2u[M]n_{E_0} + (w + p + \alpha)n_{E_1} + (w + p)n_{E_1'} + u([D] + [S])n_{E_2S} \\
&+ (\alpha + w)n_{E_3} + (\alpha + w)n_{E_2S}) \left. \right) P \left[n_{E_0}, n_{E_1}, n_{E_1'}, n_{E_2}, n_{E_3}, n_{E_2S}, n_{E_2^{(0)}}, n_P; t \right]
\end{aligned} \tag{6.15}$$

Following the same mathematical procedure as adopted for the previous models, we get Eq.6.16.

$$\begin{bmatrix} \hat{P}_{E_0}(s) \\ \hat{P}_{E_1}(s) \\ \hat{P}_{E_1'}(s) \\ \hat{P}_{E_2}(s) \\ \hat{P}_{E_3}(s) \\ \hat{P}_{E_2S}(s) \\ \hat{P}_{E_2^{(0)}}(s) \end{bmatrix} = \begin{bmatrix} \frac{s^4 + h s^3 + j s^2 + l s + n}{s^5 + s^4 q + s^3 x + s^2 y + s z + \lambda_1} \\ \frac{[M]u s^3 + \lambda_2 s^2 + \lambda_3 s + \lambda_4}{s^5 + s^4 q + s^3 x + s^2 y + s z + \lambda_1} \\ \frac{[M]u s^3 + \lambda_5 s^2 + \lambda_6 s + \lambda_7}{s^5 + s^4 q + s^3 x + s^2 y + s z + \lambda_1} \\ \frac{\alpha[M]u s^2 + \lambda_8 s + \lambda_9}{s^5 + s^4 q + s^3 x + s^2 y + s z + \lambda_1} \\ \frac{\alpha[D][M]u^2 s + \alpha[D][M]u^2(2p+w)}{s^5 + s^4 q + s^3 x + s^2 y + s z + \lambda_1} \\ \frac{\alpha[M][S]u^2 s + \alpha[M][S]u^2(2p+w)}{s^5 + s^4 q + s^3 x + s^2 y + s z + \lambda_1} \\ 0 \end{bmatrix} \tag{6.16}$$

Here $h = 2\alpha + 2p + ([D] + [S])u + 3w$,

$j = \alpha([D] + [S])u + \alpha(p + w) + w(2p + w) + (\alpha + ([D] + [S])u + w)(\alpha + 2(p + w))$,

$l = \alpha([D] + [S])u(\alpha + 2(p + w)) + (\alpha + ([D] + [S])u + w)(\alpha(p + w) + w(2p + w))$,

$n = \alpha([D] + [S])u(\alpha(p + w) + w(2p + w))$,

$q = 2p + ([D] + 2[M] + [S])u + 3w + \alpha(2 + \alpha[M][S]u^2(2p + w))$,

$x = \alpha^2 + (2[M]u + w)(([D] + [S])u + w) + (2p + w)(([D] + 2[M] + [S])u + 2w) + \alpha(3p + 2([D] + 2[M] + [S])u + 4w)$,

$$y = (2p + w)(2[M]u + w)(([D] + [S])u + w) + \alpha^2(p + ([D] + 2[M] + [S])u + w) \\ + \alpha(6[M]p u + ([D] + [S])u(3p + 4[M]u) + 3p w + (3[D] + 5[M] + 3[S])u w \\ + 2w^2),$$

$$z = \alpha u((2p + w)(3[M]([D] + [S])u + ([D] + [M] + [S])w) + \alpha([S](p + w) + [D](p + [M]u \\ + w) + [M](2p + 2[S]u + w))),$$

$$\lambda_1 = \alpha^2[M][S]u^2(2p + w), \lambda_2 = [M]u(\alpha + 2p + ([D] + [S])u + 2w),$$

$$\lambda_3 = [M]u(\alpha([D] + [S])u + (2p + w)(\alpha + ([D] + [S])u + w)),$$

$$\lambda_4 = \alpha[M]([D] + [S])u^2(2p + w), \lambda_5 = \lambda_2 + \alpha[M]u,$$

$$\lambda_6 = \lambda_3 + [M]u(\alpha(\alpha + ([D] + [S])u + w)), \lambda_7 = \lambda_4 + \alpha^2[M]([D] + [S])u^2,$$

$$\lambda_8 = \alpha[M]u(\alpha + 2(p + w)), \text{ and } \lambda_9 = \alpha[M]u(\alpha + w)(2p + w).$$

Eq. 6.17 represents the waiting-time distribution for the model shown in Figure 6.5.

$$\hat{f}(s) = \alpha \hat{P}_{E_2S}(s) = \alpha^2 \left(\frac{[M][S]u^2 s + [M][S]u^2(2p+w)}{s^5 + q s^4 + x s^3 + y s^2 + z s + \lambda_1} \right). \quad (6.17)$$

From Eq. 6.17, we get the mean reaction time.

$$\langle t \rangle = \frac{\alpha(p+[M]u+w)+(2p+w)(3[M]u+w)}{\alpha[M]u(2p+w)} + \frac{(2p+w)(3[D][M]u+([D]+[M])w)+\alpha([M](2p+w)+[D](p+[M]u+w))}{\alpha[M][S]u(2p+w)} \quad (6.18)$$

The mean time for the substrate phosphorylation follows the MM equation. Eq. 6.19 shows the analytical expression for the randomness parameter for the scheme shown in Figure 6.5.

$$R = 1 - \frac{2MS\xi_8}{\xi_9} \quad (6.19)$$

$$\text{Here } \xi_5 = (2p + w)^2(2[M]u + w)(([D] + [S])u + w),$$

$$\xi_6 = \alpha^2(2p^2 + p([D] + 2[M] + [S])u - [M]([D] + [S])u^2 + 3pw + [M]uw + w^2),$$

$$\xi_7 = \alpha(2p + w)(u(3p([D] + 2[M] + [S]) + [M]([D] + [S])u) + (3p + 2([D] + 2[M] + [S])u)w \\ + 2w^2),$$

$$\xi_8 = \xi_5 + \xi_6 + \xi_7, \text{ and}$$

$$\xi_9 = ((2p + w)(3[M]([D] + [S])u + ([D] + [M] + [S])w) + \alpha([S](p + w) + [D](p + [M]u + w) \\ + [M](2p + [S]u + w)))^2.$$

In Eq. 6.19, if we put the limit $[S] \rightarrow 0$ then R attains the value unity, as the substrate-binding event becomes the rate-determining step. Also in the limit, $[M] \rightarrow 0$, the activation of ERK2 enzyme becomes the slowest step so $R = 1$.

For this model (Figure 6.5), the presence of conformational fluctuations between two activator bound enzymatic states affects the randomness in the system. When the enzyme is in the inactive E'_1 state, it has to reach to the E_1 state for the reaction to proceed towards product formation. When the rate constant characterizing these conformational transitions (p) is smaller or comparable in magnitude to the other rate constants then it can lead to dynamic disorder. This is evident from the significant deviation in the value of R from unity (Eq.18) as shown in Figure 6.5. With an increase in the magnitude of p , E'_1 readily converts to E_1 and the dynamic disorder decreases, R is equal to one. As seen from the data listed in Table II, all other dependencies of R on u , $[M]$ and $[D]$ follows the same trend as observed for the model shown in Figure 6.2.

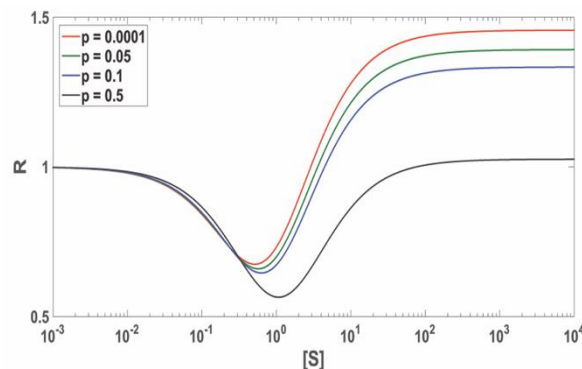


Figure 6.6: Plot showing the variation of R as a function of $[S]$ for the reaction scheme represented in Figure 6.5 to analyse the effect of the rate constant p at four different values 0.0001, 0.05, 0.1 and 0.5 represented by the red, green, blue and black solid lines, respectively. The common set of reaction parameters $u = 1$, $w = 1$, $\alpha = 5$, $[M] = 10$ and $[D] = 0.1$.

Table 6.2:

6.2(a) Effect of the binding rate constant u at high $[S]$ for Figure 6.5:

Kinetic Parameters	u	R
$w = 1, \alpha = 5, p = 1, [M] = 1, [D] = 0.1, [S] = 5 * 10^4$	0.001	~ 1
	0.5	0.7174
	1	0.6790
	5	0.7837
$w = 1, \alpha = 500, p = 1, [M] = 1, [D] = 0.1, [S] = 5 * 10^4$	1 (fixed)	~ 1

6.2(b) Effect of the activator concentration $[M]$ at high $[S]$ for Figure 6.5:

Kinetic Parameters	$[M]$	R
$u = 1, w = 1, \alpha = 5, p = 1, [D] = 0.001, [S] = 5 * 10^4$	0.001	~ 1
	0.1	0.8940
	1	0.6790
	10	0.8384
$u = 1, w = 1, \alpha = 500, p = 1, [D] = 0.001, [S] = 5 * 10^4$	1 (fixed)	~ 1

6.2(c) Effect of the deactivator concentration $[D]$ at high $[S]$ for Figure 6.5:

Kinetic Parameters	$[D]$	R
$u = 1, \omega = 1, \alpha = 5, p = 1, [M] = 1, [S] = 5 * 10^4$	0.001	0.6790
	1	0.6790
	$1 * 10^3$	0.6852
	$5 * 10^6$	~ 1
$u = 1, \omega = 1, \alpha = 500, p = 1, [M] = 1, [S] = 5 * 10^4$	1 (fixed)	~ 1

6.3 Conclusions:

In this chapter, we have applied the waiting-time distribution formalism to understand the dynamical picture associated with the substrate phosphorylation process catalysed by the activated ERK2 enzyme. For such reaction systems, we find that the reaction velocity follows the MM type relation. However, there are multiple rate-determining steps in different physical scenarios depending on the given parameter space as well as the concentrations of the activator, substrate, and deactivator. When there is sufficient availability of the activated ERK2 (E_2), and the substrate concentration is considerably higher than the $[D]$, the phosphorylation of the substrate will be favored over the deactivation/dephosphorylation of the active enzyme (E_2).

At high $[S]$, the enzyme present in the substrate-bound state can either form the product or E_2S can simply revert-back to E_2 . Thus, there are multiple rate determining steps contributing to the randomness of the system. For the cases when the $[D]$ and $[S]$ both are significantly high, the probabilities of transitions from the deactivator bound and substrate-bound enzymatic states increases leading to the deviation in the value of R from unity. For the reaction model shown in Figure 6.4, the presence of conformational fluctuations between E_1 and E'_1 neither affects the reaction rate nor the randomness parameter. If the activated enzymatic state is not directly accessible to one of the activator bound state as shown in Figure 6.5, then the enzyme will be trapped in the E'_1 state and the formation of the activated ERK2 (E_2) form is hindered. If the conformational fluctuations are faster, then it will readily go back to E_1 state from which the formation of E_2 takes place and the disorder in the system decreases.

The applied theoretical formalism provides justifications to explain the causes contributing to the system randomness and emphasizes on how the rate-determining step changes in different physical situations. These analyses provides a platform for dynamical interpretations associated with the phosphorylation/de-phosphorylation network reactions.

6.4 References:

- (1) Futran, A. S.; Link, A. J.; Seger, R.; Shvartsman, S. Y. *Curr Biol* **2013**, *23*, R972.
- (2) Lavoie, H.; Therrien, M. *Nature Reviews Molecular Cell Biology* **2015**, *16*, 281.
- (3) Anderson, N. G.; Maller, J. L.; Tonks, N. K.; Sturgill, T. W. *Nature* **1990**, *343*, 651.
- (4) Wu, Z.; Elgart, V.; Qian, H.; Xing, J. J. *Phys. Chem. B* **2009**, *113*, 12375.
- (5) Snir, E.; Joore, J.; Timmerman, P.; Yitzchaik, S. *Langmuir* **2011**, *27*, 11212.
- (6) Canagarajah, B. J.; Khokhlatchev, A.; Cobb, M. H.; Goldsmith, E. J. *Cell* **1997**, *90*, 859.
- (7) Lee, T.; Hoofnagle, A. N.; Resing, K. A.; Ahn, N. G. *Journal of Molecular Biology* **2005**, *353*, 600.
- (8) Misiura, M. M.; Kolomeisky, A. B. *J. Phys. Chem. B* **2016**, *120*, 10508.
- (9) Misiura, M.; Kolomeisky, A. B. *J. Phys. Chem. B* **2019**, *150*, 155101.
- (10) Tanoue, T.; Adachi, M.; Moriguchi, T.; Nishida, E. *Nature Cell Biology* **2000**, *2*, 110.
- (11) Gardiner, C. W. *Handbook of Stochastic Methods: for Physics, Chemistry, and the Natural Sciences*; Springer: New York, 1996.
- (12) Kou, S. C.; Cherayil, B. J.; Min, W.; English, B. P.; Xie, X. S. *J. Phys. Chem. B* **2005**, *109*, 19068.
- (13) Singh, D.; Chaudhury, S. *J. Chem. Phys.* **2017**, *146*, 145103.

7. A stochastic theoretical approach to study the size-dependent catalytic activity of metal nanoparticle at the single molecule level

Reprinted from “Singh, D.; Chaudhury, S., *Phys. Chem. Chem. Phys.* 2017, 19, 8889-8895.” with the permission from the Royal Society of Chemistry publishing.

Reproduced by permission of The Royal Society of Chemistry

<https://pubs.rsc.org/en/content/articlepdf/2017/cp/c6cp07895h>

7.1 Introduction

Catalysis can be homogenous as well as heterogeneous. Enzymatic activity is usually associated with the homogenous turnover characteristics where the transformation of a specific substrate type to its corresponding product occurs with the regeneration of the free enzyme. However, in case of certain enzymes more than one substrate molecule can be processed at a time owing to the oligomeric nature (equivalent multiple active sites) of proteins but the catalytic action would remain restricted to a particular substrate.¹ Some enzymes exhibit the well-known allosteric effect, where a non-active (docking) site is present along with the active site. In these mechanisms, occupancy of the docking site introduces configurational rearrangements, which modulate the substrate-binding event and eventually both of these sites are vacant after the successful execution of the turnover event.^{2,3} Experimental evidences and theoretical investigations related to the kinetics of an enzyme in the presence of varying substrates have shed light on the multiple binding pathways and its stochastic dependencies on the sequence and site specificity.⁴ Reaction models describing such catalytic systems have clarified the cooperative effect⁵ and explained the ternary complex formation mechanisms, which leads to the turnover (final product) event. In other words, we can say that the fundamental homogeneity associated with the activity of an enzyme (monomeric/oligomeric) signifies the conversion of a definite substrate to its product. In our previous thesis chapters, we have described all these effects in details by considering different enzymatic models undergoing reversible conformational interconversions.

On the contrary, nanoparticles are heterogeneous catalysts pertaining to different types of surface active sites, spontaneous or induced surface restructuring dynamics, which affects the adsorption equilibrium kinetics of different catalytic channels. Metal nanoparticles play an important role as catalysts in many chemical transformations and have many industrial applications.⁶⁻⁸ Unlike enzymes, in NP catalysis there are many simultaneous chemical reactions occurring on different active sites. This can lead to a distribution of time-dependent catalytic rate constants.⁹ The heterogeneous and dynamic behaviour of metal nanoparticles remains hidden in ensemble-averaged measurements. Electrochemical microscopy techniques,¹⁰ surface plasmon resonance,¹¹ electro generated chemiluminescence¹² and single fluorescence microscopy⁸ are among the few techniques that have been

used to study the catalytic activity of a single metal nanoparticle in real time. Zhou *et al.* has used single-molecule fluorescence microscopy to study the redox catalysis of single gold nanoparticle that catalyses the reduction of resazurin to a fluorescent product, resorufin in an aqueous environment.⁸ The product formation and product dissociation events were respectively characterized by the off and on behaviour of the intensity in the fluorescence trajectory. The calculated autocorrelation functions of the off and on times were not found to be zero which indicates the presence of time-dependent fluctuations in both the off and the on reaction rates.

Further single molecule studies reveal that the size of a nanoparticle plays an important role, which consequently leads to different catalytic reactivity and selectivity between the two parallel product dissociation pathways.¹³ The experimental results show that the surface restructuring time scales are different for individual nanoparticles of different dimension. Also, the rate of activity fluctuations for both the off and on reactions are higher for nanoparticles of smaller size. It was also explained theoretically that the surface dynamic restructuring occurs readily in smaller size nanoparticles due to high surface energies.¹³ We know that the measurements of average rate from the first moment of the off and on distributions does not provide enough information about the temporal fluctuations in the off and on rates. In order to obtain a quantitative measure of the temporal variations, one can calculate the randomness parameter.¹⁴

Unlike enzymes, nanoparticles do not follow the classical Michaelis-Menten (MM) mechanism. Xu *et al.*¹⁵ has proposed a single-molecule kinetic theory based on the Langmuir Hinshelwood mechanism to describe the catalytic product formation event which could explicitly account for the multitude of catalytic sites on the nanoparticle surface by considered two parallel product dissociation pathways as reported earlier in experiments.⁸ Using this Langmuir Hinshelwood mechanism,¹⁶ the randomness parameter was calculated for the off and on state from the respective probability densities, which successfully described the stochastic dynamics associated with different pathways. When the substrate adsorption-desorption is low, the Langmuir adsorption isotherm breaks down. In such a scenario, Xu *et al.* considered a modified Michaelis-Menten mechanism for heterogeneous nanoparticle catalysis.¹⁵ But this modified theory employed one "effective" active site assumption which represented

all the catalytic sites.¹⁵ Therefore, it could not explain the actual effect of size on the catalytic activity of a single metal nanoparticle.

However, experimental studies indicated that the inclusion of a multitude of surface active sites on a single nanoparticle surface could enhance disorder.¹³ In order to account for the effect of heterogeneity in nanoparticle catalysis, Ochoa *et al.* has calculated the time correlation functions in the off and on state for an experimental fluorescence trajectory.¹⁷ Das *et al.* has proposed a theoretical model¹⁸ based on the first passage time distribution formalism where they have considered multiple non-equivalent catalytic sites and quantified the time dependent fluctuations in the activity of a single NP.

In this chapter, we utilize a stochastic approach that is based on the superposition of renewal processes (SRP)¹⁹ to obtain the first passage time distribution of product formation and dissociation event for single nanoparticle of different sizes. The number of surface active sites increases with the increase in particle dimension. We consider an arbitrary N number of independent and identical non-interacting sites on the nanoparticle. We can calculate the distribution of the off and on events of N such identical and independent catalytic sites starting from the distributions of a single active site on the nanoparticle surface. Here, the main aim is to develop a generalized theoretical framework in order to analyse the size-dependent activity of single nanoparticle and the temporal fluctuations in the catalytic rates.

7.2 Reaction Model and Analyses:

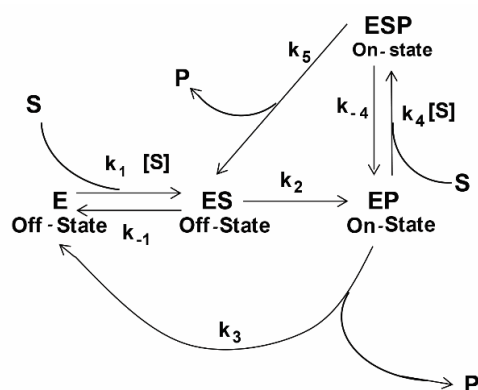


Figure 7.1: Modified MM scheme of enzyme catalysis with multiple product dissociation pathways applicable to single nanoparticle catalysis.

For the given model, we obtain the first passage time distribution of N -number of identical surface catalytic sites on a single nanoparticle. In the context of heterogeneous nanoparticle catalysis, each product formation, and dissociation event corresponds to a renewal process.²⁰ The off and on time distribution for a single catalytic site is used to obtain the pooled output which corresponds to the distribution of N independent and equivalent catalytic sites. Following the SRP method by Cox and Smith,¹⁹ the first passage time distribution of N surface sites is given by Eq. 7.1.

$$\phi_{off/on}(t, N) = N\phi_{off/on}(t, 1)\left(\int_t^\infty \phi_{off/on}(\tau, 1)d\tau\right)^{N-1} \quad (7.1)$$

Here $\phi_{off/on}(t, 1) \equiv \phi_{off/on}(t)$ corresponds to the first passage time distribution between two successive off/on events for a single catalytic site on the surface of a nanoparticle. Eq. 7.2 written below represents the PDF for the fluorescent product formation event.

$$\widehat{\phi}_{off}(s) = C_1\widehat{\phi}_1(s) + C_2\widehat{\phi}_2(s) \quad (7.2)$$

In the above equation C_1 and C_2 are the weight coefficients for the two product dissociation pathways such that $C_1 + C_2 = 1$.

$$C_1 = \frac{k_3(1+K_2[S])}{k_3(1+K_2[S])+k_5K_2[S]}, C_2 = \frac{k_5K_2[S]}{k_3(1+K_2[S])+k_5K_2[S]} \text{ and } K_2 = \frac{k_4}{k_{-4}+k_5}.$$

Eq. 7.3 represents the PDF for the direct dissociation pathway.

$$\widehat{\phi}_1(s) = \frac{\widehat{Q}_{E \rightarrow ES}(s)\widehat{Q}_{ES \rightarrow EP}(s)}{1 - \widehat{Q}_{E \rightarrow ES}(s)\widehat{Q}_{ES \rightarrow E}(s)} \quad (7.3)$$

Similarly, Eq. 7.4 shows the PDF for the substrate-assisted pathway.

$$\widehat{\phi}_2(s) = \frac{\widehat{Q}_{ES \rightarrow EP}(s)}{1 - \widehat{Q}_{E \rightarrow ES}(s)\widehat{Q}_{ES \rightarrow E}(s)} \quad (7.4)$$

The waiting time distributions characterizing the transitions between any two consecutive states have the following functional form.

$$\widehat{Q}_{ES \rightarrow EP}(s) = \frac{k_2}{s+k_2+k_{-1}} \quad (7.5.a)$$

$$\widehat{Q}_{ES \rightarrow E}(s) = \frac{k_{-1}}{s+k_2+k_{-1}} \quad (7.5.b)$$

$$\widehat{Q}_{E \rightarrow ES}(s) = \frac{k_1[S]}{s+k_1[S]} \quad (7.5.c)$$

After substituting the above set of equations in Eq. 7.2, we get Eq. 7.6.

$$\widehat{\Phi}_{off}(s) = \frac{k_2[S](k_1k_3(k_{-4}+k_5)+k_4k_5s+k_1k_4(k_3+k_5)[S])}{(k_3(k_{-4}+k_5)+k_4(k_3+k_5)[S])(k_{-1}s+(k_2+s)(s+k_1[S]))} \quad (7.6)$$

The inverse Laplace transform of the above equation will yield Eq. 7.7.

$$\widehat{\Phi}_{off}(t) = \frac{e^{Bt} k_2[S]((G+K[S])(1-e^{At})+(k_4k_5A)(1+e^{At}))}{(I+J[S])A} \quad (7.7)$$

Here $A = \sqrt{-4k_1k_2[S] + (k_{-1} + k_2 + k_1[S])^2}$, $B = -\frac{1}{2}(k_{-1} + k_2 + k_1[S] + A)$,

$G = -2k_1k_3(k_{-4} + k_5) + k_4k_5(k_{-1} + k_2)$, $K = -k_1k_4(2k_3 + k_5)$, $I = 2k_3(k_{-4} + k_5)$ and $J = 2k_4(k_3 + k_5)$.

Next, we construct the PDF for the product dissociation event, given as Eq. 7.8.

$$\widehat{\Phi}_{on}(s) = \frac{\widehat{Q}_{EP \rightarrow ESP}(s)\widehat{Q}_{ESP \rightarrow ES}(s)+\widehat{Q}_{EP \rightarrow E}(s)}{1-\widehat{Q}_{EP \rightarrow ESP}(s)\widehat{Q}_{ESP \rightarrow EP}(s)} \quad (7.8)$$

Eq. 7.9 shows the waiting time distributions for each step associated with the on route.

$$\widehat{Q}_{EP \rightarrow ESP}(s) = \frac{k_4[S]}{s+k_4[S]+k_3} \quad (7.9.a)$$

$$\widehat{Q}_{ESP \rightarrow ES}(s) = \frac{k_5}{s+k_{-4}+k_5} \quad (7.9.b)$$

$$\widehat{Q}_{EP \rightarrow EP}(s) = \frac{k_{-4}}{s+k_{-4}+k_5} \quad (7.9.c)$$

$$\widehat{Q}_{EP \rightarrow E}(s) = \frac{k_3}{s+k_4[S]+k_3} \quad (7.9.d)$$

Substituting the above expressions in Eq. 7.8, we will get Eq. 7.10.

$$\widehat{\Phi}_{on}(s) = \frac{k_5k_4[S]+k_3(s+k_{-4}+k_5)}{(s+k_{-4}+k_5)(s+k_4[S]+k_3)-k_{-4}k_4[S]} \quad (7.10)$$

By taking an inverse Laplace Transform of Eq. 7.10, we can obtain the PDF for the on event (fluorescent product dissociation) in the time domain.

$$\phi_{on}(t) = \frac{e^{B't}[(C'+D'[S])(1-e^{A't})+k_3A'(1+e^{A't})]}{2A'} \quad (7.11)$$

$$\text{Here } A' = \sqrt{(k_3 + k_{-4} + k_5 + k_4[S])^2 - 4(k_3(k_{-4} + k_5) + k_4k_5[S])},$$

$$B' = -\frac{1}{2}[(k_3 + k_{-4} + k_5 + k_4[S]) + A'], \quad C' = k_3(k_3 - k_{-4} - k_{-5}) \text{ and } D' = k_4(k_3 - 2k_{-5}).$$

In order to account for the heterogeneity of a single nanoparticle, one needs to consider the effect of multiple surface active sites explicitly. For deducing the distribution of the on and off times for N independent, identical catalytic sites, we substitute Eq. 7.7 and 7.11 in Eq. 7.1. From the first and second moment of these distributions, we can account for the substrate concentration dependence of the randomness parameter in the off and on state for a single nanoparticle of different dimensions and a varying number of surface catalytic sites.

To illustrate the effect of the dimension of the nanoparticle, we consider single nanoparticles of three different dimensions; Type I having only two catalytic sites ($N = 2$), Type II with five catalytic sites ($N = 5$), and Type III with ($N = 10$). The number of catalytic sites is proportional to the size of the nanoparticle. Experimental findings of Zhou and co-workers, have shown that the binding of the substrate to the Au-nanoparticle is weaker for smaller particle size and they preferentially dissociate via substrate assisted pathway.¹³ The catalytic reactivity per surface site increases with the dimension of the single nanoparticle. For bigger size nanoparticles, single-particle measurements show that the selectivity decreases and the two dissociation pathways are equally likely. Thus, the kinetic parameters show size-dependent activity and hence the parameter values for the different rate constants chosen in our theoretical investigation are such that they follow the experimental trends.

Figure 7.2 shows the temporal variation of the turnover time distribution in the off state for three different nanoparticle sizes as calculated from Eq. 7.1. For all three dimensions, the turnover times decay mono-exponentially at low and high substrate concentration $[S]$ (Figures 7.2(a) and 7.2(c)). At intermediate $[S]$, for particles of smaller dimension, the distribution is multi-exponential (Figure 7.2(b))

and becomes narrower with the increasing particle size.

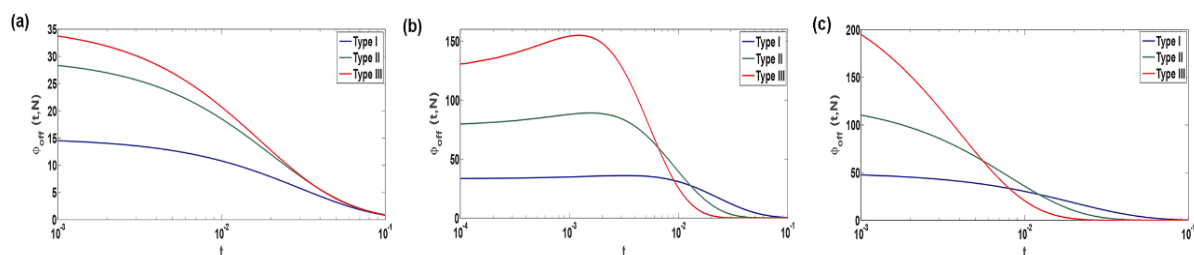


Figure 7.2: The temporal variation of first passage time distribution in the off state for different size of nanoparticle. For (a) and (c) distribution is monoexponential at low $[S] = 0.01$ and high $[S] = 10^4$ for Type I: $N = 2$ (blue line), Type 2: $N = 5$ (green line) and Type III: $N = 10$ (red line). For (b) the distribution is multiexponential at an intermediate substrate concentration $[S] = 100$ for all three types of nanoparticle. Parameter values for Type I: $k_1 = 2, k_3 = 4, k_5 = 8$, Type II: $k_1 = 5, k_3 = 6, k_5 = 10$ and Type III: $k_1 = 6, k_3 = k_5 = 12$. Common parameter values in (a)-(c) are $k_{-1} = 1, k_2 = 25, k_4 = 300, k_{-4} = 3$.

Similarly, Figure 7.3 gives the first passage time distribution for the on state for three different particle sizes. The parameter values of the kinetic parameters are same as used in Figure 7.2. For all three sizes ($N = 2, N = 5, N = 10$), the distributions show an exponential decay at low and high $[S]$ (Fig. 3(a) and (c)). At intermediate substrate concentrations, for small and medium size nanoparticles ($N = 2, N = 5$), the distribution is multi-exponential as shown in Figure 7.3(b). Similar to the off time distributions, the multi-exponential behaviour decreases with the increase in the single nanoparticle size.

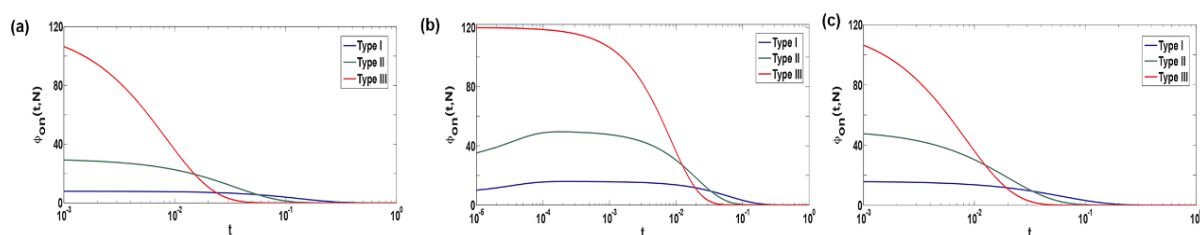


Figure 7.3: The first passage time distribution in the on state is mono-exponential at low substrate concentration ($[S] = 0.01$) and high substrate concentration ($[S] = 10000$) for Type I: $N = 2$ (blue line), Type II: $N = 5$ (green line) and Type III: $N = 10$ (red line). The distributions at a moderate substrate concentration ($[S] = 100$) are multi exponential for Type I: $N = 2$ (blue line), Type II: $N = 5$ (green line) and mono-exponential for Type III: $N = 10$ (red line). Parameter values for Type I: $k_3 = 4, k_5 = 8$, Type II: $k_3 = 6, k_5 = 10$ and Type III: $k_3 = k_5 = 12$. Common parameter values are $k_4 = 300$ and $k_{-4} = 3$.

At the single molecule level, such multi exponential behaviour in the first passage time distributions

arises due to dynamic surface reconstruction, which can lead to time-dependent activity fluctuations. The multi-exponential behaviour decreases with increasing particle size. For bigger size nanoparticles, $N = 10$ ($k_3 = k_5$), the on time distribution decays exponentially at all substrate concentrations, $[S]$. This indicates that for nanoparticles of larger dimension, the product dissociation process has a single rate-determining step.

The first moment of the off and on time distribution gives the rate of product formation and dissociation respectively. Figure 7.4 graphically shows the variation in the product formation and the dissociation rate with the substrate concentration, $[S]$ for single nanoparticles of three different dimensions. For all the three particle sizes, the rate of product formation ($\langle t_{off} \rangle^{-1}$), shows different saturation levels and a similar MM-like behaviour. For the product dissociation rate, $\langle t_{on} \rangle^{-1}$ saturates at high substrate concentration, $[S]$. For type III, with more number of surface sites, $k_3^{Type III} \approx k_5^{Type III}$, and the product dissociation rate is a constant and independent of $[S]$ (black line in Fig. 4b).

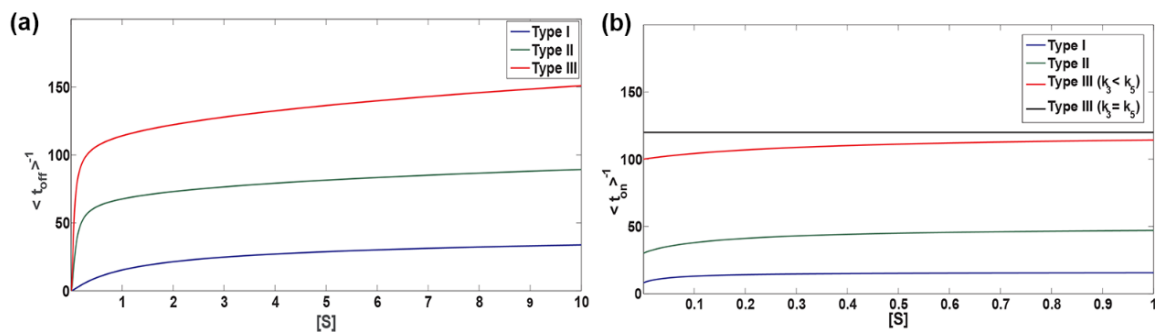


Figure 7.4: The reciprocal of the (a) off and (b) on times for three types of nanoparticles as a function of substrate concentration, $[S]$. The parameters values for the off and on rates as same as in Figure 7.2 and 7.3, respectively.

Next, we compute the randomness parameter to quantify the measure of the temporal fluctuations in the reaction pathway. Following Eq. 1, one can obtain the second moments of the first passage time distributions and hence the randomness parameter in the off and on state.

Figure 7.5(a) shows the variability of the randomness parameter in the off state as a function of particle size. For all three sizes of the particle, R_{off} is equal to unity for low and infinite substrate

concentration. The value of R_{off} significantly deviates from unity at intermediate substrate concentrations for all particle sizes. This is in agreement with Fig. 7.2 where we observed the multi-exponential decay behaviour of the off time distributions at intermediate $[S]$. This indicates the presence of dynamic disorder due to multiple competing time steps in the reaction. Figure 7.5(b) shows the variation of the randomness parameter with the number of surface active sites, N at some intermediate substrate concentration. For less number of identical catalytic sites, R_{off} is less than unity. Initially, with an increase in the number of surface catalytic sites the dynamic disorder increases and then decreases. Eventually, it saturates to unity. This indicates that the effect of dynamic surface restructuring is less prominent for particles of larger dimension.

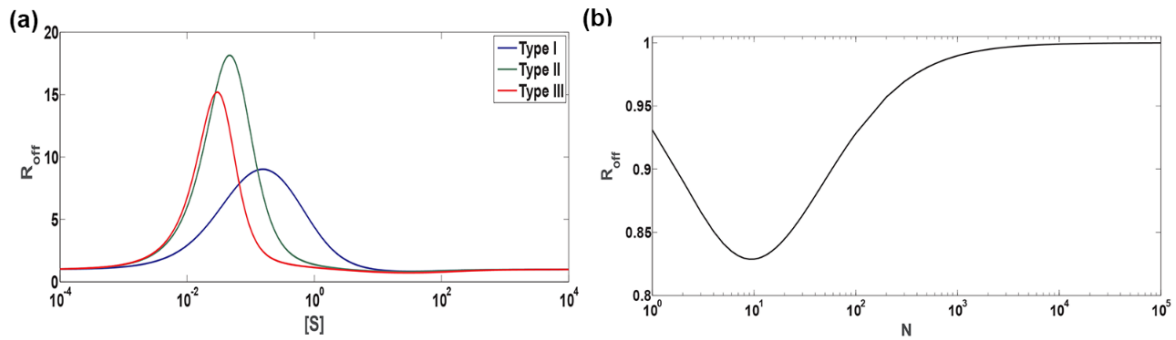


Figure 7.5: (a) The randomness parameter as a function of substrate concentration $[S]$ for the given scheme in the off state for Type I: $N = 2$ (blue line), Type II: $N = 5$ (green line) and Type III: $N = 10$ (red line). Parameter values are same as in Fig. 7.2. (b) The randomness parameter as a function of N for the given scheme at $[S] = 100$, $k_1 = 2$, $k_{-1} = 1$, $k_2 = 25$, $k_3 = 4$, $k_5 = 8$, $k_4 = 300$, $k_{-4} = 3$.

Figure 7.6(a) shows R_{on} as a function of $[S]$. For all three sizes of the particle, R_{on} is equal to unity for low and infinite substrate concentration. At intermediate substrate concentrations, for smaller particle size (Type I and II), where the substrate-assisted dissociation pathway is more likely than the direct dissociation step ($k_3 < k_5$), $R_{on} < 1$. This indicates that at intermediate $[S]$, dynamic disorder is present in a single nanoparticle of smaller dimension (Type I and Type II). For Type III, where N is large and both the product dissociation routes are equally likely ($k_3 = k_5$), the product dissociation is dominated by a single rate-determining step and R_{on} is equal to unity at all $[S]$. Thus, for large size nanoparticles with a multitude of surface active sites, there is no dynamic disorder in the product

dissociation reaction. Figure 7.6(b) shows the variation of R_{on} with the number of surface sites N at intermediate value of $[S]$. For less number of surface active sites R_{on} deviates more from unity that is randomness increases. With a further increase in N , the randomness decreases (R approaches unity).

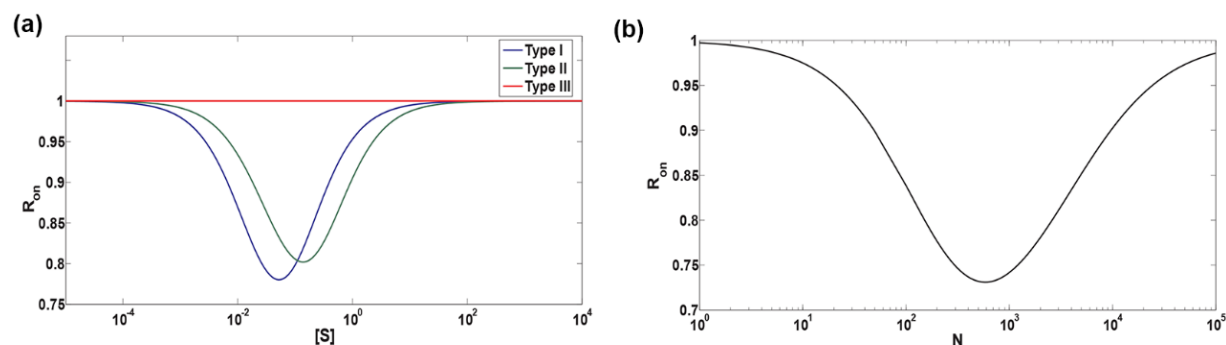


Figure 7.6: (a) Randomness parameter as a function of substrate concentration $[S]$ in the on state for the given scheme for Type I: $N = 2$ (blue line), Type II: $N = 5$ (green line) and Type III: $N = 10$ (red line). Parameter values are same as in Fig. 3. (b) Randomness parameter R_{on} as a function of N for the given scheme at $[S] = 10, k_3 = 4, k_5 = 8, k_4 = 300$ and $k_{-4} = 3$.

All these studies show that dynamic disorder arises due to the temporal fluctuations in the catalytic activity, attributed to the dynamic surface restructuring. For single nanoparticles of higher dimension with a large number of surface catalytic sites, the effect of dynamic surface restructuring decreases and it thereby reduces the effect of temporal activity fluctuations. R_{off} and R_{on} show deviation from unity at intermediate substrate concentrations for less number of surface catalytic sites indicating the presence of dynamic disorder. With further increase in the number of catalytic sites for a given nanoparticle, the dynamic disorder decreases.

7.3 Conclusions:

In this chapter, we have presented a theoretical approach based on the superposition of the renewal process (SRP) to understand the effect of particle size on the catalytic activity of metal nanoparticle. Within this approach, we obtain the off and on time distribution of N identical surface catalytic sites from the distribution function of one site. The off and on time distribution of a single nanoparticle with one catalytic site is obtained using the first passage time distribution formalism.²¹ The parameter values of the rate constants are chosen based on the experimental predictions of the dependence of kinetic rate constants on the size of the nanoparticle.^{13,15} The shape of the PDF and the value of the randomness

parameter in the off and on state support the fact that the effect of dynamic surface restructuring which can lead to activity fluctuations in the single metal nanoparticle is suppressed with the increase in the dimension of the nanoparticle. Our results show that there exists a close correlation between dynamic disorder and dynamic surface structural dynamics in single nanoparticle catalysis. It also provides a strong basis for the experimental findings on the size-dependent catalytic activity of nanoparticle at the single molecule level.

7.4 References:

- (1) Segel, I. H.; John, W.; Sons *Enzyme kinetics : behavior and analysis of rapid equilibrium and steady-state enzyme systems*; John Wiley & Sons: New York, 2014.
- (2) Lavoie, H.; Therrien, M. *Nat Rev Mol Cell Biol* **2015**, *16*, 281.
- (3) Misiura, M. M.; Kolomeisky, A. B. *J. Phys. Chem. B* **2016**, *120*, 10508.
- (4) Wallace Cleland, W. *Biochim. Biophys. Acta.* **1989**, *1000*, 209.
- (5) Qian, H. *Biophys. J.* **2008**, *95*, 10.
- (6) Ertl, G.; Knozinger, H.; Weitkamp, J. *Handbook of Heterogeneous Catalysis*; VCH: Weinheim, 1997.
- (7) Burda, C.; Chen, X.; Narayanan, R.; El-Sayed, M. A. *Chem. Rev.* **2005**, *105*, 1025.
- (8) Xu, W.; Kong, J. S.; Yeh, Y.-T. E.; Chen, P. *Nat. Mater.* **2008**, *7*, 992.
- (9) Zwanzig, R. *Acc. Chem. Res.* **1990**, *23*, 148.
- (10) Vered, R. T.; Bard, A. J. *J. Phys. Chem. B* **2006**, *110*, 25279.
- (11) Novo, C.; Funston, A. M.; Mulvaney, P. *Nat. Nanotechnol.* **2008**, *3*, 598.
- (12) Fan, F.-R. F.; Bard, A. *Nano Lett.* **2008**, *8*, 1746.
- (13) Zhou, X.; Xu, W.; Liu, G.; Panda, D.; Chen, P. *J. Am. Chem. Soc.* **2010**, *132*, 138.
- (14) Moffitt, J. R.; Bustamante, C. *FEBS J.* **2013**, *281*, 498.
- (15) Xu, W.; Kong, J. S.; Chen, P. *J. Phys. Chem C* **2009**, *113*, 2393.
- (16) Satterfield, C. N. *Heterogeneous Catalysis in Practice*; McGraw-Hill Book Company: New York, 1980.
- (17) Ochoa, M. A.; Chen, P.; Loring, R. F. *J. Phys. Chem. C* **2013**, *117*, 19074.
- (18) Das, A.; Chaudhury, S. *Chem. Phys. Lett.* **2015**, *641* 193.
- (19) Cox, D. R.; Smith, W. L. *Biometrika* **1954**, *41*, 91.
- (20) Cao, J.; Silbey, R. J. *J. Phys. Chem. B* **2008**, *112*, 12867.
- (21) Chaudhury, S.; Cao, J.; Sinitzyn, N. A. *J. Phys. Chem. B* **2013**, *117*, 503.

8. Theoretical investigations of the dynamics of chemical reactions on nanocatalysts with multiple active sites

Reprinted from “Chaudhury, S.; Singh, D.; Kolomeisky, A. B., *J. Phys. Chem. Lett.* 2020, 11, 2330-2335.” with the permission from the American Chemical Society publishing.

© 2020, American Chemical Society

8.1 Introduction:

Application of numerous experimental methods with high temporal and spatial resolutions and analytical frameworks, help in understanding multiple chemical processes on nanocatalysts.¹⁻⁵ However, the molecular mechanism of these phenomena remains not well understood. Single-molecule experimental approaches give much detailed stochastic information. By analysing a certain number of fluorescence trajectories comprising a specific number of products in a defined time range, one can obtain the waiting time distributions of the fluorescent product formation and dissociation event, which corresponds to one-on and one-off-event, respectively. These studies confirm that there is a wide distribution in the rates of product formations and dissociations on nanocatalysts, and that the size of the nanocatalyst affects the dynamic surface restructuring, leading to the temporal dependence of the catalytic activities.

In our previous thesis chapter, we have employed a theoretical framework for modelling the size-dependent heterogeneous⁶ catalysis by a single nanocatalyst. For deriving the PDF, which could describe the different catalytic events occurring on the multiple surface active sites, we utilized the distribution corresponding to one site. In this way, one can analyse the required temporal effects from a pool of events. The statistical quantities of interest (the mean time and higher moments of the PDF) calculated using this approach gave the stochastic measurements obtained from the time distribution, which represented the overall time required for the turnover to happen on each site. In other words, only after the completion of the chemical reaction on all the surface sites there will be the commencement of the next set of events and this time between any two consecutive cumulative sets of processes gave the first passage distribution. The chemical model taken into account was quite simplistic.

On the contrary, at nanocatalysts, reactions occur simultaneously on multiple sites and the recorded times between any two consecutive fluorescence bursts, yields the PDF. The main objective of this chapter deals with the development and application of another theoretical approach based on the first passage analysis, which could establish a direct link between the experimentally measured time and the time distribution deduced from the analytical methods. This also emphasizes on exploring the

mechanistic details of the chemical reaction occurring on different catalytic sites of a single nanocatalyst. Unlike the previous theoretical methods, here we use a complex general reaction occurring on each site, which comprises an arbitrary number of catalytic active sites and intermediates. For a given network, based on the specific site descriptions (number of free or substrate-bound/occupied sites) of a particular state, one can determine the productivity and the probability of the chemical reaction to begin from there. Availability of a single or multiple free sites will ensure initiation of the chemical reaction from there. Similarly, for the product formation to happen from any state there must be a single or multiple bound sites.

Using a discrete-state stochastic model that takes into account the stochasticity of individual chemical reactions at each catalytic site, one can examine the molecular details of these processes and understand its relation with experimentally measured distributions of reaction times. The mean time analysis is insufficient to capture the stochastic effects so we need higher moments of the PDF. From these moments, one can quantify the temporal fluctuations present in the system and analyse the noise dependence for systems with varying number catalytic sites and number of intermediates.

8.2 Reaction Model and Analyses:

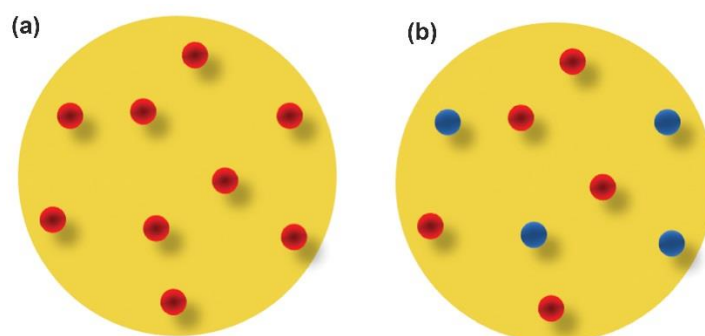


Figure 8.1: Schematic representation of a nanocatalyst with N (a) identical catalytic sites and (b) two different types of catalytic sites.

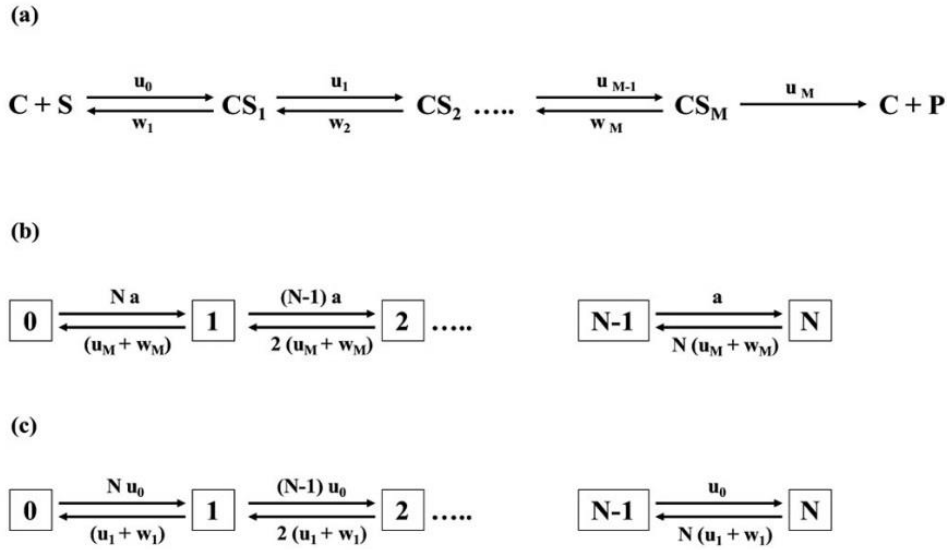


Figure 8.2: (a) Schematic representation of (a) catalytic reaction taking place at each catalytic site (b) system with N number of catalytic sites with M number of intermediate steps (c) system with one intermediate state, $M = 1$.

We consider a system consisting of a single nanocatalyst particle with N identical active sites as illustrated in Figure 8.1a. We assume that all catalytic sites are independent of each other and all of them are equally accessible to the substrate molecules. At each site, the chemical reaction with M ($M = 1, 2, 3, \dots$) sequential intermediate states is taking place. In this scheme, CS_j describes the intermediate chemical state j ($j = 1, 2, 3, \dots, M$) at the given catalytic site. From the state CS_j the reaction moves forward to the state CS_{j+1} with a rate u_j , while the backward transition that leads to the state CS_{j-1} has a rate, w . The substrate first binds to the catalytic site with a rate proportional to the concentration of substrates, $u_0 = k[S]$, while the final transition that creates the product molecule P is irreversible and it has a transition rate u_M (Figure 8.2a). Just like the experimental measurements, we calculate the catalytic time distribution and the related statistical quantities associated with the consecutive product formation events where we consider the possibility of one or more products formation from single or few sites. It depends on the number of catalytic sites present in the CS_M state. Chemical reactions are simultaneously happening at different catalytic sites, and a discrete-state stochastic scheme represents the overall dynamics in the system as shown in Figure 8.2b. Here the state n refers to a situation when n active sites are present in the chemical state CS_M just before the product formation is taking place. From the state n , the transition rates to the state $n + 1$ and $n - 1$ are given

by $(N - n)a$ and $n(u_M + w_M)$, respectively. The parameter a is the effective rate of reaching the state n from the state $n - 1$, and it can be always explicitly determined in terms of transition rates (u_j, w_j) for any M as shown later.

At large times, the dynamics in the system reaches stationary conditions. We define P_n as a steady-state probability to find the system in the state n , i.e. with n sites in the conformation, S_M . Because at $t \rightarrow \infty$, the discrete-state stochastic model (see Figure 8.2b) attains an effective equilibrium, with the following form of probabilities.

$$\begin{aligned} N a P_0 &= (u_M + w_M)P_1 \\ (N - 1) a P_1 &= 2(u_M + w_M)P_2 \dots \\ a P_{N-1} &= N(u_M + w_M)P_N \end{aligned} \tag{8.1}$$

Taking into account the normalization condition, $\sum_{n=0}^N P_n = 1$, one can solve these equations.

$$P_n = \frac{N! x^n}{(N-n)!n!(1+x)^N} \tag{8.2}$$

Using Eq.2, one can estimate the total flux from N sites, under stationary conditions.

$$J_N = u_M P_1 + 2u_M P_2 + 3u_M P_3 + \dots + Nu_M P_N = N \left(\frac{a u_M}{a + u_M + w_M} \right) \tag{8.3}$$

The reciprocal of the flux gives the mean time between the products release events, $\langle \tau \rangle_N = \frac{1}{J_N}$ which is also the average reaction times as measured in the single-molecule experiments.

$$\langle \tau \rangle_N = \frac{\langle \tau \rangle_1}{J_N} \tag{8.4}$$

In other words, the mean reaction times are inversely proportional to the number of active sites. It means that if one considers only the mean reaction times as a measure of the chemical processes occurring at the nanocatalyst, the stochastic effects remain hidden. This does not depend on the specific details of the chemical reactions at each site, which, however, affect the amplitude of reaction times. Considering only the mean reactions times, a system with N sites with the rates (u_j, w_j) [$j = 1, 2, 3, \dots, M$] behaves

exactly like a system with one "effective" single catalytic site with the rescaled rates, (Nu_j, Nw_j) . Figure 8.3 represents these observations.

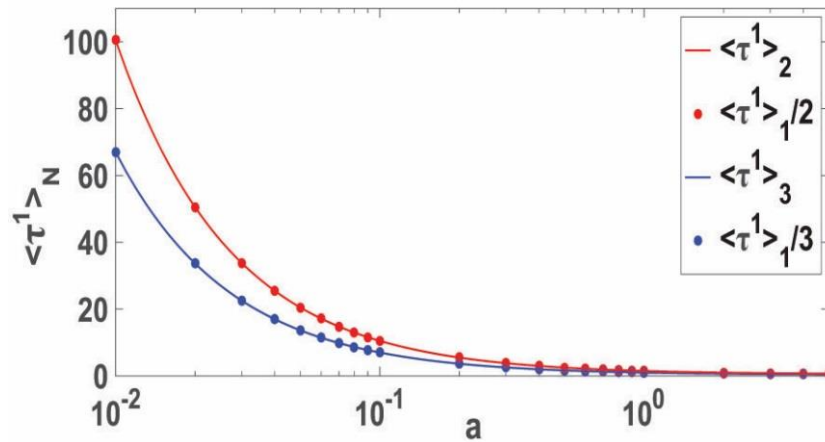


Figure 8.3: Mean reaction times $\langle \tau \rangle_N$ for the system with N catalytic sites as function of a , using $u_M = w_M = 1$.

The effective rate a can be explicitly expressed in terms of the intrinsic transition rates (u_j, w_j) . a depends only on the number of intermediate states M , but it is independent of the number of catalytic sites N .⁷ For $N = 1$, Eq. 8.5 represents the flux.

$$J_1 = \left(\frac{a u_M}{a + u_M + w_M} \right) = \frac{1}{R_M} \quad (8.5)$$

$$\text{Here } R_M = \sum_{j=0}^M r_j \quad (8.6)$$

$$r_j = \frac{1}{u_j} \left[1 + \sum_{k=1}^M \prod_{l=j+1}^{j+k} \frac{w_l}{u_l} \right] \quad (8.7)$$

From Eq. 5, we derive Eq. 8.8.

$$a = \left(\frac{u_M + w_M}{u_M R_M - 1} \right) \quad (8.8)$$

For $M = 1$, $a = u_0$.

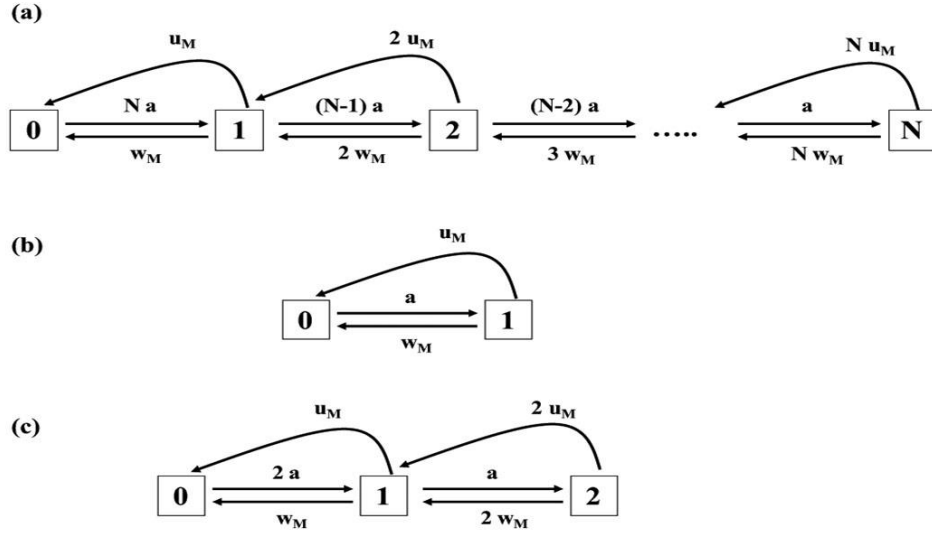


Figure 8.4: Theoretical framework for first-passage analysis for a system with N catalytic sites involving chemical reactions with M intermediate states. (b) Representation of the system for one catalytic site ($N = 1$) and (c) for two catalytic sites ($N = 2$) for M intermediates.

Since the mean reaction times do not reflect the stochasticity of the system and do not yield the molecular information on the mechanisms of chemical reactions at each site, we have to investigate the higher moments of the reaction times. For this purpose, we introduce a method based on the first-passage probability calculations of the catalytic times distributions. Figure 8.4 describes the discrete-state stochastic scheme for this approach. We define $F_n(t)$ as a probability density function to complete the catalytic cycle and to make the product P for the first time at time t , provided, at $t = 0$, the system is present in the state n . A set of backward master equations represents the temporal evolution of these first-passage probabilities.⁸

$$\frac{\partial F_0(t)}{\partial t} = N a F_1(t) - N a F_0(t) \quad (8.9.a)$$

$$\frac{\partial F_1(t)}{\partial t} = (N - 1)a F_2(t) + w_M F_0(t) + u_M F_P(t) - [(N - 1)a + w_M + u_M]F_1(t) \quad (8.9.b)$$

$$\frac{\partial F_n(t)}{\partial t} = (N - n)a F_{n+1}(t) + n w_M F_{n-1}(t) + n u_M F_P(t) - [(N - n)a + n(u_M + w_M)]F_n(t) \quad (8.9.c)$$

$$\frac{\partial F_N(t)}{\partial t} = N w_M F_{N-1}(t) + N u_M F_P(t) - N(u_M + w_M)F_N(t) \quad (8.9.d)$$

Here $F_P(t)$ represents the product state, such that, $F_P(t) = \delta(t)$. The physical meaning of this relation is that if the system is already in the product state, the reaction is immediately finished. One can solve these equations for any number of active sites using the Laplace transformations. From these transformed densities, one can derive the moments.

$$\langle T_n \rangle = - \left(\frac{\partial \hat{F}_n(s)}{\partial s} \right)_{s=0}, \langle T_n^2 \rangle = - \left(\frac{\partial^2 \hat{F}_n(s)}{\partial s^2} \right)_{s=0} \quad (8.10)$$

For $N = 1$, we will have the following equations for the probability densities. The reaction can begin from the state 0, as it has one free site. The product formation can exclusively take place from the reaction state 1, due to the availability of one CS_M conformer (Figure 8.4b).

$$\hat{F}_0(s) = \frac{a u_M}{s^2 + s(a + u_M + w_M) + a u_M} \quad (8.11.a)$$

$$\hat{F}_1(s) = \frac{u_M(s+a)}{s^2 + s(a + u_M + w_M) + a u_M} \quad (8.11.b)$$

For the given scheme, Eq. 8.12 shows the mean first passage time.

$$\langle \tau \rangle_1 = \langle T_0 \rangle = \frac{a + u_M + w_M}{a u_M} \quad (8.12)$$

Eq. 8.13 represents the second moment for the model shown in Figure 8.4b.

$$\langle \tau^2 \rangle_1 = 2 \left[\left(\frac{a + u_M + w_M}{a u_M} \right)^2 - \frac{1}{a u_M} \right] = 2(\langle \tau \rangle_1)^2 - \frac{2}{a u_M} \quad (8.13)$$

Similarly, one can analyse the catalytic systems with $N = 2$ and $N = 3$. Eq. 8.14 represents the backward CME for the system with two active sites (Figure 8.4c).

$$\frac{\partial F_0(t)}{\partial t} = 2a F_1(t) - 2a F_0(t) \quad (8.14.a)$$

$$\frac{\partial F_1(t)}{\partial t} = w_M F_0(t) + u_M F_P(t) + a F_2(t) - (w_M + u_M + a) F_1(t) \quad (8.14.b)$$

$$\frac{\partial F_2(t)}{\partial t} = 2 w_M F_1(t) + 2 u_M F_P(t) - 2(w_M + u_M) F_2(t) \quad (8.14.c)$$

$$\frac{\partial F_2(t)}{\partial t} = 2 w_M F_1(t) + 2 u_M F_P(t) - 2(w_M + u_M) F_2(t) \quad (8.14.d)$$

One can solve Eq. 8.14 using the Laplace transforms, which will give Eq. 8.15.

$$\hat{F}_0(s) = \frac{2a u_M (s + 2a + 2(u_M + w_M))}{(s + a + u_M + w_M)((s + 2a)(s + 2u_M) + 2s u_M)} \quad (15.a)$$

$$\hat{F}_1(s) = \frac{(2a + s) u_M (s + 2a + 2(u_M + w_M))}{(s + a + u_M + w_M)((s + 2a)(s + 2u_M) + 2s u_M)} \quad (8.15.b)$$

$$\hat{F}_2(s) = \frac{2(2a+s)u_M(a+s+u_M)+4(a+s)u_Mw_M}{(s+a+u_M+w_M)(s+2a)(s+2u_M)+2su_M} \quad (8.15.c)$$

The time required to start the reaction from state 0, 1 or 2.

$$\langle T_0 \rangle = -\left(\frac{\partial \hat{F}_0(s)}{\partial s}\right)_{s=0}, \langle T_1 \rangle = -\left(\frac{\partial \hat{F}_1(s)}{\partial s}\right)_{s=0}, \langle T_2 \rangle = -\left(\frac{\partial \hat{F}_2(s)}{\partial s}\right)_{s=0} \quad (8.16)$$

For the initiation of the chemical reaction, there must be the availability at least one free site. Analogous to this logic, for the occurrence of the product formation event from a particular state, at least one CS_M conformer must be present. Because of these reasons, the reaction can start from the state 0 or 1 and the product formation can happen either from the state 1 or 2. Eq. 8.17 represents the average time between the product releases.

$$\langle \tau^1 \rangle_2 = \langle T_0 \rangle P'_0 + \langle T_1 \rangle P'_1 \quad (8.17)$$

P'_0 and P'_1 are the probabilities for the reaction to start from the state 0 and 1, respectively. One can derive them using the stationary state probabilities of respective states.

$$P_0 = \frac{u_M+w_M}{(a+u_M+w_M)^2} \quad (8.18.a)$$

$$P_1 = \frac{2a(u_M+w_M)}{(a+u_M+w_M)^2} \quad (8.18.b)$$

Substituting these relations, we get

$$\langle \tau^1 \rangle_2 = \frac{a+u_M+w_M}{2au_M} \quad (8.19)$$

As shown for Figure 8.4b, for the system with two sites also, one can derive the second moment.

$$\langle \tau^2 \rangle_2 = \frac{1}{4} \left(\langle \tau^2 \rangle_1 + \frac{2}{(a u_M)^2 (\langle \tau_1 \rangle)^2} \right) \quad (8.20)$$

Similarly, for the network with three catalytic sites, one can get Eq. 8.21 and 8.22.

$$\langle \tau^1 \rangle_3 = \frac{a+u_M+w_M}{3au_M} \quad (8.21)$$

$$\langle \tau^2 \rangle_3 = \frac{1}{9} \left(\langle \tau^2 \rangle_1 - \frac{4}{(a u_M)^2 (\langle \tau_1 \rangle)^2} + \frac{16}{2(a u_M)^2 (\langle \tau_1 \rangle)^2 + a u_M} \right) \quad (8.22)$$

On considering multiple active sites as a single new effective site with the properly rescaled transition rates, then one can expect the following scaling relation, $\left(\langle \tau^2 \rangle_N = \frac{\langle \tau^2 \rangle_1}{N^2} \right)$. However, Eq. 8.20 and 8.21 clearly show deviations from this behavior. Thus, the effect of stochasticity of individual chemical reactions exhibits itself in the second and higher moments of reaction times. In addition, the molecular details of these chemical reactions specify the degree of deviations from the above-mentioned scaling relation. Figure 8.5 illustrates these observations.

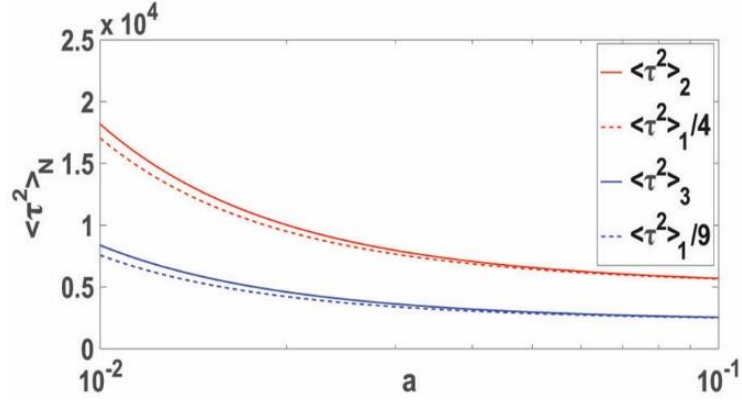


Figure 8.5: Mean squared reaction times $\langle \tau^2 \rangle_N$ (in s^2) for the system with N catalytic sites as function of the effective rate a (in s^{-1}) for $u_M = 0.01 s^{-1}$ and $w_M = 0.001 s^{-1}$.

Using the randomness parameter, one can measure the degree of stochastic fluctuations. We explicitly evaluate the randomness $R_{N,M}$ for the system with N active sites and M intermediate states. Eq. 8.23 show the randomness expression for the system with one catalytic site ($N = 1$).

$$R_{1,M} = 1 - \frac{2}{a u_M (\langle \tau_1 \rangle)^2} \quad (8.23)$$

For the system with two sites, one will get Eq. 8.24.

$$R_{2,M} = 1 - \frac{2}{a u_M (\langle \tau_1 \rangle)^2} \left(1 - \frac{1}{a u_M (\langle \tau_1 \rangle)^2} \right) \quad (8.24)$$

Eq. 8.25 represents the randomness for the system with three sites.

$$R_{3,M} = 1 - \frac{2}{a u_M (\langle \tau_1 \rangle)^2} \left(1 + \frac{2}{a u_M (\langle \tau_1 \rangle)^2} - \frac{8}{1 + 2 a u_M (\langle \tau_1 \rangle)^2} \right) \quad (8.25)$$

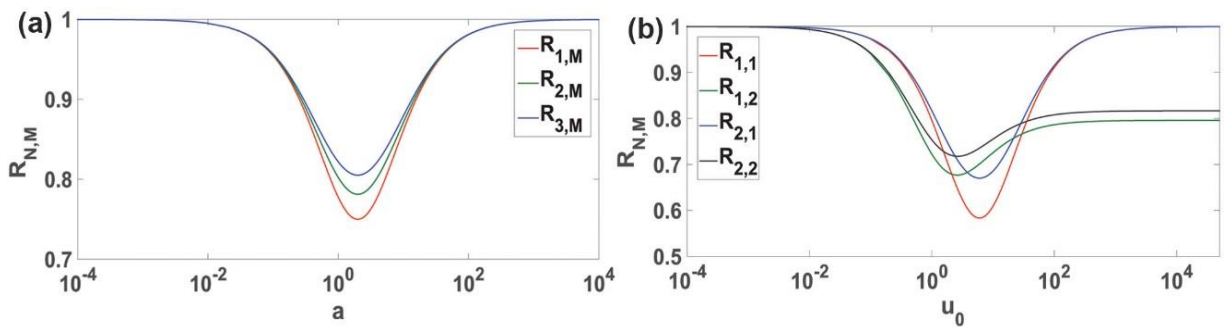


Figure 8.6: Randomness parameter $R_{N,M}$ (a) as a function of the effective rate a (in s^{-1}) for a system with $N = 1$ (red line), $N = 2$ (green line) and $N = 3$ (blue line) catalytic sites for

arbitrary number of intermediate states M and (b) as a function of the transition rate u_0 (in s^{-1}) for a system with one and two catalytic sites and having one ($M = 1$) and two ($M = 2$) intermediates.

Figure 8.6a presents the dependence of the randomness on the effective transition rate a for $N = 1, N = 2$ and $N = 3$ for arbitrary number of intermediate states, M . It shows a non-monotonic behavior of the randomness. The largest noise is expected for the intermediate values of a , while the noise is diminished for very small and very large transition rates, a . For understanding these observations, consider the discrete-state scheme described in Figure 8.2. For $a \rightarrow 0$, the system is mainly found in the state, $N - 1$ and there are not much stochastic fluctuations. Similarly, for $a \gg 1$, the system prefers to be in the state N , and this again leads to very small stochastic fluctuations. All discrete states in the system are fully explored only for intermediate values of a . One can also analyze that a decrease in the degree of stochastic fluctuations with increasing the number of catalytic sites (Figure 8.6a). This is in agreement with experimental observations.⁶ The degree of stochastic noise depends also on the complexity of the chemical reactions at each catalytic site. Figure 8.6b describes this effect, where the randomness is studied as a function of the transition rate, u_0 . One can see that increasing the number of intermediate states M , governs the degree of stochastic noise in the system. These observations suggest that the analysis of experimentally obtained randomness parameters can assist in determining the molecular details of the chemical reactions at each catalytic site.

One can extend the current theoretical framework in several directions to present a more realistic description of the complex processes on the nanocatalysts. For example, we can analyze a system with two types of catalytic sites as shown in Figure 8.1b. There are N_1 active sites where the chemical reactions with transition rates (u_j, w_j) and N_2 active sites where the chemical reactions with transition rates (p_j, q_j) , with $N = N_1 + N_2$. Assuming that all reactions have M intermediate states, we obtain the following expression for the mean reaction time.

$$\langle \tau^1 \rangle_N = \left(\frac{1}{N_1} \right) \left(\frac{1}{a} + \frac{1}{u_M} + \frac{w_M}{a u_M} \right) + \left(\frac{1}{N_2} \right) \left(\frac{1}{b} + \frac{1}{p_M} + \frac{q_M}{b p_M} \right) \quad (8.26)$$

Here a and b are the effective transition rates before the product formation steps. This result again shows that the stochasticity effects remain hidden when we are simply considering the mean turnover times. The molecular details of the underlying reactions will influence the higher moments of PDF.

8.3 Conclusions:

In this chapter, we have developed a theoretical method to analyse the dynamics of chemical processes of catalytic particles with multiple active sites. Using the discrete-state stochastic description, dynamic properties of the chemical reactions on nanocatalysts one can explicitly evaluate the stationary-state and first-passage probabilities. Our analysis shows that the mean reaction times in the system are inversely proportional to the number of active sites, independently of the details of underlying chemical reactions. This result suggests that the stochastic effects remain covered for the mean chemical reaction rates, and the nanocatalyst with multiple active sites behaves as one new effective catalyst with a single site. Careful consideration of higher moments of reaction times leads to a different conclusion. For this situation, the stochastic effects are important. In addition, the details of the chemical reactions at each active site affects the higher moments of the PDF. The proposed theoretical method provides platforms for uncovering the quantitative features of the complex processes on nanocatalysts. It will be critically important to test our theoretical predictions in experimental studies as well as in the more advanced computational methods.

8.4 References:

- (1) Kalz, K. F.; Kraehnert, R.; Dvoyashkin, M.; Dittmeyer, R.; Gläser, R.; Krewer, U.; Reuter, K.; Grunwaldt, J.-D. *ChemCatChem* **2017**, *9*, 17.
- (2) Xu, W.; Kong, J. S.; Yeh, Y.-T. E.; Chen, P. *Nat. Mater.* **2008**, *7*, 992.
- (3) Xu, W.; Kong, J. S.; Chen, P. *J. Phys. Chem. C* **2009**, *113*, 2393.
- (4) Chen, P.; Zhou, X.; Andoy, N. M.; Han, K.-S.; Choudhary, E.; Zou, N.; Chen, G.; Shen, H. *Chem. Soc. Rev.* **2014**, *43*, 1107.
- (5) Roeffaers, M. B. J.; Sels, B. F.; Uji-i, H.; De Schryver, F. C.; Jacobs, P. A.; De Vos, D. E.; Hofkens, J. *Nature* **2006**, *439*, 572.
- (6) Zhou, X.; Xu, W.; Liu, G.; Panda, D.; Chen, P. *J. Am. Chem. Soc.* **2010**, *132*, 138.
- (7) Kolomeisky, A. B.; Fisher, M. E. *Phys. A* **2000**, *279*, 1.
- (8) Kolomeisky, A. B. *Motor proteins and molecular motors*; CRC Press: Boca Raton, 2015.

9. Effect of memory and inertial contribution on transition time distributions: theory and simulations

9.1 Introduction:

In the previous thesis chapters, we have applied different analytical frameworks to model the stochastic kinetics and dynamics of catalytic systems at the SM level. We took into consideration different enzymatic networks comprising single/multiple substrate types, reaction models equivalent to intracellular compartment reactions with substrate number fluctuations, mechanisms covering dynamic cooperative and allosteric effects of an enzyme. We also applied our theoretical formalisms to study heterogeneous metal NP catalysis for theoretically understanding size dependent catalytic activity and exploring mechanistic details of chemical reactions occurring on multiple active surface sites of a nanocatalyst. For solving these problems, we constructed the PDF corresponding to discrete stochastic events and determined temporal quantities of interest from the statistical moments. The obtained distribution of time relates to the probability of occurrence of an event from a particular state for the first time, beginning from an initial state, after traversing through a certain number of intermediate states. Similarly, one can derive the waiting time distribution for the catalytic turnover event from a productive substrate-bound state, which gives the corresponding rate of change in the probability density of the product formation state. The PDF takes into account the change in the number of different species participating in each step with certain a priori conditions. The fundamental basis of these theoretical methods lies in the implementation of probabilistic approach for discrete single or multi directional reversible transitions among different interconverting conformers. In other words, the random variables exclusively take discrete values.

Apart from discrete approaches applied on stochastic systems, one can also obtain the same PDF of interest, by implementing considering theoretical methods, which employ continuous random variables. The overall PDF obtained from discrete methods, constitutes of the PDFs describing changes in species involved in each sequential step, which ultimately leads to the main event under examination (say, the monitored transition). However, in the continuous state model, the PDF represents the overall change in the dynamics of the system in terms of a variable (say the reaction co-ordinate of a system representing its progression with time), rather than examining discrete sequential changes. Analogous to discrete models, here also one determines the probability of finding the system at some advance time i.e. predicting the position of the reaction coordinate, pertaining to certain initial conditions. In general,

to model such systems in one dimension using a continuous formalism, one can begin with the Langevin equation (LE) and formulate the corresponding Fokker-Planck equation (FPE). This equation represents the rate of change in the probability density of the state, which marks the event accomplishment. The solution of the FPE gives the PDF (the first passage-time distribution) of interest associated with the continuous random variable. The later sections of this chapter include descriptive explanations of the theoretical method used with a specific example.

Bio-molecular transitions like protein folding and conformation rearrangements involve a one-dimensional diffusion in a free energy landscape with two minima separated by a high-energy barrier.¹⁻⁶ Owing to the stochastic nature of biophysical events and probable reversions happening while crossing the potential barrier, both the successful as well as the failed events contribute to the PDF (the first-passage time distribution). However, in the case of steep barriers, the reversion probability becomes significantly smaller and the corresponding PDF exclusively incorporates only the successful transitions initiated from the point of origin to the final co-ordinate, which marks the completion of an event. The distribution corresponding to such processes are defined as the transit time distribution (TTD), which represent the time a single particle spends while crossing the energy barrier, beginning from an initial co-ordinate to another defined co-ordinate. Recent single-molecule measurements have now achieved sufficient time resolution to observe such individual transition paths.⁷⁻¹¹ In the context of nucleic acid and protein folding,^{9,12} zipping/unzipping transition of a DNA hairpin,¹³ experimentally one can measure the time biomolecules spend while crossing such free energy barriers known as the transition path times. The time duration of such a transition path is much shorter than the mean reaction time and only a small fraction of the stochastic trajectories contribute to the transition paths. Such experimental studies have motivated many theoretical and computational studies where one can determine the full probability distribution function of transition path times.^{12,14-17}

These theoretical studies at the earlier stage mostly employed memoryless Markovian dynamics.¹⁸⁻²⁰ Nevertheless, as pointed out in protein folding experiments and in theoretical studies, the dynamics of such macromolecular systems is anomalous/sub-diffusive in nature and one needs to include memory effects to model the dynamics along a reaction coordinate.^{21,22} One can account for such sub-diffusive behavior by implementing models that are based on fractional Fokker Planck

equation, fractional Brownian motion and so on.²³ Makarov and coworkers have looked at the effect of memory on the time duration of transition paths using a simple model defining the particle dynamics using a generalized Langevin equation with an exponential memory kernel.^{22,24,25} Later, Carlon and coworkers extended this to a power-law-type memory kernel.²⁶ Obtaining closed form analytical expressions for the transit path times are difficult but under certain approximations, analytical results are derivable. To model such systems, one can implement the high friction (overdamped) limit. However, as pointed out by Orland and coworkers, for such short duration of transition paths, it is interesting to consider inertial effects and they have calculated the full transition-path time distribution along with the average transition-path time.²⁷ However, the calculations for the Markovian limit employed an ordinary Langevin equation with the Gaussian white noise. Since memory effects are important in molecular folding, it would be interesting to consider them along with the inertial contribution. In this chapter, we present theoretical calculations of the transition time distribution and the mean transition time using a model based on the generalized Langevin equation with the fractional Gaussian noise for a parabolic barrier. We show the calculation details of the transit time distribution (TTD) and deduce the analytical expressions of the distributions in the short and the long-time regimes. We also show a comparison between the analytical results and numerical simulations performed using the absorbing boundary conditions.

9.2 Model and Analyses:

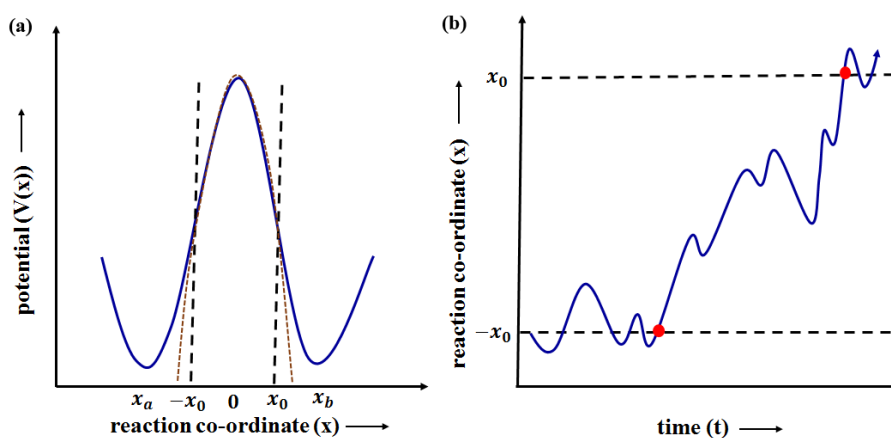


Figure 9.1: (a) Motion of a trajectory represented by the change in the position of the reaction co-

ordinate x , in a double well potential. x_a and x_b represent the equilibrium positions for the two protein conformations, which are involved in the transition. The part of the trajectory lying between the co-ordinates $-x_0$ and x_0 corresponds to the transition path in the defined inverted parabolic potential (dashed brown lines). (b) Time taken by the trajectory to reach x_0 beginning from $-x_0$ without any reversion, gives the transit path time. The red circles clearly mark the transit path and the x-axis signifies the corresponding transition time.

A generalized Langevin equation (GLE)^{28,29} well describes the stochastic dynamics of a particle in an inverted parabolic potential barrier $V(x) = -\frac{kx^2}{2}$.

$$m\dot{v}(t) = -V'(x) - \gamma \int_0^t dt' K(t-t')v(t') + \theta(t) \quad (9.1)$$

where m is the mass of the particle, γ is the friction coefficient and $K(t-t')$ is the power law memory kernel having the form

$$K(t-t') = 2H(2H-1)|t-t'|^{2H-2} = (2-\alpha)(1-\alpha)|t-t'|^{-\alpha}$$

where $\alpha = 2 - 2H$ and $0 \leq \alpha \leq 1$. (9.2)

The third term on the RHS of the GLE, $\theta(t)$ represents the colored noise of the system with the following characteristics.

$$\langle \theta(t) \rangle = 0 \text{ and}$$

$$\langle \theta(t)\theta(t') \rangle = \gamma k_B T K(t-t'). \quad (9.3)$$

Following Figure 9.1 (a), which represents the propagation of a trajectory in a double well potential, marked by the equilibrium positions x_A and x_B , we exclusively consider the transition part falling in the inverted parabolic barrier region. This is a symmetric barrier peaked at $x = 0$ with initial and final points at $-x_0$ and x_0 , respectively. The trajectories that sample the transit time enter the transition region at $-x_0$ and exit into x_0 without ever going back to $-x_0$. Thus the calculation of TPT distributions requires absorbing boundary conditions at $-x_0$ and x_0 . Equivalent to this GLE, one can obtain the propagator $P(x, v, t | -x_0, v_0, 0)$ that gives the probability of finding the system at a position x and velocity v at time t with initial position and velocity as $-x_0$ and v_0 . In the non-Markovian limit

the Fokker Planck equation (FPE) can be written as

$$\frac{\partial P}{\partial t} = -v \frac{\partial P}{\partial x} + \Xi(t) \frac{\partial (vP)}{\partial v} - W^2 x \frac{\partial P}{\partial v} + (W^2(t) - w_b^2) \frac{k_B T}{k} \frac{\partial^2 P}{\partial v \partial x} + \Xi \frac{k_B T}{m} \frac{\partial^2 P}{\partial v^2}. \quad (9.4)$$

where $P(x, v, t | -x_0, v_0, 0) \cong P$

$$\Xi(t) = \frac{\chi(t)\ddot{\chi}(t) - \dot{\chi}(t)\dot{\chi}(t)}{\dot{\chi}(t)^2 - \chi(t)\ddot{\chi}(t)} \quad (9.5)$$

$$W^2(t) = \frac{\dot{\chi}(t)\ddot{\chi}(t) - \ddot{\chi}(t)^2}{\dot{\chi}(t)^2 - \chi(t)\ddot{\chi}(t)} \quad (9.6)$$

$\chi(t)$ is the inverse Laplace transform of $\hat{\chi}(s)$.

$$\hat{\chi}(s) = \frac{s + \left(\frac{\gamma \bar{K}(s)}{m}\right)}{s^2 + s\left(\frac{\gamma \bar{K}(s)}{m}\right) - w_b^2} \quad (9.7)$$

No exact solution of Eq. 9.4 satisfies the absorbing boundary conditions. Eq. 9.8 represents the general solution of Eq. 9.4.

$$P(x, v, t) = \frac{\sqrt{C}}{2\pi} \exp \left[-\frac{1}{2} \left\{ D_{11}(x - \bar{x}(t))^2 + 2D_{12}(x - \bar{x}(t))(v - \bar{v}(t)) + D_{22}(v - \bar{v}(t))^2 \right\} \right] \quad (9.8)$$

where C is the determinant of a matrix D with general elements D_{ij}

$$D = \begin{bmatrix} C \sigma_v^2(t) & -C \sigma_{xv}(t) \\ -C \sigma_{xv}(t) & C \sigma_x^2(t) \end{bmatrix} \quad (9.9)$$

$$\bar{x}(t) = x_0 \chi(t) + \frac{v_0 \dot{\chi}(t)}{w_b^2} \quad (9.10a)$$

$$\bar{v}(t) = x_0 \dot{\chi}(t) + \frac{v_0 \ddot{\chi}(t)}{w_b^2} \quad (9.10b)$$

$$\sigma_x^2(t) = -\frac{k_B T}{m} \left(\frac{\dot{\chi}(t)^2}{w_b^4} - \frac{(\chi^2(t) - 1)}{w_b^2} \right) \quad (9.10c)$$

$$\sigma_v^2(t) = \frac{k_B T}{m} \left(1 + \frac{\dot{\chi}(t)^2}{w_b^2} - \frac{\ddot{\chi}(t)^2}{w_b^4} \right) \quad (9.10d)$$

$$\sigma_{xv}(t) = \frac{k_B T}{m} \left(\frac{\chi(t)\dot{\chi}(t)}{w_b^2} - \frac{\dot{\chi}(t)\ddot{\chi}(t)}{w_b^4} \right) \quad (9.10e)$$

This solution is with the free boundary conditions since no exact solution exists with the absorbing boundaries. In order to calculate the transit time distribution we introduce a function $Q_A(t)$, which counts all the trajectories crossing x_0 starting from $-x_0$ at a particular time t such that

$$Q_A(t) = \int_{x_0}^{\infty} P(x, t | -x_0, 0) dx \quad (9.11)$$

where $P(x, t | -x_0, 0)$ is the probability of finding the particle at position x at a time t . Using the rate of change in the absorption function at two consecutive time instants with an interval of Δt , one can obtain the transit time distribution.²⁷ As shown in the Ref. 27, the TPT distribution can be approximated as

$$f(t) \approx C \left(\frac{dQ_A(t)}{dt} \right). \quad (9.12)$$

On integrating the velocity component v in the obtained solution of the FPE (Eq. 9.8), we get

$$P(x, t | -x_0, v_0, 0) = \int_{-\infty}^{\infty} dv P(x, v, t | -x_0, v_0, 0) = \frac{1}{\sqrt{2\pi\sigma_x^2(t)}} e^{-\frac{(x-\bar{x}(t))^2}{2\sigma_x^2(t)}} \quad (9.13)$$

Further integration of Eq. 9.13 over v_0 by incorporating the equilibrium distribution of initial velocities, we get $P(x, t | -x_0, 0)$

$$P(x, t | -x_0, 0) = \int_{-\infty}^{\infty} dv_0 \rho_{eq}(v_0) P(x, t | -x_0, v_0, 0) = \frac{1}{\sqrt{2\pi\sigma^2(t)}} e^{-\frac{(x-X_0(t))^2}{2\sigma^2(t)}} \quad (9.14)$$

where $\rho_{eq}(v_0) = \sqrt{\frac{m}{2\pi k_B T}} e^{-\frac{mv_0^2}{2k_B T}}$, $\sigma^2(t) = \frac{k_B T}{k} (\chi^2(t) - 1)$ and $X_0(t) = -x_0\chi(t)$.

Substituting Eq. 9.14 in Eq. 9.11 gives Eq. 9.15.

$$Q_A(t) = \frac{1}{2} \left(1 - \text{Erf}(G(t)) \right) \quad (9.15)$$

$$\text{where } G(t) = \sqrt{\beta E} \sqrt{\frac{\chi(t)+1}{\chi(t)-1}} \quad (9.16)$$

$$\beta = \frac{1}{k_B T} \text{ and } E = \frac{k x_0^2}{2}.$$

The transit time distribution is

$$f_{TTD}(t) = \frac{1}{Q_A(\infty)} \left(\frac{dQ_A(t)}{dt} \right). \quad (9.17)$$

$$Q_A(\infty) = \frac{1}{2} \left(1 - \text{Erf}(\sqrt{\beta E}) \right) \quad (9.18)$$

Using the above equations, we get Eq. 9.19.

$$f_{TTD}(t) = -\frac{2}{\sqrt{\pi}} \frac{G'(t)e^{-G^2(t)}}{(1-\text{Erf}(\sqrt{\beta E}))} \quad (9.19)$$

This expression is approximate, as we have used the free boundary conditions instead of imposing the appropriate absorbing boundary conditions. We exclude trajectories that correspond to multiple unsuccessful attempts, and may fail to accomplish the transition. We are not counting trajectories with multiple crossings at $-x_0$ and x_0 , as it will not be the transition path. However, it had has been shown earlier that assuming a barrier that is much higher than the thermal energy, such re-crossing events become rare and the solution with free boundary conditions can be well approximated to that in the case of an absorbing boundary.^{19,23}

Using Eq.9.19 one can calculate the mean transit time defined as

$$\langle t \rangle = \int_0^\infty t f_{TTD}(t) dt = \int_0^\infty t \left(-\frac{2}{\sqrt{\pi}} \frac{G'(t)e^{-G^2(t)}}{(1-\text{Erf}(\sqrt{\beta E}))} \right) dt. \quad (9.20)$$

For the non-Markovian system with the inertial contribution, the functional form of $\chi(t)$ can be found to be

$$\chi(t) = \sum_{n=0}^{\infty} \frac{(w_b t)^{2n}}{n!} \left[E_{2-\alpha, 1+\alpha n}^{(n)} \left(\frac{-\gamma \Gamma[3-\alpha] t^{2-\alpha}}{m} \right) + \frac{\gamma \Gamma[3-\alpha] t^{2-\alpha}}{m} E_{2-\alpha, 3+\alpha(n-1)}^{(n)} \left(\frac{-\gamma \Gamma[3-\alpha] t^{2-\alpha}}{m} \right) \right]. \quad (9.21)$$

where $E_{\alpha, \beta}(z)$ is the Mittag-Leffler function defined as $E_{\alpha, \beta}(z) = \sum_{m=0}^{\infty} \frac{z^m}{\Gamma[\alpha m + \beta]}$. The n^{th} order

derivative of the same can be represented as $E_{\alpha, \beta}^{(n)}(z) = \sum_{m=0}^{\infty} \frac{(m+n)! z^m}{m! \Gamma[\alpha(m+n) + \beta]}$.

In the overdamped limit ($\gamma \rightarrow \infty$), $E_{\alpha,\beta}(-z) \sim \frac{1}{(z)\Gamma[\beta-\alpha]}$. In this case, Eq. 9.21 attains the same form as reported in the study by Orland and co-workers specific for the non-Markovian system without the inertial contributions.

As we cannot obtain a closed form of expression for $\chi(t)$, we numerically truncate the series of $\chi(t)$ in order to obtain an expression of the full transit-time distribution function. In order to do so, we write the expression of $\chi(t)$ as

$$\chi(t) = \sum_{j=0}^{\infty} \sum_{k=0}^{\infty} \left(\frac{(j+k)!(-z)^j (w_b t)^{2k}}{j! k! \Gamma[(2-\alpha)(j+k)+1+\alpha k]} + \frac{(j+k)! z (-z)^j (w_b t)^{2k}}{j! k! \Gamma[(2-\alpha)(j+k)+3+\alpha(k-1)]} \right) \quad (9.22)$$

where $z = \frac{\gamma \Gamma[3-\alpha] t^{2-\alpha}}{m}$

This is an infinite series in two indices j and k starting from zero. To evaluate this series, the inner sum over k at each j is evaluated by truncating the summation when the increment of the summation made by adding one more term is less than a very small number (here we take 10^{-8}). Then we sum over j and again truncate the series when the change in the successive terms is again less than a very small number (again we take it to be 10^{-8}). In this way, we evaluate $\chi(t)$ at each t starting from an initial time $t = 0.01$ and at small time intervals of $h = 0.01$. Next, we calculate $G(t)$ and $G'(t)$ at each time step using the relation $G'(t) = \frac{G(t+h)-G(t)}{h}$ and using these expressions we calculate the $f_{TTD}(t)$ from Eq. 9.19.

Figure 9.2 shows the transition path distribution $f_{TTD}(t)$ for two different values of α . The transition path time decreases with decreasing α . At low values of α , memory effects are dominant and that will enhance the dynamics. For a given value of the friction coefficient, the integral $\int_0^t dt' K(t-t') v(t') = \int_0^t dt' (2-\alpha)(1-\alpha) |t-t'|^{-\alpha} v(t') \equiv I(t)$ increases with an increase in α , but in the inertial limit (low γ values), the difference between $I(t)$ for different α 's is very less. Thus, the contribution from this term is negligible. At the same time because of the fact that the particle cannot go backward, the initial random force is positive (particle will only move forward) and the random forces at the subsequent times must be positive. At low values of α the random forces are

strongly-positively-correlated and this helps the particle to likely complete its trajectory faster. So these two effects compete with each other and as we have described that at low γ the difference in the frictional force at different α values is very less, the random force term dominates and hence the particle completes its trajectory faster at low α values. Also as shown in Figure 9.2, the transition path time decreases with decrease in α in the inertial regime, though the difference is very less as in general the effect of the random forces on the particle dynamics is weaker than the effect of the frictional force. Also the plot at $\alpha=1$ agrees with Eq. 9.19 in Ref. 27 which gives an expression for the transition path distribution in the Markovian limit in the presence of inertia. However at higher friction values (i.e. in the overdamped limit), the frictional force dominates over the random force term and the transition path time then increases quite significantly with decreasing α .

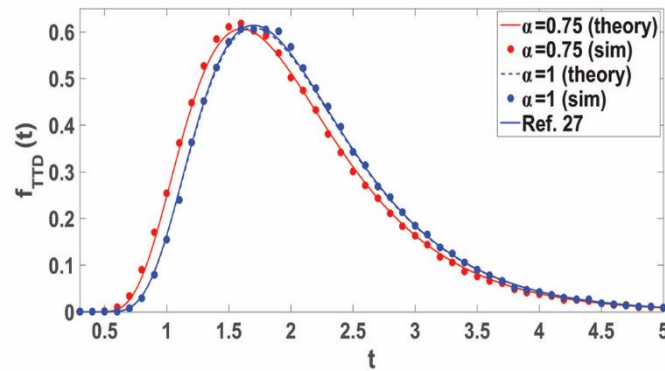


Figure 9.2: The transit time distributions obtained from Eq. 9.19 and 9.22 for various values of α . The solid red line represents the data sets obtained using Eq. 9.22 (theoretical prediction by implementing the free-boundary condition) and the filled red circles correspond to the data generated numerically using absorbing boundary conditions for the non-Markovian system, $\alpha = 0.75$. Similarly for $\alpha = 1$ there are data sets generated using Eq. 9.22 and from simulations, respectively represented by the blue dashed line and filled blue circles. The solid blue line corresponds to the TTD for the Markovian system described in Ref. 27. The other parameters are $k = 10$, $m = 1$, $\gamma = 5$, $x_0 = 1$ and $k_B T = 1$ such that $\beta E = 5$.

It is difficult to obtain the closed-form analytical expression for the transit time distribution for the non-Markovian system as it involves an infinite series associated with the n^{th} order derivative of the Mittag-Leffler function. However, we can obtain the exact asymptotic forms of quantities like $Q_A(t)$ and $G(t)$ and obtain the behavior of $f_{TTD}(t)$ at short and long times by using the properties of the Mittag-Leffler function.³⁰

In the short time limit we approximate the Mittag-Leffler function as $E_{\alpha,\beta}(-f) \sim \sum_{k=0}^3 \frac{(-f)^k}{\Gamma[\alpha k + \beta]}$. Using this, Eq. 9.21 reduces to

$$\chi(t) \sim 1 + t^2 w_b^2 \left(\frac{1}{2}\right) + \frac{1}{24} t^4 w_b^4 - \frac{t^2 w_b^2 z}{\Gamma[3-\alpha](\alpha^2 - 7\alpha + 12)} \quad (9.23)$$

The above equation does not consider higher order terms of time because of their insignificant contributions in the short time limit. This agrees with the short time approximation of $\chi(t)$ given in Ref. 27 in the Markovian limit, by considering $\alpha = 1$ in Eq. 9.23.

Substituting Eq. 9.23 in Eq. 9.16, we get

$$G(t) \sim \sqrt{\beta E} \sqrt{\frac{2}{t^2 w_b^2 \left(\frac{1}{2}\right) + \frac{1}{24} t^4 w_b^4 - \frac{t^2 w_b^2 z}{\Gamma[3-\alpha](\alpha^2 - 7\alpha + 12)}}}. \quad (9.24)$$

Eq. 9.24 shows that in this limit $t \rightarrow 0$, $G(t)$ diverges.

This expression for $G(t)$ and its derivative is used to derive transit time distribution for early times.

Figure 9.3a shows that $\chi(t)$ agrees with the short time approximation of $\chi(t)$ given in Ref 27 in the Markovian limit ($\alpha = 1$). In Figure 9.3b, we have compared TTD expressions at short times for $\alpha = 0.75$.

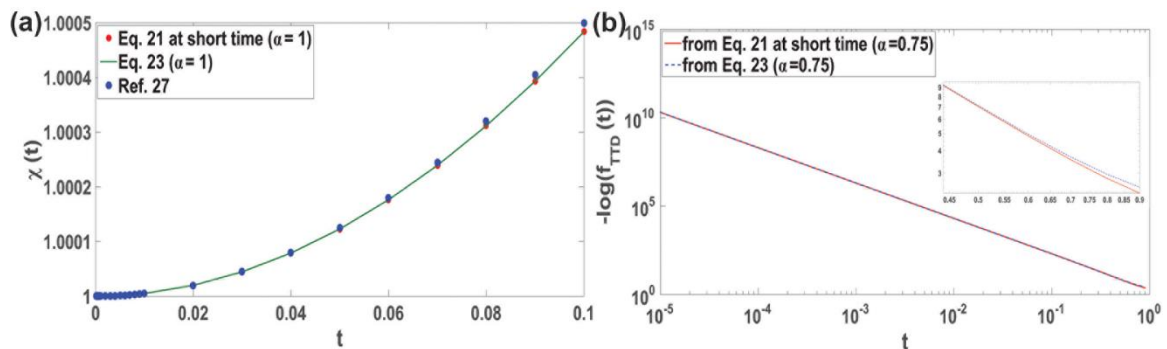


Figure 9.3: (a) Comparison between the exact expression of $\chi(t)$ (Eq. 9.21) at shorter times for $\alpha = 1$, the early time approximation of $\chi(t)$ expressed in Eq. 9.23 and the $\chi(t)$ for Markovian systems at short time as described in Ref. 27. These data sets are respectively, represented by the filled red circles, the green solid line and the filled blue circles using the following set of parameter values: $k = 0.1, m = 1, \gamma = 1$ (b) Comparison between the expression of TTD in Eq. 9.19 using the $\chi(t)$ defined in Eq. 9.21 at shorter times for $\alpha = 0.75$ (non-Markovian system) and the TTD

using the early time approximation of $\chi(t)$ in Eq. 9.23. These are respectively, represented by the red solid line and the dashed blue line, using the mentioned parameter set: $k = 0.1, m = 1, \gamma = 1$ and $x_0 = 1$.

In the long time, $E_{\alpha,\beta}(-f) = -\sum_{r=1}^N \frac{1}{(-f)^r \Gamma[\beta - \alpha k]}$. Here, N can be any natural number greater than unity. Applying this formula in Eq. 21 will give

$$\chi(t) = \sum_{r=1}^N -z^{-r} \left[E_{\alpha,1-(2-\alpha)r}^r((\Omega t)^\alpha) + z E_{\alpha,(3-\alpha)-(2-\alpha)r}^r((\Omega t)^\alpha) \right] \quad (9.25)$$

$$\text{where } \Omega = \left(\frac{mw_b^2}{\gamma \Gamma[3-\alpha]} \right)^{\frac{1}{\alpha}}.$$

Here, $E_{\alpha,\beta}^r(f) = \sum_{k=0}^{\infty} \frac{r(k)f^k}{k! \Gamma[\alpha k + \beta]}$. It represents the functional form of a three parameter Mittag-Leffler function and $r(k)$ holds the relationship mentioned below.³¹

$$r(k) = \begin{cases} 1; & k = 0 \\ r(r+1)(r+2) \dots (r+k-1); & k > 0 \end{cases}$$

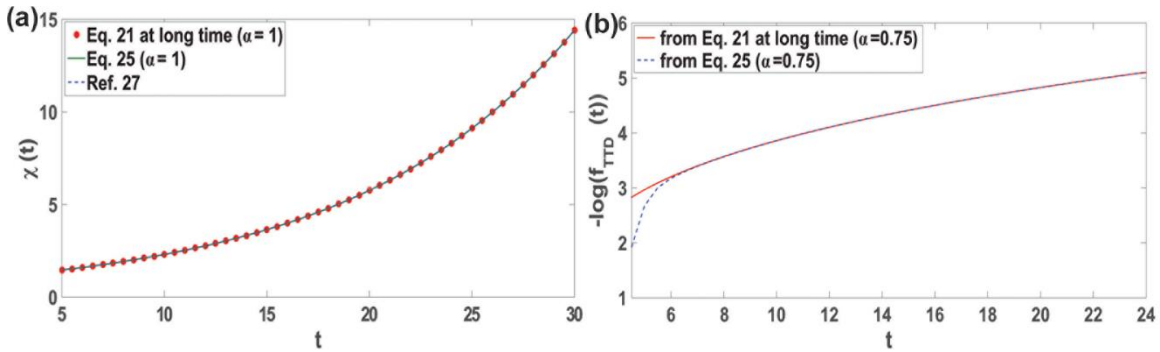


Figure 9.4: Comparison between the exact expression of $\chi(t)$ (Eq. 9.21) at long times for $\alpha = 1$, the long-time approximation of $\chi(t)$ expressed shown in Eq. 9.25, and the $\chi(t)$ for Markovian systems at short time as discussed in Ref. 27, respectively represented by the filled red circles, the green solid line and the dashed blue line. The parameter values used are $k = 0.1, m = 1$ and $\gamma = 1$. (b) Comparison between the expression of TTD in Eq. 9.19 using the $\chi(t)$ in Eq. 9.21 at long times for $\alpha = 0.75$ (non-Markovian system) and the TTD using the long-time approximation of $\chi(t)$ as shown in Eq. 25, respectively represented by the red solid line and the dashed blue line. The parameter values used are: $k = 0.1, m = 1, \gamma = 1$ and $x_0 = 1$.

In order to test our theoretical results we performed simulations by numerically integrating the full GLE given in Eq. 9.1. We compute the TPT distribution from the simulations by imposing absorbing boundary conditions in x_0 . The initial position of the particle is at $-x_0$ and the velocity is initialized from the equilibrium distribution of velocities. Then the particle evolves in time until it reaches x_0 . If the particle enters the region $x \leq -x_0$, we discard and restart the simulation of that particle. We repeat

this process until we evolve the particle to the region $x \geq x_0$ without entering into the region $x \leq -x_0$ and we record the time required for that particle. This will give us one transit path time. We repeat this process for 10^5 times to get 10^5 transit path times. This will give us our entire transit path time distribution.

As described in the former sections of the chapter, for obtaining an analytical expression for the transit time distribution associated with the barrier-crossing event one needs to apply the high barrier approximation using the free-boundary conditions. The exact solution corresponding to the absorbing boundary conditions is unobtainable. As shown in Figure 9.4a, the numerical simulations (using the absorbing boundary conditions) performed for validating our theory (based on the free boundary conditions), show excellent agreement in the high barrier limit. So, in general, the statistics obtained by implementing the free and absorbing boundary conditions using theory and simulations respectively agree well with each other for the steep barriers as under these situations, the probability of re-crossing reduces significantly. This was also observed in previous studies on the transit time distributions both in the overdamped as well as inertial limit.^{18,26,27} For smaller barriers, the agreement is good at lower friction values and disagrees in the higher friction limit (Figure 9.5b). When the friction is low, the inertial contributions saturate to a fixed value (represented by the first term of Eq. 10c) and fluctuations in the reaction coordinate are negligible (represented by the second term of Eq. 10c). On the other hand, at higher friction coefficient values, fluctuations have contributions both from the inertial term as well as from the variance of the reaction coordinate, x . Thus, in this case, there is a disagreement between the theoretical and simulation data points.

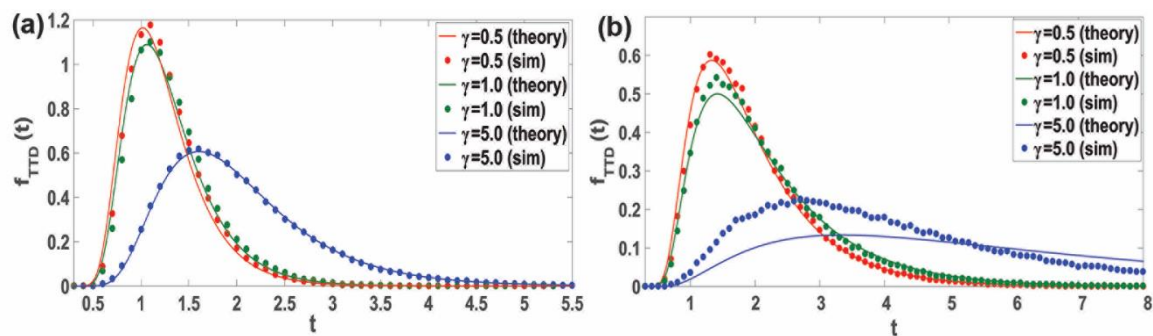


Figure 9.5: Transit time distributions obtained from Eq. 9.21 and 9.22 for various values of γ at $k = 10$ and (b) $k = 2$. The red, green and blue solid lines respectively represent the distribution

profiles obtained using Eq. 9.22 for the different values of γ : 0.5, 1 and 5. The corresponding colored symbols represents the TTDs from simulations, employing the following parameter set: $\alpha = 0.75$, $m = 1$, $x_0 = 1$ and $k_B T = 1$. We observe significant deviations between theory and simulations for the case when $k = 2$ (low barrier) at higher values of the friction coefficient γ .

9.3 Conclusions:

Transition path times takes into account the actual duration of transition between two different conformational states in the context of proteins folding, polymer translocation experiments. In this chapter, we used a simple toy model of a generalized Langevin equation with a power-law memory kernel to model the dynamics of a one-dimensional stochastic particle crossing a parabolic barrier. Previous dynamical analyses employed the overdamped limit for a non-Markovian process and later the inertial effects were included. However, the studies with inertial contributions were limited to Markovian process. As anomalous dynamics is present in macromolecular systems and recent studies have examined the effect of memory on transition path times, in this chapter we include inertial effects in the presence of memory.

The analytical approach followed for deducing the transit time distribution involves the usage of the free boundary conditions by incorporating the high barrier approximation. Inclusion of inertia and memory effects make the calculations complex and a closed form analytical form of the TPT distribution cannot be obtained. Also this solution is not exact as we do not use the absorbing boundary conditions. We have also developed a numerical algorithm to calculate the transit time distribution for non-Markovian processes with power-law memory and extended it to study systems with inertia. Our analytical results with free boundary conditions agree very well the numerical simulations for steep barriers. Such studies associated with modeling non-Markovian systems including inertial effects enhance the physical understanding of the dynamics of molecular systems that relate to realistic biochemical processes.

9.4 References:

- (1) Tanford, C. In *Adv. Protein Chem.*; Anfinsen, C. B., Anson, M. L., Edsall, J. T., Richards, F. M., Eds.; Academic Press: 1968; Vol. 23, p 121.
- (2) Kim, P. S.; Baldwin, R. L. *Annu. Rev. Biochem.* **1990**, *59*, 631.

- (3) Jackson, S. E.; Fersht, A. R. *Biochemistry* **1991**, *30*, 10428.
- (4) Haas, E. *ChemPhysChem* **2005**, *6*, 858.
- (5) Ladurner, A. G.; Fersht, A. R. *Nat. Struct. Biol.* **1999**, *6*, 28.
- (6) Jacob, M.; Schindler, T.; Balbach, J.; Schmid, F. X. *Proc. Natl. Acad. Sci. U.S.A.* **1997**, *94*, 5622.
- (7) Hänggi, P.; Talkner, P.; Borkovec, M. *Rev. Mod. Phys.* **1990**, *62*, 251.
- (8) Chung, H. S.; Louis, J. M.; Eaton, W. A. *Proc. Natl. Acad. Sci. U.S.A.* **2009**, *106*, 11837.
- (9) Neupane, K.; Ritchie, D. B.; Yu, H.; Foster, D. A. N.; Wang, F.; Woodside, M. T. *Phys. Rev. Lett.* **2012**, *109*, 068102.
- (10) Truex, K.; Chung, H. S.; Louis, J. M.; Eaton, W. A. *Phys. Rev. Lett.* **2015**, *115*, 018101.
- (11) Neupane, K.; Wang, F.; Woodside, M. T. *Proc. Natl. Acad. Sci. U.S.A.* **2017**, *114*, 1329.
- (12) Neupane, K.; Foster, D. A. N.; Dee, D. R.; Yu, H.; Wang, F.; Woodside, M. T. *Science* **2016**, *352*, 239.
- (13) Sharma, S.; Biswas, P. *J. Stat. Mech: Theory and Experiment* **2020**, *2020*, 073411.
- (14) Berezhkovskii, A.; Szabo, A. *J. Chem. Phys.* **2004**, *122*, 014503.
- (15) Orland, H. *J. Chem. Phys.* **2011**, *134*, 174114.
- (16) Kim, W. K.; Netz, R. R. *J. Chem. Phys.* **2015**, *143*, 224108.
- (17) Berezhkovskii, A. M.; Dagdug, L.; Bezrukov, S. M. *J. Phys. Chem. B* **2017**, *121*, 5455.
- (18) Chaudhury, S.; Makarov, D. E. *J. Chem. Phys.* **2010**, *133*, 034118.
- (19) Zhang, B. W.; Jasnow, D.; Zuckerman, D. M. *J. Chem. Phys.* **2007**, *126*, 074504.
- (20) Berezhkovskii, A. M.; Hummer, G.; Bezrukov, S. M. *Phys. Rev. Lett.* **2006**, *97*, 020601.
- (21) Satija, R.; Makarov, D. E. *J. Phys. Chem. A* **2019**.
- (22) Satija, R.; Das, A.; Makarov, D. E. *J. Chem. Phys.* **2017**, *147*, 152707.
- (23) Pollak, E. *Phys. Chem. Chem. Phys.* **2016**, *18*, 28872.
- (24) Medina, E.; Satija, R.; Makarov, D. E. *J. Phys. Chem. B* **2018**, *122*, 11400.
- (25) Makarov, D. E. *J. Chem. Phys.* **2015**, *143*, 194103.
- (26) Carlon, E.; Orland, H.; Sakaue, T.; Vanderzande, C. *J. Phys. Chem. B* **2018**, *122*, 11186.
- (27) Laleman, M.; Carlon, E.; Orland, H. *J. Chem. Phys.* **2017**, *147*, 214103.
- (28) Chaudhury, S.; Cherayil, B. J. *J. Chem. Phys.* **2006**, *125*, 024904.
- (29) Chaudhury, S.; Chatterjee, D.; Cherayil, B. J. *J. Chem. Phys.* **2008**, *129*, 075104.
- (30) Haubold, H. J.; Mathai, A. M.; Saxena, R. K. *Journal of Applied Mathematics* **2011**, *2011*, 298628.
- (31) Garra, R.; Garrappa, R. *Commun Nonlinear Sci Numer Simulat* **2018**, *56*, 314.

10. Conclusions and Future Directions

10.1 An Overall Outlook:

Understanding the stochastic physics associated with biomolecules like protein, DNA, RNA and polypeptides can unravel the mechanistic details of the concerned biological process. The molecular aspect of a biochemical network regulates the method of analysis, which would determine the time-dependent signatures of the system under investigation.^{1,2} Exploration of several SM experimental techniques, well comprehended with different analytical frameworks, provided tools for examining dynamic properties of biophysical/biochemical networks.^{3,4} Many studies have confirmed the existence of temporal fluctuations in the catalytic rates attributed to the slow conformational interconversions between different states.^{5,6} One cannot extract such dynamic information by simply applying the ensemble average measurements.

In this thesis, we have implemented different theoretical methods (the first-passage time distribution formalism, the waiting-time distribution formalism) for modelling the dynamics of a system with discrete conformational states. We have also applied a continuous modelling method, using the generalized Langevin equation (GLE) for deducing the distribution of time taken by a molecule in crossing a double-well potential, pertaining to frictional and random forces with the inertial and memory effects (the transit time distribution). The PDF corresponding to a certain event contains the stochastic signatures of that particular system. From the first moment of the PDF, one can deduce the exact analytical expression for the mean reaction time. However, using the mean analysis one cannot capture any fluctuation characteristics. Additionally, two different systems can show similar mean behaviour. In order to quantify the temporal fluctuations in the catalytic rates, we deduce higher moments of the PDF and calculate the randomness parameter.⁷ We have analysed different reaction models related to enzyme and NP catalyses at the SM level, where different states are mutually interconverting into each other. We have found that the statistical quantities reflect the stochasticity of systems and predict the mechanistic details of the ongoing chemical reactions.

As observed experimentally, from these mechanistic minimal models, one can successfully measure different temporal effects like the dynamic cooperativity, the allosteric effect, determination of the rate-determining step in a complicated network and the characteristic phenomenon of distribution of rates. We have also validated our theoretical predictions by employing numerical algorithms for a system with many stochastic processes. Such extended applications provide platforms for dynamic investigations of intracellular networks, multi-step catalysis, understanding the transport mechanism of chemical substances across membranes, dependence of the substrate processing rate on different physical-chemical factors and associated stochastic kinetics of biopolymers.

Factually, any slight change in the reaction environmental conditions can introduce conformational (structural) modifications in the native state of a protein. This protein structure-function dependence and its corresponding consequences in a complex biological framework is a wholesome challenging research problem in itself.⁸ Beginning from the protein activation to the required activity, there can be many intermediate steps. Identifying a particular state in a multistep reaction will depend on its lifetime and the resolution of the spectroscopic technique adopted for the characterization. However, in the course of a reaction, denaturation of the active protein can also happen, leading to the malfunctioning in a given biological process and rare deadly diseases.^{9,10} Based on the mechanistic insights, suggesting alternative pathways to inhibit the unfolding process, developing models to understand the dynamics of a certain class of proteins and investigating the rare event statistics, could be some of the engaging problems. In future, we would like to develop similar theoretical formalisms and extend their applicability to many more cellular reactions and catalytic networks in a general way.

Similar to biomolecules, materials also exhibit phenomena of change in their magnetic properties, realignment of its composite atoms, reordering and restructuring, driven by thermodynamic and kinetic principles.¹¹⁻¹³ We wish to extend and modify the existing

analytical formalisms for probing the stochastic behaviour. By applying the concepts of statistical mechanics, one can compute the thermodynamic and kinetic parameters of interest. Developing model mechanisms and computing theoretical analogues of some experimental quantities could help in establishing a link between the observed data and the developed theoretical method. Active coherence between experiments and theory would open new vistas for better understanding and future developments in a definite domain of research.

10.2 References:

- (1) Moerner, W. E. *J. Phys. Chem. B* **2002**, *106*, 910.
- (2) Cornish, P. V.; Ha, T. *ACS Chem. Biol.* **2007**, *2*, 53.
- (3) Michalet, X.; Weiss, S.; Jäger, M. *Chem. Rev.* **2006**, *106*, 1785.
- (4) Ambrose, W. P.; Goodwin, P. M.; Jett, J. H.; Van Orden, A.; Werner, J. H.; Keller, R. A. *Chem. Rev.* **1999**, *99*, 2929.
- (5) English, B. P.; Min, W.; van Oijen, A. M.; Lee, K. T.; Luo, G.; Sun, H.; Cherayil, B. J.; Kou, S. C.; Xie, X. S. *Nat. Chem. Biol.* **2006**, *2*, 87.
- (6) Zwanzig, R. *Acc. Chem. Res.* **1990**, *23*, 148.
- (7) Chaudhury, S. *J. Phys. Chem. B* **2014**, *118*, 10405.
- (8) Brucale, M.; Schuler, B.; Samorì, B. *Chem. Rev.* **2014**, *114*, 3281.
- (9) Nettels, D.; Müller-Späth, S.; Küster, F.; Hofmann, H.; Haenni, D.; Rügger, S.; Reymond, L.; Hoffmann, A.; Kubelka, J.; Heinz, B.; Gast, K.; Best, R. B.; Schuler, B. *Proc. Natl. Acad. Sci. U.S.A.* **2009**, *106*, 20740.
- (10) Soranno, A.; Koenig, I.; Borgia, M. B.; Hofmann, H.; Zosel, F.; Nettels, D.; Schuler, B. *Proc. Natl. Acad. Sci. U.S.A.* **2014**, *111*, 4874.
- (11) Wu, L.; Mendoza-Garcia, A.; Li, Q.; Sun, S. *Chem. Rev.* **2016**, *116*, 10473.
- (12) Elnaggar, H.; Wang, R.-P.; Lafuerza, S.; Paris, E.; Tseng, Y.; McNally, D.; Komarek, A.; Haverkort, M.; Sikora, M.; Schmitt, T.; de Groot, F. M. F. *ACS Appl. Mater. Interfaces* **2019**, *11*, 36213.
- (13) Rodina, A.; Efros, A. L. *Nano Lett.* **2015**, *15*, 4214.

List of Publications

- Chaudhury, S.; Singh, D.; Kolomeisky, A. B., Theoretical Investigations of the Dynamics of Chemical Reactions on Nanocatalysts with Multiple Active Sites. *J. Phys. Chem. Lett.* 2020, *11*, 2330-2335.
- Singh, D.; Chaudhury, S., Single-Molecule Kinetics of an Enzyme in the Phosphorylation-Dephosphorylation Cycle. *J. Indian Chem. Soc.* 2019, *96*, 967-979. (invited article)
- Singh, D.; Chaudhury, S., Theoretical Study of the Conditional Non-Monotonic Off Rate Dependence of Catalytic Reaction Rates in Single Enzymes in the Presence of Conformational Fluctuations. *Chem. Phys.* 2019, *523*, 150-159.
- Singh, D.; Chaudhury, S., Stochastic Simulations Data for Figure 1 and the Phase Diagram Construction for Defining Monotonic and Non-Monotonic Regimes of the Velocity as a Function of K_{off} . *Data in Brief* 2019, *25*, 104211-104215.
- Singh, D.; Chaudhury, S., Effect of Substrate Number Fluctuations in Stochastic Enzyme Kinetics. *ACS Omega* 2018, *3*, 5574-5583. (invited article)
- Singh, D.; Chaudhury, S., Single-Molecule Kinetics of an Enzyme in the Presence of Multiple Substrates. *ChemBioChem* 2018, *19*, 842-850.
- Singh, D.; Chaudhury, S., Statistical Properties of Fluctuating Enzymes with Dynamic Cooperativity Using a First Passage Time Distribution Formalism *J. Chem. Phys.* 2017, *146*, 145103-145107.
- Singh, D.; Chaudhury, S., A Stochastic Theoretical Approach to Study the Size-Dependent Catalytic Activity of a Metal Nanoparticle at the Single Molecule Level. *Phys. Chem. Chem. Phys.* 2017, *19*, 8889-8895.

Rights and Permissions:

12/10/2020 RightsLink Printable License

**AIP PUBLISHING LICENSE
TERMS AND CONDITIONS**

Dec 10, 2020

This Agreement between Ms. Divya Singh ("You") and AIP Publishing ("AIP Publishing") consists of your license details and the terms and conditions provided by AIP Publishing and Copyright Clearance Center.

License Number 4965260903037

License date Dec 10, 2020

Licensed Content Publisher AIP Publishing

Licensed Content Publication Journal of Chemical Physics

Licensed Content Title Statistical properties of fluctuating enzymes with dynamic cooperativity using a first passage time distribution formalism

Licensed Content Author Divya Singh, Srabanti Chaudhury

Licensed Content Date Apr 14, 2017


Licensed Content Volume 146


Licensed Content Issue 14

Type of Use Thesis/Dissertation

Requestor type Author (original article)

<https://i100.copyright.com/AppDispatchServlet> 1/3

 **RightsLink**Home ? Email Support Sign in Create Account



Theoretical study of the conditional non-monotonic off rate dependence of catalytic reaction rates in single enzymes in the presence of conformational fluctuations
Author: Divya Singh, Srabanti Chaudhury
Publication: Chemical Physics
Publisher: Elsevier
Date: 1 July 2019
© 2019 Published by Elsevier B.V.

Please note that, as the author of this Elsevier article, you retain the right to include it in a thesis or dissertation, provided it is not published commercially. Permission is not required, but please ensure that you reference the journal as the original source. For more information on this and on your other retained rights, please visit: <https://www.elsevier.com/about/our-business/policies/copyright#Author-rights>

[BACK](#) [CLOSE WINDOW](#)

© 2020 Copyright - All Rights Reserved | Copyright Clearance Center, Inc. | Privacy statement | Terms and Conditions
Comments? We would like to hear from you. E-mail us at customer@copyright.com

**JOHN WILEY AND SONS LICENSE
TERMS AND CONDITIONS**

Dec 10, 2020

This Agreement between Ms. Divya Singh ("You") and John Wiley and Sons ("John Wiley and Sons") consists of your license details and the terms and conditions provided by John Wiley and Sons and Copyright Clearance Center.

License Number	4965260517283
License date	Dec 10, 2020
Licensed Content Publisher	John Wiley and Sons
Licensed Content Publication	ChemBioChem
Licensed Content Title	Single-Molecule Kinetics of an Enzyme in the Presence of Multiple Substrates
Licensed Content Author	Srabanti Chaudhury, Divya Singh
Licensed Content Date	Mar 23, 2018
Licensed Content Volume	19
Licensed Content Issue	8
Licensed Content Pages	9
Type of use	Dissertation/Thesis

12/15/2020

IISER, Pune Mail - Regarding Incident 4002590 Issuing Copyrights (URGENT)



DIVYA SINGH <divya.dhyia@students.iiserpune.ac.in>

Regarding Incident 4002590 Issuing Copyrights (URGENT)

2 messages

support@services.acs.org <support@services.acs.org>
To: divya.dhyia@students.iiserpune.ac.in

Thu, Dec 10, 2020 at 4:35 PM



Dear Dr. Singh,

Thank you for contacting us.

Your permission requested is granted and there is no fee for this reuse. In your planned reuse, you must cite the ACS article as the source, add this direct link <https://pubs.acs.org/doi/10.1021/acsomega.8b00611> and include a notice to readers that further permissions related to the material excerpted should be directed to the ACS.

Kind regards,

Nikola Markovic
ACS Publications
Customer Services & Information
Website: <http://help.acs.org>

Incident Information:

Incident #: 4002590
Date Created: 2020-12-10T10:43:25
Priority: 3
Customer: Divya Singh
Title: Issuing Copyrights (URGENT)
Description: Dear Team,

Kindly, issue the copyrights of my paper (Singh, D.; Chaudhury, S., Effect of Substrate Number Fluctuations in Stochastic Enzyme Kinetics. ACS Omega 2018, 3, 5574-5583.) published in ACS

<https://mail.google.com/mail/u/0/?ik=def03907c1&view=pt&search=all&permthid=thread-F63A168568011964060538&impl=msg-F63A16856801196...> 1/2

12/15/2020

IISER, Pune Mail - RE: Issuing Copyrights



DIVYA SINGH <singh.divya@students.iiserpune.ac.in>

RE: Issuing Copyrights

2 messages

CONTRACTS-COPYRIGHT (shared) <Contracts-Copyright@rsc.org>
To: "singh.divya@students.iiserpune.ac.in" <singh.divya@students.iiserpune.ac.in>

Mon, Nov 2, 2020 at 9:10 PM

Many thanks for sending the permissions request below. The Royal Society of Chemistry (RSC) hereby grants permission for the use of your paper(s) specified below in the printed and microfilm version of your thesis. You may also make available the PDF version of your paper(s) that the RSC sent to the corresponding author(s) of your paper(s) upon publication of the paper(s) in the following ways: in your thesis via any website that your university may have for the deposition of theses, via your university's intranet or via your own personal website. We are however unable to grant you permission to include the PDF version of the paper(s) on its own in your institutional repository. The Royal Society of Chemistry is a signatory to the STM Guidelines on Permissions (available on request).

Please note that if the material specified below or any part of it appears with credit or acknowledgement to a third party then you must also secure permission from that third party before reproducing that material.

Please ensure that the thesis states the following:

Reproduced by permission of The Royal Society of Chemistry

and include a link to the paper on the Royal Society of Chemistry's website.

Please ensure that your co-authors are aware that you are including the paper in your thesis.

Best wishes,

Chloe Szebrat
Contracts and Copyright Executive
Royal Society of Chemistry
Thomas Graham House
Science Park, Milton Road
Cambridge, CB4 0WF, UK
www.rsc.org

---Original Message---

From: singh.divya@students.iiserpune.ac.in <singh.divya@students.iiserpune.ac.in>
Sent: 02 November 2020 15:23
To: CONTRACTS-COPYRIGHT (shared) <Contracts-Copyright@rsc.org>
Subject: Issuing Copyrights

Name: Divya Singh
Message: Dear Team,

Please issue the copyrights for my paper published in the PCCP. I want to use the full article in my thesis. Please find the details for the same:

Singh, D.; Chaudhury, S., A Stochastic Theoretical Approach to Study the Size-Dependent Catalytic Activity of a Metal Nanoparticle at the Single-Molecule Level. Phys. Chem. Chem. Phys. 2017, 19, 8889-8895. (<https://pubs.rsc.org/en/content/articlelanding/2017/CP/c6cp07895h#divAbstract>).

Thanks and Regards,
Divya Singh
IISER Pune

This communication is from The Royal Society of Chemistry, a company incorporated in England by Royal Charter (registered number RC000524) and a charity registered in England and Wales (charity number 207890). Registered

<https://mail.google.com/mail/u/0/?ikv=del05907c1&view=pt&search=all&permthid=thread-F43A1682263677386033202&siml=msg-F43A16822636773...> 1/2



RightsLink[®]

Home ? Email Support Sign In Create Account

Theoretical Investigations of the Dynamics of Chemical Reactions on Nanocatalysts with Multiple Active Sites

Author: Srabanti Chaudhury, Divya Singh, Anatoly B. Kolomeisky

Publication: Journal of Physical Chemistry Letters

Publisher: American Chemical Society

Date: Mar 1, 2020

Copyright © 2020, American Chemical Society



PERMISSION/LICENSE IS GRANTED FOR YOUR ORDER AT NO CHARGE

This type of permission/license, instead of the standard Terms & Conditions, is sent to you because no fee is being charged for your order. Please note the following:

- Permission is granted for your request in both print and electronic formats, and translations.
- If figures and/or tables were requested, they may be adapted or used in part.
- Please print this page for your records and send a copy of it to your publisher/graduate school.
- Appropriate credit for the requested material should be given as follows: "Reprinted (adapted) with permission from (COMPLETE REFERENCE CITATION). Copyright (YEAR) American Chemical Society." Insert appropriate information in place of the capitalized words.
- One-time permission is granted only for the use specified in your request. No additional uses are granted (such as derivative works or other editions). For any other uses, please submit a new request.

BACK

CLOSE WINDOW